Development and Assessment of Multifunctional Fluorescent-Magnetic Liposomes for Bioanalysis

Dissertation zur Erlangung des

Doktorgrades der Naturwissenschaften

(Dr. rer. nat.)

an der Fakultät Chemie und Pharmazie

der Universität Regensburg

Deutschland

Vorgelegt von

Cornelia Hermann

aus Altötting

im Jahr 2019

Die vorliegende Dissertation entstand in der Zeit von Januar 2016 bis August 2019 am Institut für Analytische Chemie, Chemo- und Biosensorik der Universität Regensburg.

Die Arbeit wurde angeleitet von Prof. Dr. Antje J. Bäumner.

Promotionsgesuch eingereicht am: 02.09.2019

Voraussichtlicher Kolloquiumstermin: 30.10.2019

Prüfungsausschuss

Vorsitzender: Prof. Dr. Oliver Tepner

Erstgutachterin: Prof. Dr. Antje J. Bäumner

Zweitgutachter: PD Dr. Axel Dürkop

Drittprüfer: Prof. Dr. Achim Göpferich

Danksagung

Besonders bedanken möchte ich mich bei meiner Betreuerin **Prof. Dr. Antje Bäumner** für die Möglichkeit zur Bearbeitung dieses interessanten Themas, sowie für die großartige Betreuung und Unterstützung während der gesamten Promotion. Auch **PD Dr. Axel Dürkop** danke ich vielmals für die ausführlichen Diskussionen und die geduldige Beantwortung meiner Fragen. Außerdem danke ich ihm für die Übernahme des Zweitgutachtens für diese Arbeit. Weiterhin gilt mein Dank **Prof. Dr. Achim Göpferich** und **Prof. Dr. Oliver Tepner** dafür, dass sie die Rollen des Drittgutachters und des Vorsitzenden in meiner Promotionsprüfung übernehmen.

Joachim Rewitzer dank ich herzlich für seine Unterstützung bei den ICP-OES/-MS Messungen, ebenso auch **Vanessa Tomanek**. Ihr danke ich auch für ihre wundervollen Zeichnungen, die diese Arbeit aufwerten. Auch **Dr. Sandy Himmelstoß** danke ich für ihre 3D Graphik sowieso für die Geduld, mit der sie diverse TEM Bilder für mich aufgenommen hat – was bei Liposomen nicht immer so ganz einfach ist.

Ich danke der Abbott Arbeitsgruppe, besonders **Sergey Tetin** und **Patrick MacDonald** dafür, dass sie mich so freundlich aufgenommen und mir die Forschung in ihrem Labor ermöglicht haben.

Außerdem möchte ich mich bei meiner Arbeitsgruppe bedanken, sowohl bei den Kollegen im **4. Stock** für die angenehme Gestaltung der Mittagspausen und die vielen schönen Freizeitabende, als auch beim **1. Stock** für die Unterstützung bei den vielen Fragen zur Mikrofluidik und den Fluoreszenzmessungen. Mein Dank gilt hierbei ins Besondere **Carola Hofmann** und **Rosi Walter** für die vielen langen Gespräche und die Aufmunterung, wenn es mal wieder nicht so lief wie geplant.

Ein großes Dankeschön auch an meine Freundinnen **Johanna Hinkel** und **Kathryn Zevenbergen**, die meine endlosen Fragen zur englischen Grammatik mit viel Geduld ertragen haben und die sprachliche Qualität der Arbeit sicher deutlich aufwerten konnten.

Last but not least gilt mein größter Dank **meiner Familie**, besonders meinen Eltern **Helga und Richard Hermann**, sowieso meinem Freund **Christian Rogoll**, die immer an meiner Seite waren und mich in jeglicher Hinsicht mit ganzer Kraft und Liebe unterstützt haben.

Vielen Dank Ihnen/Euch allen!

Declaration of Collaborations

This work was conducted in large degrees of experimental and theoretical work solely by the author. However, at some points collaborations with other researchers were conducted to generate results, which is stated in this chapter in accordance with §8 Abs. 1 Satz 2 Punkt 7 of the "Ordnung zum Erwerb des akademischen Grades eines Doktors der Naturwissenschaften (Dr. rer. nat.) an der Universität Regensburg vom 18. Juni 2009".

Food Safety Analysis enabled through Biological and Synthetic Materials: A Critical Review of Current Trends (Chapter 1)

This chapter has been published as a review article, except for the abstract. The author performed literature search and wrote the manuscript. The article was revised by Axel Duerkop and Antje J. Baeumner. Antje J. Baeumner is corresponding author.

Evaluation of Different Encapsulation Strategies for Magnetosomes (Chapter 3)

This chapter is intended for submission for publication. The experimental work was carried out by the author. Carola Hofmann, Thomas Hirsch, Axel Duerkop and Antje J. Baeumner contributed with strategic discussions. Antje J. Baeumner was the leader of this project.

A Microfluidic Magnetic-Coupling Device for the Production of Multifunctional Conjugates (Chapter 4)

This chapter is prepared to be submitted for publication. The experimental work was carried out by the author. Franziska Beck assisted in magnetic setup optimization. Christian Griesche, Michael Mayer and Antje J. Baeumner contributed with discussions to microfluidic design and strategic ideas. Antje J. Baeumner was the leader of this project.

Studies for the Preconcentration of P24 by Liposomes (Chapter 5)

This chapter has not been published. All experiments described in this chapter were performed by the author herself, and were conducted at Abbott Diagnostics in Lake Forest, IL, in cooperation with Patrick MacDonald, who also conducted preliminary functionalization of antibodies and other reagents and drew parts of the schemes. The author wrote this chapter. Liposome synthesis and functionalization were carried out by Carola Hofmann. Sergey Tetin, Thomas Hirsch, Axel Duerkop and Antje J. Baeumner contributed with strategic discussions. Antje J. Baeumner was the leader of this project.

Table of Contents

1 Food Safety Analysis enabled through Biological and Synthetic Materials: A Critical Review of Current Trends

1.1 Abstract

Food safety analysis is of tremendous importance to ensure high quality food and avoid any risk for the consumer. Nevertheless, there is still a high demand for faster, more reliable techniques, capable of action at the point of need, which may be the production site, a supermarket or the consumer's home.

This review focuses on the progress in development of new methods and materials applied in these analyses, distinguishing between biological und synthetic materials as well as *macro* versus *nano*. It is critically evaluating the pros and cons of each method, comparing them with emphasis on their field-portability, including analysis time and ease of application for the end user, but also on the limits of detection and material production effort.

Eventually, no significant improvement in food safety analysis was found when comparing total ranks of research from the early 2000s with recent publications. However, with a closer look, it can be observed that the trend moves away from solely lab-based methods and towards field-portable analysis systems, comparable to point of care detection for medical samples. As this also requires a huge increase in the investigation of complicated synthetic rather than biological materials, the intensified production effort compensates the portability assessment.

This chapter has been published, except for the abstract.

Hermann CA, Duerkop A, Baeumner AJ (2019) Food Safety Analysis Enabled through Biological and Synthetic Materials: A Critical Review of Current Trends. Analytical Chemistry 91:569–587. doi: 10.1021/acs.analchem.8b04598.

Author contributions

The author performed literature search and wrote the manuscript. The article was revised by Axel Duerkop and Antje J. Baeumner. Antje J. Baeumner is corresponding author.

1.2 Introduction

In summer 2017, a food safety scandal in which the insecticide fipronil was found in eggs produced in Belgium and the Netherlands [1] caused a huge outcry across Western Europe. Although the German Federal Institute for Risk Assessment quickly issued a declaration that the content of fipronil in eggs was too low to be harmful in the short time of exposure [2], this incident together with EHEC and *Salmonella* outbreaks in recent years demonstrate how utterly important food safety analysis is for the protection of all consumers. Routine food safety analysis is a stronghold across the food production chain, however much improvement in techniques that provide rapid, in-field and low-cost answers is needed, which is reflected by a very vibrant research field. As the development of new (nano)materials for analytical purposes has increased immensely in the last decade, this review focuses on the large variety of materials – *biological* as well as *synthetic*, *nano* as well as *macro* - that are under investigation in order to advance food safety analysis capabilities beyond today's standards. In this context, it provides a critical overview and comparison of these materials over a broad range of analytes and detection strategies.

For more narrowly defined reviews, the readers are directed to a number of excellent articles that focus on the diversity of analytes and detection principles. Some are limited to specific methods, e.g., the use of electrochemiluminescence [3], microfluidics [4] or electrochemical aptasensors [5]. Others choose one analyte, e.g., inorganic arsenic [6] or food borne pathogens [7] and review the different methods to detect these. Furthermore, some articles reflect the use of one specific material for the detection of different analytes with various methods [8, 9]. Also nanomaterials in general have been reviewed recently as they are applied in the analysis of food contaminants, such as those articles focusing on one class of materials or analytes, e.g., nanoparticles or pesticides [10–12] or giving a broader overview about the use of various nanomaterials for different analytes [13–15].

This critical review article provides an overview of literature published in the last four years (01/2015 to 07/2018) and evaluates the performance of technologies described. Only well-cited publications were chosen covering a broad range of analytes, detection methods and in particular the employed materials. The "Web of Science" citation service was used selecting publications for 2015 with at least 20 citations, for 2016 more than 15, 2017 more than 5 and 2018 at least two citations (as of July 2018). To enable a critical evaluation and comparison between the various sensing techniques described, the following ranking strategy was devised:

The publications were grouped within the classes of analytes that were found most frequently in the reviewed literature, which are "microbes", "mycotoxins", "veterinary drugs", "pesticides",

"preservatives", "packaging components", "seafood toxins" and "others". Within each analyte class, technologies were ranked based on (i) the effort of materials and sensor production, (ii) the effort of the analysis itself for the user, (iii) the duration of the analysis method including – if given – the preparation time of real samples, (iv) the limits of detection (LODs) relative to each other and finally (v) an evaluation about the portability of the new technology *vs*. a purely lab-based system. For a field-portable system, standard evaluation criteria of point-of-care systems were adopted (Table 1):

Table 1. Criteria and classification for portable devices

Portability evaluation criteria	Classification of portability
• close to user/product • no sample pre-treatment, no pipetting • ready-to-use chemicals, e.g., in tanks • no advanced training necessary for use • fast availability of results • consequence gathered directly from results	1 purely lab based 2 lab based, but with potential for portability 3 on the way to field-portable sensor, but still a lot to do 4 almost portable, but some points missing, e.g., a lot of pipetting needed or laborious data analysis 5 complete field-portable sensor

The sheer number of citations a publication gained according to the Web of Science was not used as an aspect for its rank, as this factor is too inhomogeneous, e.g., dependent on the year of publication, on the reputation of the respective research group or on the size of the community that is served by the applied method or material.

1.3 Analytes in Food Safety Analysis

The analytes of interest (Table 2) reflect contaminants of great concern with respect to food safety. These match in general with lists published by others, i.e., the index of Dzantiev et al. [16] matches well with the one in this review. More limited lists are published by the Food and Drug Administration [17] as, e.g., no veterinary drugs or preservatives are specified as food contaminants of great concern. The Food and Agriculture Organization of the United Nations together with the World Health Organization assembled even fewer contaminants in their 'general standard for contaminants and toxins in food an feed' [18], as they explicitly exclude pesticides, veterinary drugs and microbes due to being within the terms of reference of other committees. Interestingly, metal ions and radionuclides seem to be of great concern, too, but are not addressed in the literature collected for this review, which indicates a demand for more intensive research focus in that direction. In Table 3 all reviewed publications are sorted by analytes providing the respective LODs, field-portability status, required assay time, evaluated ranks within the analyte group, and the citation frequency.

Table 2. Comparison of analytes of great concern in food safety analysis

found for this review	Dzantiev et al. (2014) [16]	FDA [17]	FAO/WHO [18]
microbes	pathogens (microorganisms, viruses)	pathogens	
mycotoxins	natural toxins	natural toxins	mycotoxins
pesticides	pesticides	pesticides	
packaging components	packaging derived hazards	chemical contaminants	packaging components
seafood toxins	natural toxins	natural toxins	
veterinary drugs	veterinary drugs		
preservatives	preservatives		
others (PCB, PAH, colorants, melamine, GMF)	PCB, PHAs, colorants, melamine, GMOs	PCBs, melamine	melamine
	heavy metals, radionuclides, dioxin, organic chemicals	metals, radionuclides, dioxin	metals, radionuclides, organic chemicals
	fertilizers, allergens		

FAO: Food and Agriculture Organization of the United Nations; FDA: Food and Drug Administration; GMF: genetically modified food; GMO: genetically modified organisms; PAH: polycyclic aromatic hydrocarbon; PCB: polychlorinated biphenyl; WHO: World Health Organization.

Table 3. Reviewed publications sorted by analytes with LODs, portability status, assay time, ranks and citation number

analyte class	(model) analyte	LOD	porta-bility 1 - 5	time	rank	lit	cit
microbes	*Escherichia coli* ATCC 25922	10 - 10^3 CFU·mL^{-1}	4	1 h	2	[19]	45
	Escherichia coli ATCC 8739	3 CFU·mL^{-1}	2	20 min	4	[20]	16
	Escherichia coli O157:H7	10 CFU·mL^{-1}	3	~ 1 ¾ h	4	[21]	41
	Escherichia coli O157:H7	10^2 CFU·mL^{-1}	3	< 1h	6	[22]	19
	Escherichia coli O157:H7	1 CFU·mL^{-1} (standard), 10 CFU·mL^{-1} (yoghurt, egg)	2	2 h	8	[23]	2
	Escherichia coli O157:H7	~ 10 CFU·mL^{-1}	2	1 - 3 h	13	[24]	28
	Escherichia coli	8 CFU·mL^{-1}	2	n.a.	14	[25]	20
	Salmonella typhimurium	10^2 CFU·mL^{-1} (egg), 10^3 CFU·mL^{-1} (milk, juice)	5	1 h	1	[26]	11

	Salmonella typhimurium	6 CFU·mL^{-1}	2	~ 1 h	8	[27]	30
	Salmonella typhimurium	10^3 CFU·mL^{-1}	4	~ 1 h	10	[28]	42
	Salmonella typhimurium	10^3 - 10^5 cells·mL^{-1}	4	~ 5 min	12	[29]	6
	Salmonella enteritidis	5 ng·mL^{-1} DNA	3	~ 1 ¼ h	11	[30]	33
	Salmonella enterica	10 cells·µL^{-1}	3	40 min	18	[31]	31
	Bacillus atrophaeus	n.a.	5	~ 2 ½ h	2	[32]	30
	Staphylococcus aureus	4 · 10^3 CFU·mL^{-1}	3	1 ½ h	16	[33]	18
	Vibrio parahaemolyticus	14 CFU·mL^{-1}	2	~ 2 ½ h	17	[34]	6
	Campylobacter jejuni	40.7 pM DNA (UV/vis), 2.45 fM DNA (DLS)	2	< 3 h	18	[35]	7
	Escherichia coli O157:H7, *Salmonella sp.*	57 CFU·mL^{-1} (cucumber, *E.c.*), 17 CFU·mL^{-1} (hamburger, *E.c.*), 7.4·10^3 CFU·mL^{-1} (cuc., *S.sp.*), 11.7·10^3 CFU·mL^{-1} (hamb., *S.sp.*)	3	~ 1 h	6	[36]	38
	Escherichia coli O157:H7, *Salmonella typhimurium*	10^2 - 10^6 CFU·mL^{-1}	3	~ 2 h	20	[37]	40
	Salmonella typhimurium, *Vibrio parahaemolyticus*	10^4 CFU·mL^{-1}	3	80 min	20	[38]	16
	Salmonella enterica, *Escherichia coli*, *Staphylococcus xylosus*	10^3 CFU·mL^{-1} (*E.c.*), 10^2 CFU·mL^{-1} (*S.x.*)	2	~ 2 ½ h	22	[39]	6
	Escherichia coli, *Salmonella typhimurium*, *Salmonella enteritidis*, *Pseudomonas aeruginosa*, *Listeria monocytogenes*, *Listeria innocua*, *MRSA* 35, *MRSA* 86	distinguish	4	n.a.	15	[40]	20
mycotoxins	ochratoxin A	0.08 pM = 0.032 pg·mL^{-1}	3	~ 1 h	4	[41]	16
	ochratoxin A	0.39 ng·mL^{-1}	4	< 10 min	6	[42]	31
	ochratoxin A	0.5 ng·mL^{-1}	4	~ 25 min	7	[43]	18
	ochratoxin A	5.4 pg·mL^{-1}	3	~ 1 ¼ h	7	[44]	42

	ochratoxin A	30 $pg \cdot mL^{-1}$	3	~ 1 ½ h	9	[45]	38
	ochratoxin A	0.02 $pg \cdot mL^{-1}$	2	~ 10 h	9	[46]	47
	ochratoxin A	20 nM = 8000 $pg \cdot mL^{-1}$	3	~ 2 h	15	[47]	47
	ochratoxin A	9.8 nM = 4000 $pg \cdot mL^{-1}$	3	~ 2 ½ h	15	[48]	6
	ochratoxin A	0.32 $g \cdot L^{-1}$	1	> 3 h	17	[49]	19
	aflatoxin B_1	0.32 $pg \cdot mL^{-1}$	4	~ 1 ½ h	1	[50]	22
	aflatoxin B_1	1.77 nM = 553 $pg \cdot mL^{-1}$	4	~ 3 h	12	[51]	20
	aflatoxin B_1	2.1 $pg \cdot mL^{-1}$	2	~ 2 h	14	[52]	35
	zearalenones	62.5 $pg \cdot mL^{-1}$ (standard), 3.6 $mg \cdot kg^{-1}$ (corn)	5	10 min	3	[53]	30
	zearalenones	1.5 $pg \cdot mL^{-1}$	3	~ 30 min	4	[54]	17
	vomitoxin	0.70 $pg \cdot mL^{-1}$	3	n.a.	2	[55]	8
	deoxynivalenol (DON), T-2 toxin, fumonisin B_1 (FB_1)	242.0 (DON), 17.8 (T-2), 331.5 (FB_1) $\mu g \cdot kg^{-1}$	2	< 30 min	9	[56]	21
	aflatoxin B1, B2, G1, G2, ochratoxin A, zearalanone, T-2 toxin	0.1 (AFB1), 0.04 (AFB2), 0.1 (AFG1), 0.04 (AFG2), 0.2 (OTA), 0.1 (ZEN), 0.4 (T-2) $\mu g \cdot kg^{-1}$	1	~ 30 min	12	[57]	16
veterinary drugs	chloramphenicol	0.3 $pg \cdot mL^{-1}$	3	~ 1 h	2	[58]	25
	chloramphenicol	1 pM = 0.3 $pg \cdot mL^{-1}$	2	~ 1 h	4	[59]	17
	chloramphenicol	15 $pg \cdot mL^{-1}$	2	~ 2 h	12	[60]	22
	chloramphenicol	0.03 nM = 9 $pg \cdot mL^{-1}$	1	~ 3 h	13	[61]	15
	ampicillin	3 pM = 1 $pg \cdot mL^{-1}$	4	~ 45 min	1	[62]	8
	ampicillin	4.0 pM = 1.4 $pg \cdot mL^{-1}$	2	~ 2 h	5	[63]	23
	streptomycin	94 nM = 55 $ng \cdot mL^{-1}$	3	~ 45 min	8	[64]	3
	streptomycin	0.028 $ng \cdot mL^{-1}$	3	~ 2 h	9	[65]	13

	sulfadimethoxine	10 ng·mL^{-1}	3	< 15 min	9	[66]	7
	kanamycin	321 pM = 155 pg·mL^{-1}	3	~ 4 ¼ h	11	[67]	42
	ciprofloxacin	0.1 µg·mL^{-1}	2	1 h	15	[68]	2
	tetracycline	0.0978 ng·mL^{-1}	1	~ 2 ½ h	16	[69]	26
	chloramphenicol (CAP), kanamycin (KANA)	0.19 pM (CAP), 0.16 pM (KANA) = 0.06 - 0.08 pg·mL^{-1}	2	~ 1 h	5	[70]	10
	14 sulfonamides (SA), 13 quinolones (QN)	0.13 ng·mL^{-1} (SA), 62 pg·mL^{-1} (QN)	3	~ 10 min	7	[71]	23
	chloramphenicol, oxytetracycline (OTC)	0.15 ng·mL^{-1} (CAP), 0.10 ng·mL^{-1} (OTC)	3	~ 3 h	13	[72]	27
	phenylethanolamine (PHL), clenbuterol (CLB), ractopamine (RAC), salbutamol (SAL), procaterol (PRO)	0.04 ng·mL^{-1} (RAC), 0.35 pg·mL^{-1} (CLB), 1.0 pg·mL^{-1} (PHL), 0.53 pg·mL^{-1} (SAL), 1.73 pg·mL^{-1} (PRO)	3	~ 50 min	2	[73]	22
pesticides	parathion	52 pg·L^{-1} = 0.00018 nM	4	~ 10 min	1	[74]	23
	paraquat	3.4 nM	4	~ 10 min	2	[75]	24
	glyphosate	0.1 ppb (standard), 0.01 ppm (beer) = 0.29 nM	3	~ 30 min	3	[76]	14
	triazophos	0.93 nM (UV/vis), 0.32 nM (GC)	2	~ 1 h	5	[77]	6
	paraoxon-ethyl	0.22 ± 0.02 µM	4	~ 15 min	6	[78]	8
	chlorpyrifos	5 mg·L^{-1} (color), 0.01 mg·L^{-1} (SERS) =19 nM	3	< 25 min	7	[79]	7
	malathion, cadusafos	0.1 nM	3	~ 30 min	4	[80]	12
preservatives	nitrite	20 nM	3	~ 15 min	1	[81]	6
	propyl gallate	25.1 nM	3	~ 12 ¼ h	2	[82]	28
	formaldehyde	0.2 ppm = 7 µM	4	~ 15 min	3	[83]	4
	sulfur dioxide / bisulfite	0.44 µM	2	realtime	4	[84]	6
packaging components	bisphenol A	0.19 pM	2	~ 3 ½ h	1	[85]	21
	bisphenol A	2 nM	3	~ 1 h	3	[86]	6

	13 phthalate esters	0.01 - 1.2 $\mu g \cdot L^{-1}$ = ~36 pM	1	~ 1 h	2	[87]	14
seafood toxins	azaspiracids	63 $\mu g \cdot kg^{-1}$ or 1 $\mu g \cdot L^{-1}$	2	~ 1 h	1	[88]	8
	paralytic shellfish toxins	n.a.	1	~ 1 ¼ h	2	[89]	42
	saxitoxin	3.8 nM = 1.1 $\mu g \cdot L^{-1}$	1	> 4 h	3	[90]	6
Other	alkaline phosphatase	0.1 $U \cdot L^{-1}$	5	10 min		[91]	33
	polychlorinated biphenyl-72	0.3 $pg \cdot mL^{-1}$	3	~ 1 h		[58]	25
	16 polycyclic aromatic hydrocarbons	0.05 - 0.30 $\mu g \cdot kg^{-1}$	1	~ 1 h		[92]	7
	Sudan I in spices	1 ppm	2	~ 30 min		[93]	31
	sunset yellow	4.2 nM	4	~ 5 min		[94]	23
	melamine	200 ppm	3	~ 5min		[95]	25
	melamine	1.4 ppb	4	~ 5 min		[96]	16
	genetically modified food (cauliflower mosaic virus promoter)	12 pM	2	~ 3 ½ h		[97]	2

Field-portability classification according to Table 1; assay times as given in publications or estimated according to experimental procedure where possible, including real sample preparation where given; ranks were given within analyte classes, the ranking process is described above; citation number as of July 2018; CFU: colony-forming unit; color: colorimetric readout; DLS: dynamic light scattering; GC: gas chromatography; Lab: analysis in laboratory; LOD: limit of detection; n.a.: not available; SERS: surface enhanced Raman spectroscopy; UV/vis: UV/VIS-spectroscopy.

1.4 Methods applied in Food Safety Analysis

Similar to the target analytes represented by the here reviewed publications, also sensing strategies reflect the dominant technologies under development and investigation within the sensor/bioassay community (Table 4).

The three predominantly applied detection principles are *electrochemical detection*, *fluorescence measurements* and *colorimetric readout*. *Raman* and *mass spectrometry* and a few *others* (surface plasmon resonance spectroscopy, flame photometric detection or near-infrared hyperspectral imaging) are less often reported techniques for food safety analysis. This reflects the robustness of the former methods to deal with the complexity of food matrices and the necessity of ultra-low limits of detection. Interestingly, when to identify possible correlations between detection method (Table 4) and analytes (Table 3), no significant relationship could be discovered. In contrast, it was found instead that, in general, each method is applied to almost every analyte class and seems to be equally successful according to the distribution of ranks within the groups.

The most frequently used detection principle is electrochemistry. Variations within this method include the use of different electrodes and their modification with synthetic materials to increase the surface area and electron transport efficiency. Also, various different electrochemical modes are proposed, e.g., differential pulse voltammetry, electrochemical impedance spectroscopy or cyclic voltammetry. The maturity of electrochemical strategies for food safety analysis is verified by their frequent integration with sample preparation methods to address challenges of real-world scenarios.

In the case of photometric detection such as fluorescence and colorimetric readout, the impact of similar strategies used in medical diagnostics has led to the fact that three out of four reviewed publications that describe nearly or complete field-portable systems use photometric methods for analyzing food contaminants. Raman spectroscopy has been adapted at a slower pace for food safety analysis but is catching up especially through the help of nanomaterials and nanostructures. Finally, in the case of mass spectrometry, it remains to be a purely lab-based approach, but is a very powerful detection tool after solid phase extraction and gas or liquid chromatography, or after capillary electrophoresis.

Table 4. Reviewed publications sorted by detection principle with analysis principle, detection method and ranks

detection principle	analysis principles	detection method	rank	lit
electrochemical	immunoassay on graphene	EIS of $Fe[(CN)_6]^{3-/4-}$ on SPCE	Pes 1/7	[74]
	immunoassay on MOF	EIS of $Fe[(CN)_6]^{3-/4-}$ on gold electrode	Myc 2/17	[55]
	immunoassay on MWCNT with AuPtNPs	DPV of $Fe[(CN)_6]^{3-/4-}$ on GCE	Myc 4/17	[54]
	immunoassay on self-assembled monolayer of bifunctional 3-dithiobis-(sulfosuccinimidyl-propionate), signal amplification with wheat germ agglutinin	EIS of $Fe[(CN)_6]^{3-/4-}$ on screen-printed interdigitated microelectrodes	Mic 6/22	[22]
	competitive ELISA on magnetic beads	amperometry of TMB on carbon electrode array	Sea 1/3	[88]
	competitive immunoassay, enzyme label, photodiode converting chemiluminescence to voltage	voltage readout generated by photodiode	Myc 7/17	[43]
	immunoassay, aptamer primer probe, rolling circle amplification, HRP-mimicking DNAzyme structure, electro-reduction of H_2O_2	DPV of reduction of H_2O_2 on Au electrode	Mic 14/22	[25]
	competitive immunoassay on magnetic beads, H_2O_2-responsive decomposition of carbon QDs functionalized MnO_2 nanosheets	photoelectrochemical measurement (photo irradiation with electrochemical detection) of MnO_2 decomposition on fluorine-doped tin oxide electrode	Myc 14/17	[52]
	ELISA, enzyme reaction lowers impedance	impedance measurement of gluconic acid on screen-printed interdigitated microelectrode	Mic 20/22	[37]
	competitive immunoassay on magnetic beads, enzyme tracer	amperometric measurement of hydroquinone on SPCE	Myc 17/17	[49]
	competitive aptamer assay, complementary strand with SiO_2@AuNPs blocks electrode surface, self-powered enzyme biofuel cell	electron flow between two AuNPs-modified carbon paper electrodes, one modified with glucose oxidase, one with laccase	Vet 1/16	[62]
	aptamer assay on electrode	DPV of $Fe[(CN)_6]^{3-/4-}$ on Au electrode	Vet 2/16	[73]

	competitive aptamer assay, release of metal ion tracers by analyte binding	SWV of Pb^{2+} and Cd^{2+} on GCE	Vet 2/16	[58]
	competitive aptamer assay with complementary strand and intercalating methylene blue	DPV of methylene blue on $MoSe_2$ nanoflowers and AuNPs modified GCE	Myc 4/17	[41]
	aptamer assay, labeled aptamer electrostatic repelled by ITO, analyte opens hairpin, methylene blue label is split of by enzyme, free methylene blue not repelled by ITO, signal amplification by exonuclease	DPV of methylene blue on ITO	Vet 5/16	[63]
	competitive aptamer assay on magnetic beads, MOF(M^{n+})-labeled complementary probe	SWV of Pb and Cd ions in MOF on GCE	Vet 5/16	[70]
	competitive aptamer assay, ferrocene-labeled aptamer, methylene blue-labeled complementary probe	SWV of BPA, ferrocene and methylene blue on planar gold electrode	Pac 1/3	[85]
	aptamer assay, electrochemically grafted sensor	EIS of $Fe[(CN)_6]^{3-/4-}$ on SPCE	Mic 8/22	[27]
	aptamer assay, porous carbon nanorods and graphene-Fe_3O_4-AuNPs-composite on electrode	DPV of $Fe[(CN)_6]^{3-/4-}$ on CGE	Vet 9/16	[65]
	competitive aptamer assay, magnetic hollow particle tracers bind to immobilized complementary strand if analyte releases aptamer, signal amplification by exonuclease	SWV of Pb^{2+} and Cd^{2+} on GCE	Vet 13/16	[72]
	GO-Mn_3O_4 microcubes composite interacting with analyte	CV of nitrite on modified SPCE	Pre 1/4	[81]
	PtAu bimetallic nanoparticles-capped graphene–carbon nanotube with MIP electrode surface blocking by target molecule	chronoamperometric measurement of $Fe[(CN)_6]^{3-/4-}$ on CGE	Pre 2/4	[82]
	various graphene hybrid nanocomposites, principle component analysis, impedimetric electronic tongue	impedance spectroscopy of analytes with gold interdigitated electrodes	Pes 4/7	[80]
	direct label-free measurement of analyte	CV of sunset yellow on GO-PtNPs modified GCE	other	[94]
fluorescence	immunoassay, LFA with QD submicrobeads label	fluorescence spectroscopy of QDs	Myc 3/17	[53]
	sandwich immunoassay on magnetic beads	fluorescence measurement of fluorescein isothiocyanate by smartphone	Mic 8/22	[23]

flow-through immunoaffinity chromatography	optical density of liposome encapsulated QDs	Vet 7/16	[71]
sandwich immunoassay on magnetic beads in microfluidics	fluorescence spectroscopy of QDs	Mic 10/22	[28]
competitive immunoassay, fluorescence polarization	fluorescence spectroscopy of alexa, fluorescein and rhodamine derivatives	Myc 9/17	[56]
immunoassay, fluorescence quenching by analyte binding	fluorescence spectroscopy of TiO_2 NPs	Mic 12/22	[29]
competitive aptamer assay via FRET	fluorescence spectroscopy of upconversion nanoparticles	Mic 4/22	[20]
competitive aptamer assay with ssDNA binding protein labeled fluorescent liposomes	fluorescence spectroscopy of DIL	Vet 4/16	[59]
competitive aptamer assay in microfluidics, analyte immobilized on fiber, labeled aptamer	evanescent wave all-fiber biosensing platform	Myc 6/17	[42]
competitive aptamer assay on magnetic beads with QD loaded silica nanocarriers	fluorescence spectroscopy of QDs	Myc 7/17	[44]
competitive aptamer assay with complementary strand and intercalating SYBR Green 1	fluorescence spectroscopy of SYBR Green 1 (Smartphone)	Vet 8/16	[64]
competitive aptamer assay, hyperbranched rolling circle amplification induced when analyte releases aptamer, ECL tracer intercalates	ECL measurement of $Ru(phen)_3^{2+}$	Myc 9/17	[46]
competitive aptamer assay, labeled complementary strand quenched by AuNPs, signal amplification by enzyme	fluorescence spectroscopy of 6-carboxy fluorescein	Vet 11/16	[67]
competitive aptamer assay, aptamer label quenched by nano graphite without analyte, signal amplification by enzyme recycling	fluorescence spectroscopy of carboxy fluorescein	Myc 15/17	[47]
competitive aptamer assay, luminol-gold nanoparticles, aptamer with quencher, internal reference (QDs)	ECL measurement of luminol, one-cycle voltammetry on SPCE	Vet 13/16	[61]
competitive aptamer assay, single-walled carbon nanohorn quenching of fluorescein label, signal amplification by DNase I	fluorescence spectroscopy of carboxy fluorescein	Myc 15/17	[48]
competitive aptamer assay, quenching of NMM, background reduction by Mo_2C nanotubes	fluorescence spectroscopy of NMM	Pac 3/3	[86]

	bead-beating lysis, PCR, DNA microarray, full lab on chip	fluorescence microscopy of Cy3 and Cy5	Mic 2/22	[32]
	Hantzsch reaction of analyte with dye forming fluorescent complex	fluorescence spectroscopy of formaldehyde-acetoacetanilide complex	Pre 3/4	[83]
	magnetic bead DNA separation and loop-mediated isothermal amplification in microfluidics, gel electrophoresis	fluorescence spectroscopy of SYTO-62 in microchamber and gel	Mic 18/22	[31]
	quenching of CD fluorescence by analyte	fluorescence spectroscopy of CDs	Pes 6/7	[78]
	analyte captured by cyanine-derivative, FRET inactivation	fluorescence spectroscopy of cyanine-GO-composite	Pre 4/4	[84]
colorimetric	immunoassay, LFA, enzyme cleaves off antigen	optical density of AuNPs (Smartphone)	other	[91]
	immunoassay, LFA, second labeled AB binds to AuNPs	optical density of AuNPs	other	[96]
	immunoassay, LFA	optical density of Au nanoflowers (optical strip reader)	Myc 1/17	[50]
	ELISA on magnetic beads	UV-vis spectroscopy of TMB	Mic 16/22	[33]
	flow-through immunoaffinity chromatography, enzyme activation	optical density of TMB	Vet 7/16	[71]
	aptamer assay, isothermal strand displacement amplification, LFA	optical density of AuNPs (optical strip reader)	Mic 4/22	[21]
	competitive aptamer assay, peroxidase like activity of AuNPs on complementary probe	UV-vis spectroscopy of TMB	Myc 9/17	[45]
	competitive aptamer assay, analyte binding destroys hydrogel, release of NPs	UV-vis spectroscopy of AuNPs or movement of color indicator by gas production	Myc 12/17	[51]
	competitive aptamer assay, complementary DNA and HRP labeled dsDNA-AB release	UV-vis spectroscopy of TMB	Vet 12/16	[60]
	competitive enzyme-linked aptamer assay, microtiter plate assay	UV-vis spectroscopy of TMB	Vet 16/16	[69]
	nucleic acid extraction, helicase-dependent isothermal amplification, LFA, full lab on chip	optical density of AuNPs (Smartphone)	Mic 1/22	[26]
	nucleic acid extraction, loop-mediated isothermal amplification, fully integrated paper based LFA	optical density of AuNPs (Smartphone)	Mic 2/22	[19]

	loop-mediated isothermal amplification, intercalation of SYBR Green I in dsDNA	bare eye detection of color change of SYBR Green I	Mic 11/22	[30]
	DNA-RNA heteroduplex structures, RNAse H cleavage, AuNP aggregation	UV-vis spectroscopy of AuNP aggregation	Mic 18/22	[35]
	nucleic acid extraction and loop-mediated isothermal amplification in microfluidics, LFA	optical density of digoxigenin and Texas-Red	Mic 20/22	[38]
	peroxidase-like activity of AuNPs, inhibition by aptamers	UV-vis spectroscopy of TMB	Vet 9/16	[66]
	endogenous β-galactosidase activity as indirect measure of cell proliferation of *E.coli*	UV-vis spectroscopy of 5-bromo-4-chloro-3-indolyl-β-D-galactopyranoside and o-Nitrophenyl-β-D-galactopyranosid	Vet 15/16	[68]
	molecularly imprinted SPE, magnetic separation	UV-vis spectroscopy of triazophos	Pes 5/7	[77]
	molecularly imprinted SPE	UV-vis spectroscopy of AgNPs aggregation	Pes 7/7	[79]
RS	immunoassay on magnetic and AuNPs, silver intensification process	SERS on silver-coated AuNPs	Mic 13/22	[24]
	aptamer assay on Fe_3O_4@AuNPs-GO	SERS of Fe_3O_4@Au/GO-apt 1-target-apt 2-TAMRA complex	Mic 17/22	[34]
	interaction between analyte and AgNPs	SERS on AgNPs	Pes 2/7	[75]
	AgNPs attachment to bacteria, microfluidics	SERS on AgNPs	Mic 15/22	[40]
	immobilization of bacteria on nanorod supercrystals, coating with nanoplates	SERS of nanoplate aggregate-bacteria-nanorod supercrystal	Mic 22/22	[39]
	acetylcholine-esterase mediated hydrolysis of acetylthiocholine to thiocholine, inhibition by analyte	SERS of thiocholine-induced aggregation of organometallic osmium carbonyl clusters@AuNPs	Pes 3/7	[76]
	molecularly imprinted SPE	SERS on AgNPs	Pes 7/7	[79]
	MIP-thin layer chromatography on gold colloidal SERS substrate	SERS on gold colloid	other	[93]
MS	multiple immunoaffinity column, HPLC	ESI quadrupole MS/MS	Myc 12/17	[57]
	micro SPE with natural sorbent, GC	quadrupole MS	Pac 2/3	[87]

	graphitized carbon SPE, hydrophilic interaction LC	ESI quadrupole MS/MS	Sea 2/3	[89]
	magnetic dispersive SPE with 3D ionic liquid functionalized magnetic GO, GC	quadrupole MS	other	[92]
	capillary electrophoresis, metal chelate labeling with diethylenetriamine-N,N,N′,N″,N″-pentaacetic acid and Eu^{3+}	inductively coupled plasma MS	Sea 3/3	[90]
other	immunoassay, second AB with AuNP label	surface plasmon resonance spectroscopy	Mic 6/22	[36]
	molecularly imprinted SPE, magnetic separation, GC	flame photometric detector	Pes 5/7	[77]
	two partially complementary hairpins on AuNPs-rGO composite and gold film coated optical fiber probe, target mediated hybridization, label-free	surface plasmon resonance spectroscopy	other	[97]
	extensive data analysis	near-infrared hyperspectral imaging	other	[95]

AB: antibody; CD: carbon dot; DAPI: 4′,6-diamidino-2-phenylindole; DIL: 1,1′-dioctadecyl-3,3,3′,3′-tetramethyl-indocarbocyanineper-chlorate); CV: cyclic voltammetry; DPV: Differential pulse voltammetry; EIS: electrochemical impedance spectroscopy; ELISA: enzyme-linked immunosorbent assay; ESI: electrospray ionization; GC: gas chromatography; GCE: glassy carbon electrode; (r)GO: (reduced) graphene oxide; HRP: Horse Reddish Peroxidase; LC: liquid chromatograph; LFA: lateral flow assay; MIP: molecularly imprinted polymer; MOF: metal organic framework; MS: mass spectrometry; MWCNT: multi-walled carbon nanotube; NMM: N-methylmesoporphyrin IX; NP: nanoparticle; PCR: polymerase chain reaction; QD: quantum dot; RS: Raman spectroscopy; SERS: surface enhanced RS; SPCE: screen-printed carbon electrode; SPE: solid phase extraction; SWV: Square wave voltammetry; TMB: tetramethylbenzidine

1.5 Biomaterials in Food Safety Analysis

Three quarters of the publications reflected in this review use biomaterials for their detection strategy. These are mainly used for two purposes, i.e., for specific binding to the analyte (nucleic acids, aptamers or antibodies) or for signal transduction and amplification (enzymes), as well as for unique strategies (seed powder for solid phase extraction).

1.5.1 Antibodies

Immunoassays are a common method for separating an analyte from its sample matrix. The antibody binds its antigen, in this case the desired food contaminant, very specifically and with high binding constants. Antibodies are the workhorse of most medical diagnostic assays and to-date cannot be replaced by other affinity recognition elements including aptamers and molecularly imprinted polymers. Figure 1 depicts the most common immunoassay strategies that can be adapted to any other affinity recognition molecule as well.

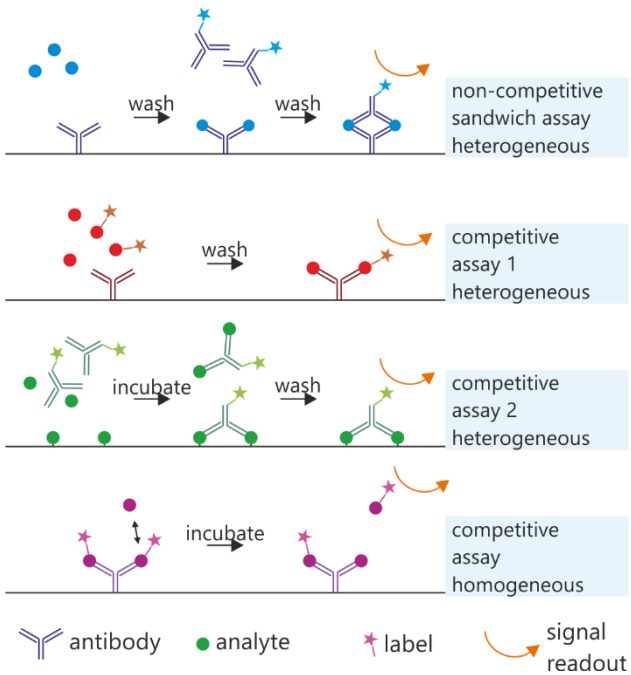

Figure 1: Examples for different immunoassay formats

In the reviewed literature, antibodies are used for the detection of almost every analyte class, namely microbes [23, 25], mycotoxins [56, 57], pesticides [74], seafood toxins [88], veterinary drugs [71] and others [91, 96].

In 2016, a method for the detection of ochratoxin A (OTA) was developed, involving a competitive immunoassay with an enzyme label [43]. A horseradish peroxidase modified antibody is added to the sample solution and injected in an OTA coated microchannel. A free antibody is binding to

the OTA at the channel surface and retained, while an already saturated antibody – in case of the presence of OTA in the sample solution – is washed out. The principle of this heterogeneous competitive assay is depicted in Figure 2. After addition of a dye solution containing luminol, chemiluminescence is observable and converted to an electrical signal by photodiodes. This promising method is simple, needs little effort and time, and is close to a completely field-portable device, but unfortunately the LOD is quite high in comparison to other mycotoxin detection methods.

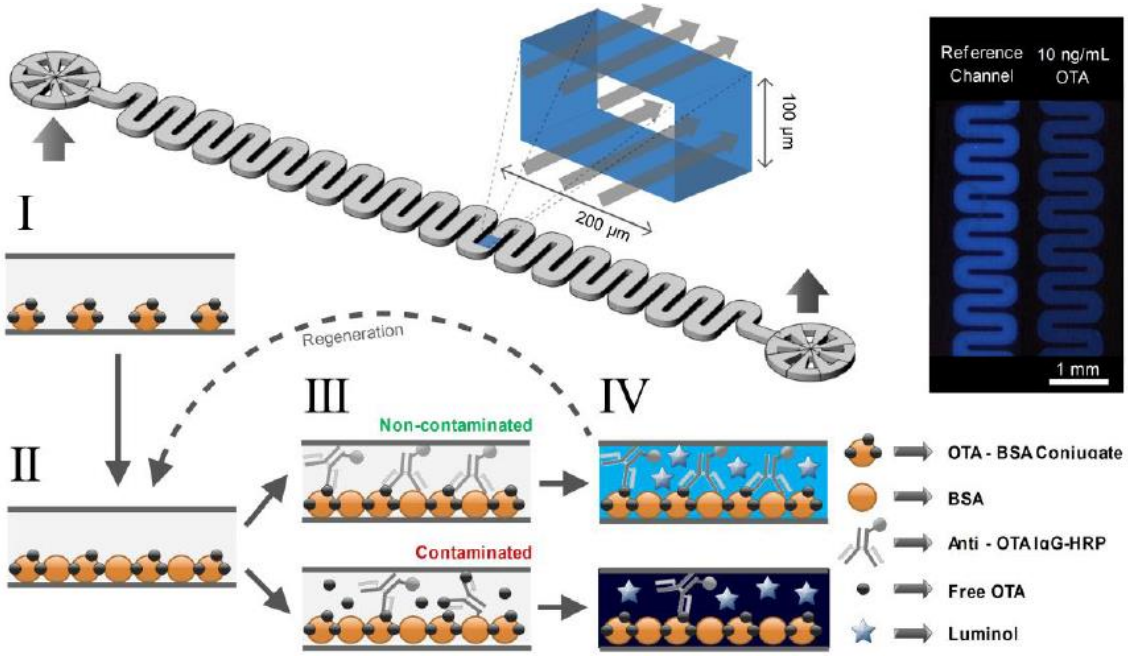

Figure 2: Schematic showing a system for ochratoxin A detection by a heterogeneous competitive immunoassay conducted in a microchannel with chemiluminescence readout (OTA: ochratoxin A; BSA: bovine serum albumin; HRP: horse reddish peroxidase). Reprinted from Sensors and Actuators B: Chemical, 235, Soares, R.R.G.; Ramadas, D.; Chu, V.; Aires-Barros, M. R.; Conde, J. P.; Viana, A. S.; Cascalheira, A. C., An ultrarapid and regenerable microfluidic immunoassay coupled with integrated photosensors for point-of-use detection of ochratoxin A, 554–562, Copyright (2016) [43], with permission from Elsevier.

Another interesting, yet improvable example is a fluorescence polarization immunoassay, a simple homogeneous competitive assay with fluorescent dye labeled artificial analytes (deoxynivalenol, T-2 toxin and fumonisin B1) [56]. Free dye-analyte-conjugates can be distinguished from antibody-bound ones in solution due to the change in fluorescence polarization. This approach holds great portability potential, as it is fast, requires no washing steps and allows multi-analyte detection by the use of different fluorophores. However, the current described method still requires lab facilities such as centrifuges and takes place in pipetting-intensive format of microtiter plates, which is why further research is necessary here.

1.5.2 Aptamers

As an alternative to antibodies, aptamers have been described for over 20 years now, as their production does not rely on cells or animals. They have a high batch-to-batch reproducibility and can easily be adapted to alterations in structure or demands on assay conditions, such as stability regarding a change of assay pH or temperature. Also, they are smaller than antibodies, allowing easier two-site-binding in sandwich assays even for small analytes [98]. Hope thus remains to be high that aptamers can reach binding efficiencies of antibodies in the future and much research is on-going improving the selection and prediction methods [99–101].

Aptamers are applied in the reviewed literature for the detection of microbes [27], veterinary drugs [63, 64, 69], mycotoxins [42, 46] and packaging components [85] and are typically used similar to antibodies in affinity assay strategies.

Chen et al. immobilized aptamers on the surface of an electrode in 2016 and measured the change of current resulting from the reaction of a redox mediator [73]. This peak current is reduced due to blocking of the electrode by bound analyte. The simplicity of this method combined with minor effort, relatively fast assay time, low LODs and the potential to be refined as portable device, results in a high rank of this publication within the detection of veterinary drugs.

In contrast, Yan et al. described a smart strategy that takes advantage of an aptamer's inherent capability to hybridize to a complementary nucleic acid strand in addition to binding to a specific analyte [72]. In this setup, the analyte displaces the complementary strand, which in turn can then be detected and quantified or serves as anchor for a labeled third strand. Using the latter strategy, chloramphenicol and oxytetracycline were detected electrochemically in milk. Even though exonuclease-assisted analyte recycling was used for signal amplification, the LODs were high compared to other veterinary drug sensors, and an increased assay time of about three hours due to the large number of steps hardly qualifies this method for a portable system at the moment.

1.5.3 Nucleic Acids

The third category of biorecognition elements are DNA and RNA molecules used for traditional hybridization reactions. Nucleic acids are only applied for microbe detection [25, 30–32, 35] in the reviewed literature and are used less often in food safety analysis, probably due to the additional processing steps needed. Instead, most microbes are detected without lysis by antigen recognition on their surface.

In analytical sensing, nucleic acids are often used in hybridization assays with detection of the binding event itself [32], e.g., in a sandwich format or by intercalating dyes, but the specific

recognition is also used for nucleic acid extraction from cellular matrix after lysis, e.g., by immobilizing the complementary strand on magnetic beads [31]. The extracted DNA is then in many cases multiplied by polymerase chain reaction or similar amplification strategies, such as loop mediated isothermal amplification with real time detection by intercalation of dyes in the grooves of dsDNA [30]. In addition, there are also completely different applications for nucleic acids, such as DNA molecules that are capable of catalyzing reactions similar to enzymes, called DNAzymes [25].

1.5.4 Enzymes

In contrast to biorecognition elements, enzymes are not used to separate or immobilize the analyte of interest, but in most cases to catalyze reactions that allow the detection itself. They act as labels and tracers to produce colored or fluorescent dyes or electrochemical marker molecules, or cleave off specific features to allow further reaction.

In the reviewed literature, enzymes are used in the detection of microbes [26, 33, 35, 37], mycotoxins [43, 47–49], veterinary drugs [60, 62, 63, 67, 69, 71, 72], pesticides [76] and others [91].

One smart strategy employs two enzymes for signal generation and amplification in one approach.[63] An aptamer, consisting of two regions, one for primer attachment and one for binding the analyte, the antibiotic residue ampicillin, is applied. These two regions are combined to form a hairpin structure that is opened by the analyte binding. The primer binds to its specific complementary region and Klenow Fragment polymerase is added with nucleotides to induce aptamer replication by polymerase chain reaction. When the analyte binding region is replicated, the analyte is recovered and can bind another aptamer. For signal generation, the other enzyme, T7-exonuclease, is digesting the double stranded aptamer-replicate and sets free a methylene blue label that, while bound to the aptamer, it is repelled from the electrode. In contrast, the free label can diffuse to the electrode and is detected electrochemically. This strategy achieves a high rank compared to other veterinary drug detection methods due to the signal amplification that yields quite low LODs, although the high user effort and relatively long assay times will require substantial engineering to serve a portable system.

Similarly, a detection strategy for *Campylobacter jejuni* was presented [35], which relies on the aggregation of gold nanoparticles and resulting color change, after RNAse H has cleaved off the stabilizing RNA after hybridization with the analyte DNA. RNAse H only cleaves double stranded nucleic acids, which is the principle of this method. Although this strategy is simple and does not

afford high effort, the LODs are moderate and the protocol is time consuming and needs a lot improvement to become portable.

Great potential can be found in enzyme biofuel cell based self-powered sensors, such as proposed by Gai et al. in 2017 for the detection of ampicillin in milk samples [62]. They use a glucose oxidase modified bioanode and a laccase modified biocathode. Electrons are generated by the oxidation of glucose to gluconolactone and consumed by the reduction of oxygen to water, respectively. An aptamer is immobilized on the bioanode and hybridized to complimentary DNA linked to gold modified silicabeads. The beads block the glucose transport to the electrode and thus prevent electron flow. When ampicillin binds to the aptamer the blocking beads are released and current is measureable. The extremely low LODs, fast assay times, high portability potential and great performance in real samples without sample pretreatment yield this technology the top position for the detection of veterinary drugs in food samples.

1.5.5 Others

The single stranded DNA binding protein uses a unique folding pattern to specifically bind to single stranded DNA. This concept was employed by Miao et al. in 2016, when they labeled fluorescent liposomes with this protein [59]. An aptamer for chloramphenicol is immobilized on the surface of magnetic beads and caught by the single stranded DNA binding protein on the liposomes surface. By binding of the analyte, the aptamer releases the liposomes and after magnetic separation, a fluorescent signal can be detected in the supernatant, depending on the amount of chloramphenicol present in the sample solution (Figure 3). Due to the very low LODs achieved with this strategy, combined with low user and time effort, a high rank in the field of veterinary drug detection was yielded.

Another unique biomaterial was applied for micro solid phase extraction: The seed powder of *Moringa oleifera*, also called horseradish tree, has a highly fibrous structure with a heterogeneous and naturally functionalized surface, and therefore was utilized for the extraction and preconcentration of phthalate esters from milk samples by Sajid et al. in 2016 [87]. Although the strategy only achieved moderate success within the group of packaging materials, it is interesting because it is a green and readily available sorbent material.

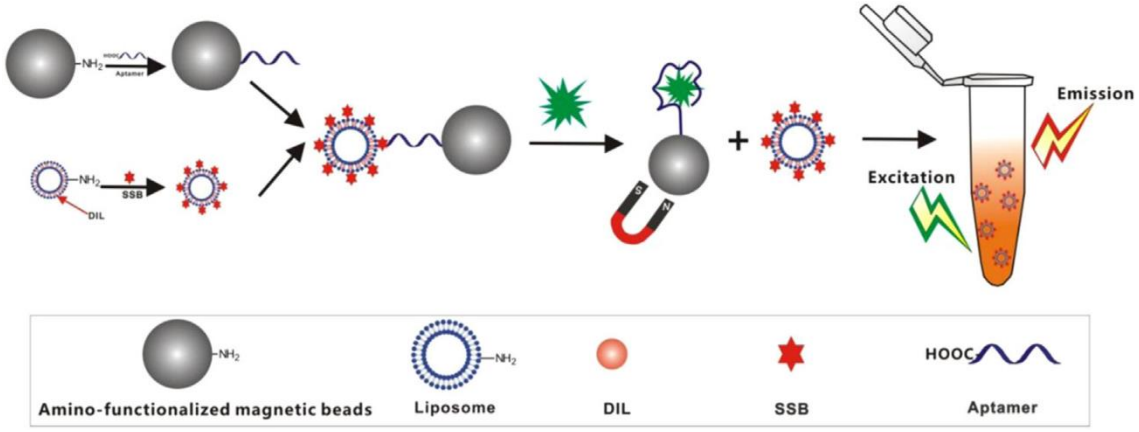

Figure 3: Schematic of a chloramphenicol detection principle based on the coupling of magnetic beads with fluorescent liposomes via an aptamer-single stranded DNA-interaction (DIL: 1,1′-dioctadecyl-3,3,3′,3′-tetramethyl-indocarbocyanineperchlorate; SSB: single stranded DNA binding protein). Reprinted from Biosensors & bioelectronics, 81, Miao, Y.-B.; Ren, H.-X.; Gan, N.; Cao, Y.; Li, T.; Chen, Y., Fluorescent aptasensor for chloramphenicol detection using DIL encapsulated liposome as nanotracer, 454–459, Copyright (2016) [59] with permission from Elsevier.

1.6 Synthetic Materials in Food Safety Analysis

Despite their countless benefits and ubiquitous use in analytical sensing, biological materials also have some drawbacks, such as high cost, laborious production and restrictions regarding temperatures, pH values, ionic strength and similar assay parameters. Therefore, synthetic materials can provide a promising alternative, mimicking the above-mentioned properties of biomaterials. An overview of synthetic materials, their role in the analytical process and their use for different analytes is given in Table 5.

Table 5. Reviewed publications sorted by application of (in)organic materials with material role, application principle, analyte and ranks

material class	material	material role	application principle	analyte	rank	lit
MIPs	o-phenylenediamine	recognition site	analyte receptor	propyl gallate	Pre 2/4	[82]
	3-methacryloxypropyl trimethoxysilane, EGDMA	solid phase extraction	separation of analyte	triazophos	Pes 5/7	[77]
	MAA, EGDMA	solid phase extraction	separation of analyte	chlorpyrifos	Pes 7/7	[79]
		stationary phase of thin layer chro-matography	analyte receptor	Sudan I	other	[93]
micro-beads	magnetic	magnetic separation	support for aptamer	chloramphenicol, polychlorinated biphenyl-72	Vet 2/16	[58]
		magnetic separation	support for aptamer	*E. coli* O157:H7	Mic 4/22	[21]
		magnetic separation	support for aptamer	chloramphenicol	Vet 4/16	[59]
		magnetic separation	support for aptamer	kanamycin, chloramphenicol	Vet 5/16	[70]
		magnetic separation	support for antibody	azaspiracids	Sea 1/3	[88]
		magnetic separation	support for antibody	*E. coli* O157:H7	Mic 8/22	[23]
		magnetic separation	support for aptamer	ochratoxin A	Myc 7/17	[44]

		magnetic separation	support for antibody	*S. typhimurium*	Mic 10/22	[28]
		magnetic separation	support for aptamer	ochratoxin A	Myc 9/17	[45]
		magnetic separation	support for antibody	*E. coli* O157:H7	Mic 13/22	[24]
		magnetic separation	support for MIP	triazophos	Pes 5/7	[77]
		magnetic separation	support for antibody	*S. aureus*	Mic 16/22	[33]
		magnetic separation	support for aptamer	chloramphenicol	Vet 12/16	[60]
		magnetic separation	support for DNA	*S. spp.*	Mic 18/22	[31]
		magnetic separation	support for antibody	aflatoxin B_1	Myc 14/17	[52]
		magnetic separation	support for antibody	*E. coli* O157:H7, *S. typhimurium*	Mic 20/22	[37]
		magnetic separation	support for antibody	ochratoxin A	Myc 17/17	[49]
	silica	electrode blocking	competition with analyte	ampicillin	Vet 1/16	[62]
		nanocarrier	signal amplification	chloramphenicol, polychlorinated biphenyl-72	Vet 2/16	[58]
		nanocarrier	signal amplification	ochratoxin A	Myc 7/17	[44]
		DNA extraction	mechanical lysis	*S. typhimurium*, *V. parahaemolyticus*	Mic 20/22	[38]
	zirconium/silica	DNA extraction	mechanical lysis	*B. atrophaeus*	Mic 2/22	[32]
nano-particles	gold	color label	signal reporter	*S. typhimurium*	Mic 1/22	[26]
		color label	signal reporter	*E. coli*	Mic 2/22	[19]
		color label	signal reporter	*E. coli* O157:H7	Mic 4/22	[21]
		color label	analyte induced release	aflatoxin B_1	Myc 12/17	[51]

color label	signal reporter	alkaline phosphatase	other	[91]
color label	signal reporter	melamine	other	[96]
color indicator	analyte induced aggregation	*C. jejuni*	Mic 18/22	[35]
color/SERS indicator	analyte inhibited aggregation	glyphosate	Pes 3/7	[76]
SERS label	signal reporter	*E. coli* O157:H7	Mic 13/22	[24]
SPR label	signal reporter	*E. coli* O157:H7, *S. sp.*	Mic 6/22	[36]
SPR label	signal reporter	cauliflower mosaic virus promoter	other	[97]
ECL label	quencher release by analyte	chloramphenicol	Vet 13/16	[61]
FRET acceptor	FRET inactivation by analyte	*E. coli* ATCC 8739	Mic 4/22	[20]
fluorescence quencher	interaction with ssDNA	kanamycin	Vet 11/16	[67]
peroxidase-like activity	color generation	ochratoxin A	Myc 9/17	[45]
peroxidase-like activity	inhibition by aptamer	sulfadimethoxine	Vet 9/16	[66]
electrode blocking	competition with analyte	ampicillin	Vet 1/16	[62]
electrode material	surface enhancement	ampicillin	Vet 1/16	[62]
electrode material	signal amplification	ochratoxin A	Myc 4/17	[41]
electrode material	signal amplification	streptomycin	Vet 9/16	[65]
electrode material	interaction with analyte	organophosphates	Pes 4/7	[80]
electrode material	signal amplification	chloramphenicol, oxytetracycline	Vet 13/16	[72]
SERS substrate	signal enhancement	*V. parahaemolyticus*	Mic 17/22	[34]

	SERS substrate	signal enhancement	Sudan I	other	[93]
	solid support	support for aptamer assay	chloramphenicol, polychlorinated biphenyl-72	Vet 2/16	[58]
	solid support	support for aptamer assay	ochratoxin A	Myc 7/17	[44]
	solid support	signal amplification	chloramphenicol	Vet 12/16	[60]
silver	SERS label	interaction with analyte	paraquat	Pes 2/7	[75]
	SERS enhancer	signal reporter	*E. coli* O157:H7	Mic 13/22	[24]
	SERS label	interaction with analyte	*E. coli*, *S. typhimurium*, *S. enteritis*, *P. aeruginosa*, *L. monocytogenes*, *L. innocua*, *MRSA* 35, *MRSA* 86	Mic 15/22	[40]
	color/SERS indicator	interaction with analyte	chlorpyrifos	Pes 7/7	[79]
iron oxide	electrode material	signal amplification	streptomycin	Vet 9/16	[65]
	SERS substrate	signal enhancement	*V. parahaemolyticus*	Mic 17/22	[34]
	magnetic separation	support for analyte receptor	16 PAHs	other	[92]
PtAu	electrode material	surface enhancement, support for antibody	zearalenones	Myc 4/17	[54]
	electrode material	surface enhancement	propyl gallate	Pre 2/4	[82]
Pt	catalyst	analyte induced activation	aflatoxin B_1	Myc 12/17	[51]
	electrode material	signal amplification	sunset yellow	others	[94]
upconversion	FRET donor	FRET inactivation by analyte	*E. coli* ATCC 8739	Mic 4/22	[20]

	TiO_2		fluorescent indicator	quenching by analyte	*S. typhimurium*	Mic 12/22	[29]
	quantum dots	CdSe/ZnS	fluorescent label	signal reporter	zearalenones	Myc 3/17	[53]
			fluorescent label	signal reporter	*S. typhimurium*	Mic 10/22	[28]
		CdTe	fluorescent label	competition with analyte	ochratoxin A	Myc 7/17	[44]
		CdS	internal reference	monitor environmental effects	chloramphenicol	Vet 13/16	[61]
		carbon	fluorescent indicator	quenching by analyte	paraoxon-ethyl	Pes 6/7	[78]
			electrode material	decomposition in absence of analyte	aflatoxin B_1	Myc 14/17	[52]
		other	fluorescent label	competition with analyte	14 sulfonamides, 13 quinolones	Vet 7/16	[71]
2D materials	graphene oxide		electrode material	surface enhancement	parathion	Pes 1/7	[74]
			electrode material	surface enhancement, interaction with analyte	nitrite	Pre 1/4	[81]
			electrode material	surface enhancement	propyl gallate	Pre 2/4	[82]
			electrode material	signal amplification	streptomycin	Vet 9/16	[65]
			electrode material	interaction with analyte	organophosphates	Pes 4/7	[80]
			electrode material	signal amplification	sunset yellow	other	[94]
			SERS substrate	signal amplification	*V. parahaemolyticus*	Mic 17/22	[34]
			FRET donor	FRET inactivation by analyte	sulfur dioxide / bisulfite	Pre 4/4	[84]
			SPR label	signal reporter	cauliflower mosaic virus promoter	other	[97]

		solid phase extraction	separation of analyte	16 PAHs	other	[92]
	multi walled carbon nanotubes	electrode material	surface enhancement, support for antibody	zearalenones	Myc 4/17	[54]
		electrode material	surface enhancement	propyl gallate	Pre 2/4	[82]
	Mo_2C nanotubes	background reduction	adsorption of free help-DNA	bisphenol A	Pac 3/3	[86]
	MnO_2 nanosheets	electrode material	decomposition in absence of analyte	aflatoxin B_1	Myc 14/17	[52]
	Ag nanoplates	SERS label	signal amplification	*S. enterica*, *E. coli*, *S. xylosus*	Mic 22/22	[39]
metal organic frame-work	aluminum based MOFs	support for antibody	inhibition of electrochemical activity by analyte	vomitoxin	Myc 2/17	[55]
	UiO-66	electro-chemical label	competition with analyte	kanamycin, chloramphenicol	Vet 5/16	[70]
nano-containers	liposomes	dye carrier	signal amplification	chloramphenicol	Vet 4/16	[59]
		dye carrier	signal amplification	14 sulfonamides, 13 quinolones	Vet 7/16	[71]
	magnetic hollow porous nanoparticles	nanocarrier, magnetic separation	signal amplification	chloramphenicol, oxytetracycline	Vet 13/16	[72]
other	Au nanoflowers	color label	signal reporter	aflatoxin B_1	Myc 1/17	[50]
	Mn_3O_4 microcubes	electrode material	electrocatalytic support	nitrite	Pre 1/4	[81]
	$MoSe_2$ nanoflowers	electrode material	signal amplification	ochratoxin A	Myc 4/17	[41]
	porous carbon nanorods	electrode material	signal amplification	streptomycin	Vet 9/16	[65]
	Au@Ag nanorods	SERS substrate	surface enhancement	*S. enterica*, *E. coli*, *S. xylosus*	Mic 22/22	[39]

organometallic osmium carbonyl clusters	SERS indicator	analyte inhibited aggregation	glyphosate	Pes 3/7	[76]
nano-graphite	fluorescence quencher	competition with analyte	ochratoxin A	Myc 15/17	[47]
single walled carbon nanohorns	fluorescence quencher	competition with analyte	ochratoxin A	Myc 15/17	[48]
graphitized non-porous carbon	solid phase extraction	separation of analyte	paralytic shellfish toxins	Sea 2/3	[89]

ECL: electrochemiluminescence; EGDMA: ethylene glycol dimethacrylate; FRET: Förster resonance energy transfer; MAA: methacrylic acid; MIPs: molecularly imprinted polymers; MOF: metal organic framework; PAH: polycyclic aromatic hydrocarbons; QD: quantum dot; SERS: surface enhanced Raman spectroscopy; SPR: surface plasmon resonance

1.6.1 Molecularly Imprinted Polymers

Specific recognition, as described for antibodies, aptamers or nucleic acids, can also be achieved by the use of molecularly imprinted polymers (MIPs), which can be applied for the separation of analytes from complex matrices as well as for binding the analyte at the detection zone. Although already introduced in 1931, MIPs gained attention first in the 1980s, after the technique was applied to organic polymers. By addition of the desired analyte during the curing process of these polymers and removal of the template afterwards, a cavity with specific binding properties for the analyte molecule is created and can be used as analyte receptor and for extraction purposes [102].

Despite their benefits such as a high mechanical and chemical robustness or the possible use in organic solvents, but maybe due to occasionally occurring imprint leakage, which lowers the sensitivity in comparison to antibodies [102], MIPs are still poorly represented in the reviewed literature and are only applied in the detection of preservatives [82], pesticides [77, 79] and food colorants [93].

For separation purposes, one strategy combined MIPs for solid phase extraction with magnetic separation for the detection of triazophos in vegetable samples, by imprinting a polymer shell on magnetic nanoparticles to utilize the large surface of nanomaterials [77].

In contrast, an electropolymerized MIP electrode was applied as analyte receptor in the quantification of the food preservative propyl gallate [82]. By inclusion of the analyte into the polymer, the electrode surface becomes blocked and a current decrease can be recorded for chronoamperometric measurement of $Fe[(CN)_6]^{3-/4-}$. Although low LODs were achieved, an extremely long preparation time for real samples disqualifies this strategy at this point for any field-portable purpose.

The dye Sudan I was likewise detected in spices by the use of MIPs as stationary phase for thin layer chromatography to specifically capture the analyte [93]. After development, a gold colloid was added and served as surface enhanced Raman spectroscopy substrate.

1.6.2 Microbeads

Nevertheless, in the majority of cases, synthetic materials serve other functions than biorecognition, and in the case of food safety analysis, particles are the predominant 3D structure of the materials developed. These can be divided further into microbeads and nanoparticles. While for nanoparticles a huge variety of materials is used, the reviewed literature only showed three different classes for microbeads: magnetic, silica and zirconium/silica beads.

The main application of magnetic beads is separation and extraction of the analyte from the sample matrix and they are applied to almost every analyte class, such as microbes [21, 23], mycotoxins [44, 45], veterinary drugs [58, 70], pesticides [77] and seafood toxins [88]. As they are not capable of analyte recognition themselves, they are combined with all of the different recognition elements and either the analyte is desorbed after separation, or detection is performed directly on the bead surface.

In contrast, silica and zirconium/silica beads are only used for the three main analyte groups, veterinary drugs [58, 62], mycotoxins [46] and microbes [32, 38] and for different purposes than magnetic beads, e.g., for DNA extraction from microbes by mechanical beat beating lysis, or for electrode blocking in competition with the analyte, as already described in the enzymes section [62].

Others use them as nanocarriers for signal amplification, such as Yan et al. in 2015, who used cadmium and lead loaded silica beads and magnetic nanoparticles, linked by an aptamer-complementary DNA couple [58]. Due to analyte binding and magnetic separation, the silica beads are released and detected in the supernatant, which leads to very low LODs. Combined with low user and time effort and the potential for field-portable application, this strategy gains a top position among veterinary drug detection methods.

1.6.3 Nanoparticles

Nanoparticles (NPs) in contrast are used for a large variety of applications. Most of the NPs are metallic, like gold, silver, iron oxide or platinum NPs, and exhibit useful effects like plasmon generation, magnetism or color change upon aggregation. They are applied as labels in colorimetric assays or Raman spectroscopy, or as electrode material in electrochemical analysis.

There are also a range of fluorescent particles, like upconversion NPs or quantum dots that are frequently used for FRET applications or as fluorescent labels.

The predominant material for NPs in the reviewed literature is gold, which is used for microbes [19, 26], mycotoxins [41, 45], veterinary drugs [58, 62], pesticides [76, 80] and others [96, 97]. These particles exhibit plasmonic effects depending on their size and aggregation state, and therefore are applied as labels in colorimetric assays [21, 51], Raman spectroscopy [24] and surface plasmon resonance spectroscopy [36]. Because of their high electron conductivity, they are also often used as electrode material [65, 72].

An interesting application for gold NPs results from their ability to mimic the catalytic activity of the enzyme peroxidase. Yan et al. utilizes the inhibition of this effect by adsorption of an aptamer on the surface of gold NPs [66]. By binding the antibiotic sulfadimethoxine the aptamer is desorbed and the pure gold NPs can convert a substrate under color generation. Unfortunately, though this method is fast and needs little user effort, the LOD is very high, which is also the case for the sensor described by Wang et al. using a similar strategy [45].

Other metallic NPs, that are employed in a similar manner, are silver NPs, that also exhibit plasmonic effects and therefore are applied for surface enhanced Raman spectroscopy of microbes [24, 40] and pesticides [75, 79]. Also, platinum and mixed platinum-gold-NPs are used as electrode material for mycotoxin [54], preservative [82] and food colorant detection [94] due to their high capacity. Platinum NPs can also serve as catalyst, as proposed by Ma et al. [51]. An aptamer based hydrogel encapsulating Pt NPs is decomposed by addition of the analyte and the free particles catalyze the conversion of hydrogen peroxide to oxygen, as depicted in Figure 4. The obtained gas is mechanically moving a color bar and thus indicating the content of aflatoxin B_1 in the sample. Although this is a great field-portable concept with simple and user-friendly readout, the high LODs and assay times still need significant improvement. Finally, also iron oxide NPs have been employed in a similar manner to gold NPs. These NPs are used as electrode material for veterinary drug detection [65], as Raman substrate for microbes [34] and, similar to the application of this material in microbeads, for magnetic separation of polycyclic hydrocarbons [92].

Another group of NPs utilizes luminescent properties for signal generation. In the reviewed literature, mainly quantum dots are used for this purpose, composed of either cadmium chalcogenides or carbon materials. Their main application area is as fluorescent label for the detection of microbes [28], mycotoxins [44, 53], veterinary drugs [71] and pesticides [78], but due to their good conductivity they are also used as electrode material [52]. Furthermore, Feng et al.

detects chloramphenicol in an electrochemiluminescence aptamer assay with luminol-gold nanoparticles and uses quantum dots on a second working electrode as internal reference to monitor environmental effects and inhibit cross talk and in this manner achieves quite low LODs [61]. Besides quantum dots, also titanium dioxide and upconversion NPs are applied in microbe detection. While Viter et al. [29] only has medium success with the application of titanium dioxide NPs as fluorescent indicator responding to *Salmonella*, Jin et al. [20] achieves a high rank within microbe detection by employing upconversion NPs composed of $NaYF_4$ doped with ytterbium and erbium ions. They are applied as donor in a FRET couple with gold NPs bridged by an aptamer link, taking advantage of the near infrared activation of upconversion NPs and subsequent background signal reduction, as most biomolecules do not absorb in the near infrared region.

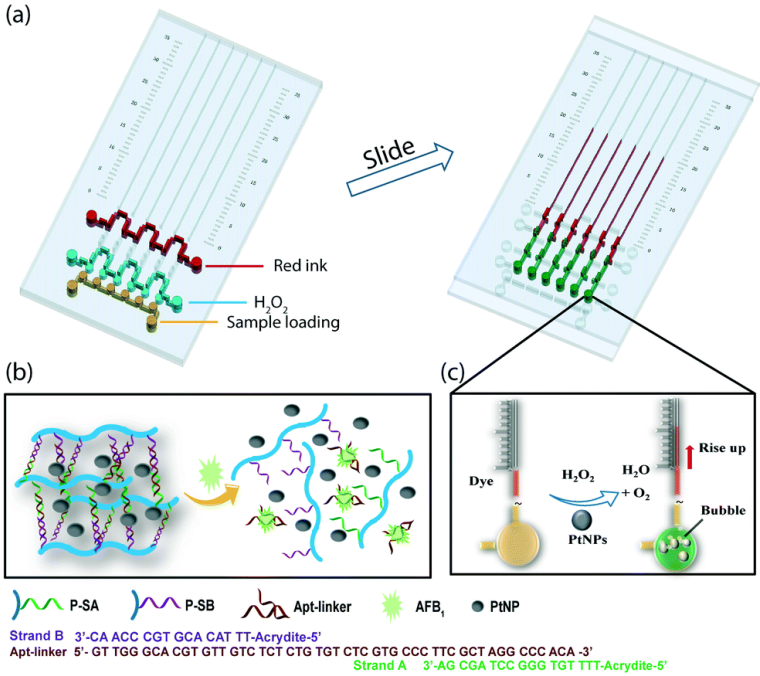

Figure 4: Bare eye detection system for aflatoxin B_1. (a) Schematic of the chip for user application. (b) A hydrogel based on polymer strands bridged with an aptamer encapsulates Pt nanoparticles, which are released upon analyte binding. (c) Pt nanoparticles catalyze the decomposition of H_2O_2 to release oxygen bubbles, which move a color bar for bare eye detection (P-SA, P-SB: polymer strand A and B; AFB_1: aflatoxin B_1; PtNP: platinum nanoparticle). Republished with permission of Lab on a chip by Royal Society of Chemistry (Great Britain), from Portable visual quantitative detection of aflatoxin B1 using a target-responsive hydrogel and a distance-readout microfluidic chip, Ma, Y.; Mao, Y.; Di Huang; He, Z.; Yan, J.; Tian, T.; Shi, Y.; Song, Y.; Li, X.; Zhu, Z.; Zhou, L.; Yang, C. J., 16, 16, 2016 [51]; permission conveyed through Copyright Clearance Center, Inc.

1.6.4 2D materials

Compared to three dimensional particles and polymers, 2D materials represent an entirely different class of synthetic materials. Due to the sp^2 character of the carbon atoms in carbon 2D materials, they have a very high conductivity and superior electron transport. Thus, graphene

oxide and carbon nanotubes are mainly used as electrode material for the detection of mycotoxins [54], pesticides [74, 80], veterinary drugs [65], preservatives [81, 82] and food colorants [94] to enhance the electrode surface, act as signal amplifier or to provide specific interaction with the analyte. Zhang et al. applies graphene oxide for solid phase extraction of polycyclic aromatic hydrocarbons from vegetable oils, due to their electrostatic interaction with the sp^2 hybridized carbon atoms [92]. Alternatively, Yu et al. modified graphene oxide with hexamethylendiamine to render it fluorescent, and used the adsorption of cyanine dyes for fluorescence resonance energy transfer [84]. When the analyte, the food preservative bisulfide, is binding to cyanine, the electrostatic interaction is fading and the energy transfer cannot take place anymore. In addition, graphene oxide was also used as Raman substrate for microbe detection [34] and surface plasmon resonance label for tracing of genetic modifications in food [97].

Other 2D nanomaterials include for example MnO_2 nanosheets, which were used by Lin et al. as electrode material for the detection of mycotoxins in similar manner than graphene oxide [52]. In absence of the analyte aflatoxin B_1, hydrogen peroxide, which is produced by an enzyme, decomposes the MnO_2 sheets and lowers the current flow. Although LODs are quite low, high production and time effort, as well as low field-portability potential, indicate a high need for improvements. Also Ag nanoplates were applied similar to graphene oxide as Raman label for the detection of microbes [39]. In contrast, He et al. uses Mo_2C nanotubes to reduce the inherent background signal [86]. Incorporation of the fluorescent dye N-methylmesoporphyrin IX in the G-quadruplex structure formed by an aptamer-complementary help-DNA-complex, increases its fluorescence. Upon binding of bisphenol A to the aptamer, dye and help-DNA are released and the fluorescence of the dye is lowered significantly. To reduce interfering background fluorescence of free help-DNA, it is adsorbed at Mo_2C nanotubes.

1.6.5 Metal Organic Frameworks

Metal organic frameworks are porous materials constructed by metallic nodes bridged with organic linker molecules. These materials provide high surface areas and exhibit electron conducting features making them applicable for electrochemical food safety analysis.

Chen et al. uses UiO-66 that is composed of $Zr_6O_4(OH)_4$ clusters with 1,4-benzodicarboxylic acid struts as host for Cd^{2+} or Pb^{2+} ions, which can be detected electrochemically [70]. This electrochemical label, attached to either kanamycin or chloramphenicol aptamers via a complementary strand, and released after analyte binding, generates very low LODs, thus,

combined with low user and time effort, this strategy gains a high rank within veterinary drug detection.

While UiO-66 is a common metal organic framework, Liu et al. used two self-synthesized aluminum based ones, $\{[Al_3(\mu_3\text{-}O)(NTB)_2(H_2O)_3](NO_3)(NMF)_{10}(H_2O)_{7.5}\}_n$ and $\{[Al_4(OH)_4(H_2O)(NTB)_2(HCOO)_3]\ (HCOO)(NMF)_{14.5}(H_2O)_4\}_n$. The high surface area of these frameworks provide the ideal support for electrochemical immunoassays, where the binding of vomitoxin hinders mass transport to the electrode [55]. This application of metal organic frameworks also yields one of the top ranks within its analyte group, mycotoxins.

1.6.6 Nanocontainers

Similar to metal organic frameworks acting as hosts for the encapsulation of signal molecules, liposomes and magnetic hollow porous nanoparticles are used for signal amplification in fluorescence, colorimetric and electrochemical assays. These nanocarriers can either encapsulate molecules in their inner cavity or bind them on their outside, but also the membranes or scaffolds can be associated with signal molecules. Interestingly, in the reviewed literature, nanocontainers are only employed for the detection of veterinary drugs.

While Jiang et al. applies liposomes encapsulating quantum dots in their aqueous inner volume as label in competitive flow-through immunoaffinity chromatography for the quantification of sulfonamides and quinolones in milk [71], Miao et al. detects chloramphenicol in fish with a competitive aptamer assay with liposomes decorated with fluorescent dyes on their outside (Figure 3) [59]. Both of them achieve quite good results with low LODs and fast assay times.

Magnetic hollow particles instead are built up by mesoporous silica spheres as scaffold, in which Yan et al. incorporates cadmium and lead ions. These act as electrochemical tracers for the detection of chloramphenicol and oxytetracyclin in milk, as already described in the aptamer section [72].

1.6.7 Others

Of course, numerous other synthetic materials that cannot be assigned to one of the above-mentioned categories are applied in the analysis of food, too, often as composites with other synthetic materials.

For example, in combination with graphene oxide and gold NPs, porous carbon nanorods and $MoSe_2$ nanoflowers are utilized as electrode material for signal amplification in veterinary

drug [65] and myxotoxin [41] detection (Figure 5). In the same way, Mn_3O_4 microcubes are applied due to their electrocatalytic activity, with great success within the group of preservatives [81].

For the detection of paralytic shellfish toxin Boundy et al. employed graphitized non-porous carbon in a solid phase extraction to reduce salt interferences from the matrix, followed by liquid chromatography and mass spectrometry [89].

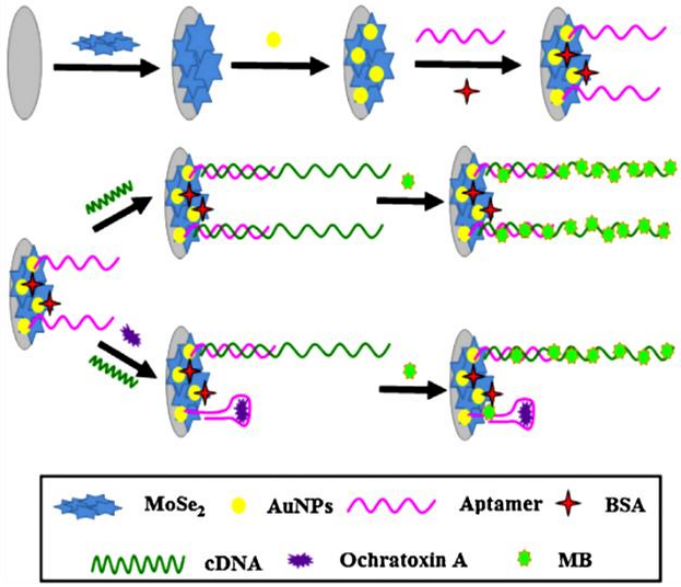

Figure 5: Scheme of an electrochemical aptasensor for the detection of ochratoxin A. Molybdenum selenide nanoflowers were used as electrode material and a competitive aptamer assay with electrochemical labeling of the remaining complementary DNA strands was conducted (AuNPs: gold nanoparticles; BSA: bovine serum albumin; MB: methylene blue). Reprinted from Sensors and Actuators B: Chemical, 225, Huang, K.-J.; Shuai, H.-L.; Chen, Y.-X., Layered molybdenum selenide stacking flower-like nanostructure coupled with guanine-rich DNA sequence for ultrasensitive ochratoxin A aptasensor application, 391–397, Copyright (2016) [41] with permission from Elsevier.

Organometallic osmium carbonyl clusters and Au@Ag nanorods in turn are used as indicators and substrates for surface enhanced Raman spectroscopy with different success. While Tan et al. achieve good results with their fast and easy-to-use glyphosate detection method [76], the strategy of Wang et al. for quantifying food borne bacteria could benefit of some improvements regarding user friendliness [39].

Analogous to gold nanoparticles, gold nanoflowers are also applied as color label by Ji et al. with great success [50]. The superior LODs, ease-of-use and high field-portability potential yield this immunochromatographic test strip for the detection of aflatoxin B_1 in rice the top rank among mycotoxin detection.

In 2015, Wei et al. published a strategy employing nano-graphite as fluorescence quencher for the detection of ochratoxin A in red wine [47]. An aptamer labeled with the fluorescent tag carboxyfluorescein is adsorbed to the surface of nano-graphite, which quenches its fluorescence.

By binding of the analyte, fluorescence is recovered, and with digestion of the aptamer by DNAse I, ochratoxin A is recovered and can bind another aptamer, which amplifies the signal. In 2017, Lv et al. uses the same strategy with single walled carbon nanohorns instead of nano-graphite [48], unfortunately with the same drawbacks such as high LODs, high assay times and a far way to go for field-portable applications.

1.7 Conclusion and Future Perspective

To observe changes in food safety analysis research over time, the reviewed literature was compared to older literature in the field. Therefore, the same search criteria as described above were employed, while the time span was expanded to the years 2000 to 2014. For this small survey, the 24 top cited publications with over 70 citations were picked and ranked in the same way as the reviewed literature.

The first observation is that the analyte classes did not change noteworthy: Microbes [103–111], mycotoxins [112, 113] and veterinary drugs [114–118] are still the analytes of highest interest, while there are also older publications dealing with preservatives [119], packaging components [120], pesticides [121, 122] and others, such as melamine [123, 124] or polycyclic aromatic hydrocarbons [125].

When, on the other hand, considering the detection methods, a clear change can be observed. While electrochemical [103–106, 112] and fluorescence [107, 108, 113, 119, 121, 125] readouts were used in the early 2000s as frequently as in the literature reviewed here, there was less colorimetric [120, 123] readout. Also, Raman spectroscopy had its breakthrough as common analytical technique in food safety analysis only in the last years, according to the sample of literature taken for this comparison. On the other hand, mass spectrometry [109, 114–117, 122, 126] is researched significantly less nowadays, which is also the case for surface plasmon resonance [110, 111, 118]. Another interesting fact is that in this small survey electrochemical readout was almost solely applied for microbes, while mass spectrometry was the method of choice for veterinary drug detection. As stated above, this is in stark contrast to today, as nowadays no correlation could be observed and all methods are applied for all analyte classes.

A significant change can also be observed in the use of synthetic materials. Research into these materials has clearly grown in importance, as the percentage of papers using synthetic materials grew from 33% in the early 2000s to 75% in the last four years.

Furthermore, in order to identify significant progress in the field of food safety analysis, the same ranking strategy as done for publications from 2015 to 2018 was then also applied to the older

literature (2000 to 2014). It was interesting to observe that there was no distinct difference in ranks between the older and newer groups of publications. This is true for all analyte classes and detection methods with many examples, such as microbes, veterinary drugs, electrochemical or fluorescent readout, and indicates that no significant breakthrough in food safety analysis research has occurred in the last four years compared to the beginning of the 2000s. In part, this is due to the degree of complexity and difficulty of the challenges that must be solved today, i.e., more straightforward food safety analysis problems have already been solved, yet the difficult tasks remain. At closer look however, it can be observed that field-portability is now increasing, indicated by fewer studies with mass spectrometry analysis and better portability classifications (according to Table 1). On the other hand, the production of biological and synthetic materials becomes more and more extensive due to increasing complexity. In the end, both factors compensate each other, equalizing ranks for old and new literature.

Thus, food safety analysis remains a highly relevant topic and solutions to gain higher certainty regarding the harmlessness of our daily diet are of great interest. Considering the global food chain and increase in our ability to share and store large sets of data, a food blockchain can be one of the solutions to prevent food fraud and food contamination. Tracing back every step a product went through from farm to fork, as it is already performed by first pioneers [127], critical contamination points can already today be identified, such as an interruption of the cold chain and thus higher risk of microbe proliferation. In the future, sensors integrated at the right point in the food production chain will be the key to detect unsafe food early. However, data exchange between the various companies involved throughout the blockchain must be enabled. The progressing Internet of Things [128] will likely play a major role in this process where a network of devices gathering and sharing all the information about a product hopefully will provide regulatory agencies with neutral oversight regarding the necessity of product annihilation without any personal or monetary engagement. Finally, the combination of the food blockchain concept with the Internet of Things might even help to overcome drawbacks of globalization, such as the difficulty to comply with standards with contributing food product components produced in different countries all over the world. Here, assays and sensors as reviewed in this article will be key to the future improvements in food safety analysis.

1.8 References

[1] Grossarth J (2017) Wie ein Insektizid in die Hühnereier kam: Lebensmittelskandal. http://www.faz.net/aktuell/gesellschaft/huehnereier-mit-insektiziden-verseucht-15133949.html. Accessed 3 August 2018.

[2] Bundesinstitut für Risikobewertung Home Page (2017) Gesundheitliche Bewertung der in Belgien nachgewiesenen Einzeldaten von Fipronilgehalten in Lebensmitteln tierischen Ursprungs: BfR-Stellungnahmen. http://www.bfr.bund.de/cm/343/gesundheitliche-bewertung-der-in-belgien-nachgewiesenen-einzeldaten-von-fipronilgehalten-in-lebensmitteln-tierischen-ursprungs.pdf. Accessed 3 August 2018.

[3] Hao N, Wang K (2016) Recent development of electrochemiluminescence sensors for food analysis. Anal. Bioanal. Chem. 408:7035–7048. doi: 10.1007/s00216-016-9548-2.

[4] Weng X, Neethirajan S (2017) Ensuring food safety: Quality monitoring using microfluidics. Trends Food. Sci. Technol. 65:10–22. doi: 10.1016/j.tifs.2017.04.015.

[5] Vasilescu A, Marty J-L (2016) Electrochemical aptasensors for the assessment of food quality and safety. Trends Anal. Chem. 79:60–70. doi: 10.1016/j.trac.2015.11.024.

[6] Llorente-Mirandes T, Rubio R, López-Sánchez JF (2017) Inorganic Arsenic Determination in Food: A Review of Analytical Proposals and Quality Assessment Over the Last Six Years. Appl. Spectrosc. 71:25–69. doi: 10.1177/0003702816652374.

[7] Mangal M, Bansal S, Sharma SK, Gupta RK (2016) Molecular Detection of Foodborne Pathogens: A Rapid and Accurate Answer to Food Safety. Crit. Rev. Food Sci. Nutr. 56:1568–1584. doi: 10.1080/10408398.2013.782483.

[8] Sundramoorthy AK, Gunasekaran S (2014) Applications of graphene in quality assurance and safety of food. Trends Anal. Chem. 60:36–53. doi: 10.1016/j.trac.2014.04.015.

[9] Warriner K, Reddy SM, Namvar A, Neethirajan S (2014) Developments in nanoparticles for use in biosensors to assess food safety and quality. Trends Food. Sci. Technol. 40:183–199. doi: 10.1016/j.tifs.2014.07.008.

[10] Malhotra BD, Srivastava S, Ali MA, Singh C (2014) Nanomaterial-based biosensors for food toxin detection. Appl. Biochem. Biotechnol. 174:880–896. doi: 10.1007/s12010-014-0993-0.

[11] Arduini F, Cinti S, Scognamiglio V, Moscone D (2016) Nanomaterials in electrochemical biosensors for pesticide detection: Advances and challenges in food analysis. Microchim. Acta 183:2063–2083. doi: 10.1007/s00604-016-1858-8.

[12] Sharma R, Ragavan KV, Thakur MS, Raghavarao KSMS (2015) Recent advances in nanoparticle based aptasensors for food contaminants. Biosens. Bioelectron. 74:612–627. doi: 10.1016/j.bios.2015.07.017.

[13] Yang T, Huang H, Zhu F, Lin Q, Zhang L, Liu J (2016) Recent Progresses in Nanobiosensing for Food Safety Analysis. Sensors 16:1118. doi: 10.3390/s16071118.

[14] Lim M-C, Kim Y-R (2016) Analytical Applications of Nanomaterials in Monitoring Biological and Chemical Contaminants in Food. J. Microbiol. Biotechnol. 26:1505–1516. doi: 10.4014/jmb.1605.05071.

[15] Liu J-M, Hu Y, Yang Y-K, Liu H, Fang G-Z, Lu X, Wang S (2018) Emerging functional nanomaterials for the detection of food contaminants. Trends Food. Sci. Technol. 71:94–106. doi: 10.1016/j.tifs.2017.11.005.

[16] Dzantiev BB, Byzova NA, Urusov AE, Zherdev AV (2014) Immunochromatographic methods in food analysis. Trends Anal. Chem. 55:81–93. doi: 10.1016/j.trac.2013.11.007.

[17] U.S. Food and Drug Administration Home Page (2018) Foodborne Illness & Contaminants. https://www.fda.gov/food/foodborneillnesscontaminants/default.htm. Accessed 7 August 2018.

[18] Joint FAO/WHO Codex Alimentarius Commission (1995 (last amended 2017)) General Standard for Contaminants and Toxins in Food and Feed. Codex Alimentarius CXS 193-1995. World Health Organization; Food and Agriculture Organization of the United Nations.

[19] Choi JR, Hu J, Tang R, Gong Y, Feng S, Ren H, Wen T, Li X, Wan Abas WAB, Pingguan-Murphy B, Xu F (2016) An integrated paper-based sample-to-answer biosensor for nucleic acid testing at the point of care. Lab Chip 16:611–621. doi: 10.1039/c5lc01388g.

[20] Jin B, Wang S, Lin M, Jin Y, Zhang S, Cui X, Gong Y, Li A, Xu F, Lu TJ (2017) Upconversion nanoparticles based FRET aptasensor for rapid and ultrasenstive bacteria detection. Biosens. Bioelectron. 90:525–533. doi: 10.1016/j.bios.2016.10.029.

[21] Wu W, Zhao S, Mao Y, Fang Z, Lu X, Zeng L (2015) A sensitive lateral flow biosensor for *Escherichia coli* O157:H7 detection based on aptamer mediated strand displacement amplification. Anal. Chim. Acta 861:62–68. doi: 10.1016/j.aca.2014.12.041.

[22] Li Z, Fu Y, Fang W, Li Y (2015) Electrochemical Impedance Immunosensor Based on Self-Assembled Monolayers for Rapid Detection of *Escherichia coli* O157:H7 with Signal Amplification Using Lectin. Sensors 15:19212–19224. doi: 10.3390/s150819212.

[23] Zeinhom MMA, Wang Y, Song Y, Zhu M-J, Lin Y, Du D (2018) A portable smart-phone device for rapid and sensitive detection of *E. coli* O157:H7 in Yoghurt and Egg. Biosens. Bioelectron. 99:479–485. doi: 10.1016/j.bios.2017.08.002.

[24] Cho I-H, Bhandari P, Patel P, Irudayaraj J (2015) Membrane filter-assisted surface enhanced Raman spectroscopy for the rapid detection of *E. coli* O157:H7 in ground beef. Biosens. Bioelectron. 64:171–176. doi: 10.1016/j.bios.2014.08.063.

[25] Guo Y, Wang Y, Liu S, Yu J, Wang H, Wang Y, Huang J (2016) Label-free and highly sensitive electrochemical detection of *E. coli* based on rolling circle amplifications coupled peroxidase-mimicking DNAzyme amplification. Biosens. Bioelectron. 75:315–319. doi: 10.1016/j.bios.2015.08.031.

[26] Tang R, Yang H, Gong Y, You M, Liu Z, Choi JR, Wen T, Qu Z, Mei Q, Xu F (2017) A fully disposable and integrated paper-based device for nucleic acid extraction, amplification and detection. Lab Chip 17:1270–1279. doi: 10.1039/c6lc01586g.

[27] Bagheryan Z, Raoof J-B, Golabi M, Turner APF, Beni V (2016) Diazonium-based impedimetric aptasensor for the rapid label-free detection of *Salmonella typhimurium* in food sample. Biosens. Bioelectron. 80:566–573. doi: 10.1016/j.bios.2016.02.024.

[28] Kim G, Moon J-H, Moh C-Y, Lim J-g (2015) A microfluidic nano-biosensor for the detection of pathogenic *Salmonella*. Biosens. Bioelectron. 67:243–247. doi: 10.1016/j.bios.2014.08.023.

[29] Viter R, Tereshchenko A, Smyntyna V, Ogorodniichuk J, Starodub N, Yakimova R, Khranovskyy V, Ramanavicius A (2017) Toward development of optical biosensors based on photoluminescence of TiO_2 nanoparticles for the detection of *Salmonella*. Sens. Actuators B Chem. 252:95–102. doi: 10.1016/j.snb.2017.05.139.

[30] Sayad AA, Ibrahim F, Uddin SM, Pei KX, Mohktar MS, Madou M, Thong KL (2016) A microfluidic lab-on-a-disc integrated loop mediated isothermal amplification for foodborne pathogen detection. Sens. Actuators B Chem. 227:600–609. doi: 10.1016/j.snb.2015.10.116.

[31] Sun Y, Quyen TL, Hung TQ, Chin WH, Wolff A, Bang DD (2015) A lab-on-a-chip system with integrated sample preparation and loop-mediated isothermal amplification for rapid and quantitative detection of *Salmonella spp.* in food samples. Lab Chip 15:1898–1904. doi: 10.1039/c4lc01459f.

[32] Roy E, Stewart G, Mounier M, Malic L, Peytavi R, Clime L, Madou M, Bossinot M, Bergeron MG, Veres T (2015) From cellular lysis to microarray detection, an integrated thermoplastic elastomer (TPE) point of care Lab on a Disc. Lab Chip 15:406–416. doi: 10.1039/c4lc00947a.

[33] Yu J, Zhang Y, Li H, Yang H, Wei H (2016) Sensitive and rapid detection of *Staphylococcus aureus* in milk via cell binding domain of lysin. Biosens. Bioelectron. 77:366–371. doi: 10.1016/j.bios.2015.09.058.

[34] Duan N, Shen M, Wu S, Zhao C, Ma X, Wang Z (2017) Graphene oxide wrapped Fe_3O_4@Au nanostructures as substrates for aptamer-based detection of *Vibrio parahaemolyticus* by surface-enhanced Raman spectroscopy. Microchim. Acta 184:2653–2660. doi: 10.1007/s00604-017-2298-9.

[35] McVey C, Huang F, Elliott C, Cao C (2017) Endonuclease controlled aggregation of gold nanoparticles for the ultrasensitive detection of pathogenic bacterial DNA. Biosens. Bioelectron. 92:502–508. doi: 10.1016/j.bios.2016.10.072.

[36] Vaisocherová-Lísalová H, Víšová I, Ermini ML, Špringer T, Song XC, Mrázek J, Lamačová J, Scott Lynn N, Šedivák P, Homola J (2016) Low-fouling surface plasmon resonance biosensor for multi-step detection of foodborne bacterial pathogens in complex food samples. Biosens. Bioelectron. 80:84–90. doi: 10.1016/j.bios.2016.01.040.

[37] Xu M, Wang R, Li Y (2016) Rapid detection of *Escherichia coli* O157:H7 and *Salmonella typhimurium* in foods using an electrochemical immunosensor based on screen-printed interdigitated microelectrode and immunomagnetic separation. Talanta 148:200–208. doi: 10.1016/j.talanta.2015.10.082.

[38] Park BH, Oh SJ, Jung JH, Choi G, Seo JH, Kim DH, Lee EY, Seo TS (2017) An integrated rotary microfluidic system with DNA extraction, loop-mediated isothermal amplification, and lateral flow strip based detection for point-of-care pathogen diagnostics. Biosens. Bioelectron. 91:334–340. doi: 10.1016/j.bios.2016.11.063.

[39] Wang W, Hynninen V, Qiu L, Zhang A, Lemma T, Zhang N, Ge H, Toppari JJ, Hytönen VP, Wang J (2017) Synergistic enhancement via plasmonic nanoplate-bacteria-nanorod supercrystals for highly efficient SERS sensing of food-borne bacteria. Sens. Actuators B Chem. 239:515–525. doi: 10.1016/j.snb.2016.08.040.

[40] Mungroo NA, Oliveira G, Neethirajan S (2016) SERS based point-of-care detection of food-borne pathogens. Microchim. Acta 183:697–707. doi: 10.1007/s00604-015-1698-y.

[41] Huang K-J, Shuai H-L, Chen Y-X (2016) Layered molybdenum selenide stacking flower-like nanostructure coupled with guanine-rich DNA sequence for ultrasensitive ochratoxin A aptasensor application. Sens. Actuators B Chem. 225:391–397. doi: 10.1016/j.snb.2015.11.070.

[42] Liu L-H, Zhou X-H, Shi H-C (2015) Portable optical aptasensor for rapid detection of mycotoxin with a reversible ligand-grafted biosensing surface. Biosens. Bioelectron. 72:300–305. doi: 10.1016/j.bios.2015.05.033.

[43] Soares RRG, Ramadas D, Chu V, Aires-Barros MR, Conde JP, Viana AS, Cascalheira AC (2016) An ultrarapid and regenerable microfluidic immunoassay coupled with integrated photosensors for point-of-use detection of ochratoxin A. Sens. Actuators B Chem. 235:554–562. doi: 10.1016/j.snb.2016.05.124.

[44] Wang C, Qian J, Wang K, Wang K, Liu Q, Dong X, Wang C, Huang X (2015) Magnetic-fluorescent-targeting multifunctional aptasensor for highly sensitive and one-step rapid detection of ochratoxin A. Biosens. Bioelectron. 68:783–790. doi: 10.1016/j.bios.2015.02.008.

[45] Wang C, Qian J, Wang K, Yang X, Liu Q, Hao N, Wang C, Dong X, Huang X (2016) Colorimetric aptasensing of ochratoxin A using Au@Fe_3O_4 nanoparticles as signal indicator and magnetic separator. Biosens. Bioelectron. 77:1183–1191. doi: 10.1016/j.bios.2015.11.004.

[46] Yang L, Zhang Y, Li R, Lin C, Guo L, Qiu B, Lin Z, Chen G (2015) Electrochemiluminescence biosensor for ultrasensitive determination of ochratoxin A in corn samples based on aptamer and hyperbranched rolling circle amplification. Biosens. Bioelectron. 70:268–274. doi: 10.1016/j.bios.2015.03.067.

[47] Wei Y, Zhang J, Wang X, Duan Y (2015) Amplified fluorescent aptasensor through catalytic recycling for highly sensitive detection of ochratoxin A. Biosens. Bioelectron. 65:16–22. doi: 10.1016/j.bios.2014.09.100.

[48] Lv L, Li D, Cui C, Zhao Y, Guo Z (2017) Nuclease-aided target recycling signal amplification strategy for ochratoxin A monitoring. Biosens. Bioelectron. 87:136–141. doi: 10.1016/j.bios.2016.08.024.

[49] Jodra A, Hervás M, López MÁ, Escarpa A (2015) Disposable electrochemical magneto immunosensor for simultaneous simplified calibration and determination of ochratoxin A in coffee samples. Sens. Actuators B Chem. 221:777–783. doi: 10.1016/j.snb.2015.07.007.

[50] Ji Y, Ren M, Li Y, Huang Z, Shu M, Yang H, Xiong Y, Xu Y (2015) Detection of aflatoxin B_1 with immunochromatographic test strips: Enhanced signal sensitivity using gold nanoflowers. Talanta 142:206–212. doi: 10.1016/j.talanta.2015.04.048.

[51] Ma Y, Mao Y, Di Huang, He Z, Yan J, Tian T, Shi Y, Song Y, Li X, Zhu Z, Zhou L, Yang CJ (2016) Portable visual quantitative detection of aflatoxin B1 using a target-responsive hydrogel and a distance-readout microfluidic chip. Lab Chip 16:3097–3104. doi: 10.1039/c6lc00474a.

[52] Lin Y, Zhou Q, Tang D, Niessner R, Knopp D (2017) Signal-On Photoelectrochemical Immunoassay for Aflatoxin B1 Based on Enzymatic Product-Etching MnO_2 Nanosheets for Dissociation of Carbon Dots. Anal. Chem. 89:5637–5645. doi: 10.1021/acs.analchem.7b00942.

[53] Duan H, Chen X, Xu W, Fu J, Xiong Y, Wang A (2015) Quantum-dot submicrobead-based immunochromatographic assay for quantitative and sensitive detection of zearalenone. Talanta 132:126–131. doi: 10.1016/j.talanta.2014.08.076.

[54] Liu N, Nie D, Tan Y, Zhao Z, Liao Y, Wang H, Sun C, Wu A (2017) An ultrasensitive amperometric immunosensor for zearalenones based on oriented antibody immobilization on a glassy carbon

electrode modified with MWCNTs and AuPt nanoparticles. Microchim. Acta 184:147–153. doi: 10.1007/s00604-016-1996-z.

[55] Liu C-S, Sun C-X, Tian J-Y, Wang Z-W, Ji H-F, Song Y-P, Zhang S, Zhang Z-H, He L-H, Du M (2017) Highly stable aluminum-based metal-organic frameworks as biosensing platforms for assessment of food safety. Biosens. Bioelectron. 91:804–810. doi: 10.1016/j.bios.2017.01.059.

[56] Li C, Wen K, Mi T, Zhang X, Zhang H, Zhang S, Shen J, Wang Z (2016) A universal multi-wavelength fluorescence polarization immunoassay for multiplexed detection of mycotoxins in maize. Biosens. Bioelectron. 79:258–265. doi: 10.1016/j.bios.2015.12.033.

[57] Zhang Z, Hu X, Zhang Q, Li P (2016) Determination for multiple mycotoxins in agricultural products using HPLC-MS/MS via a multiple antibody immunoaffinity column. J. Chromatogr. B 1021:145–152. doi: 10.1016/j.jchromb.2016.02.035.

[58] Yan Z, Gan N, Wang D, Cao Y, Chen M, Li T, Chen Y (2015) A "signal-on" aptasensor for simultaneous detection of chloramphenicol and polychlorinated biphenyls using multi-metal ions encoded nanospherical brushes as tracers. Biosens. Bioelectron. 74:718–724. doi: 10.1016/j.bios.2015.07.024.

[59] Miao Y-B, Ren H-X, Gan N, Cao Y, Li T, Chen Y (2016) Fluorescent aptasensor for chloramphenicol detection using DIL-encapsulated liposome as nanotracer. Biosens. Bioelectron. 81:454–459. doi: 10.1016/j.bios.2016.03.034.

[60] Miao Y, Gan N, Li T, Zhang H, Cao Y, Jiang Q (2015) A colorimetric aptasensor for chloramphenicol in fish based on double-stranded DNA antibody labeled enzyme-linked polymer nanotracers for signal amplification. Sens. Actuators B Chem. 220:679–687. doi: 10.1016/j.snb.2015.05.106.

[61] Feng X, Gan N, Lin S, Li T, Cao Y, Hu F, Jiang Q, Chen Y (2016) Ratiometric electrochemiluminescent aptasensor array for antibiotic based on internal standard method and spatial-resolved technique. Sens. Actuators B Chem. 226:305–311. doi: 10.1016/j.snb.2015.11.131.

[62] Gai P, Gu C, Hou T, Li F (2017) Ultrasensitive Self-Powered Aptasensor Based on Enzyme Biofuel Cell and DNA Bioconjugate: A Facile and Powerful Tool for Antibiotic Residue Detection. Anal. Chem. 89:2163–2169. doi: 10.1021/acs.analchem.6b05109.

[63] Wang X, Dong S, Gai P, Duan R, Li F (2016) Highly sensitive homogeneous electrochemical aptasensor for antibiotic residues detection based on dual recycling amplification strategy. Biosens. Bioelectron. 82:49–54. doi: 10.1016/j.bios.2016.03.055.

[64] Lin B, Yu Y, Cao Y, Guo M, Zhu D, Dai J, Zheng M (2018) Point-of-care testing for streptomycin based on aptamer recognizing and digital image colorimetry by smartphone. Biosens. Bioelectron. 100:482–489. doi: 10.1016/j.bios.2017.09.028.

[65] Yin J, Guo W, Qin X, Zhao J, Pei M, Ding F (2017) A sensitive electrochemical aptasensor for highly specific detection of streptomycin based on the porous carbon nanorods and multifunctional graphene nanocomposites for signal amplification. Sens. Actuators B Chem. 241:151–159. doi: 10.1016/j.snb.2016.10.062.

[66] Yan J, Huang Y, Zhang C, Fang Z, Bai W, Yan M, Zhu C, Chen A (2017) Aptamer based photometric assay for the antibiotic sulfadimethoxine based on the inhibition and reactivation of the peroxidase-like activity of gold nanoparticles. Microchim. Acta 184:59–63. doi: 10.1007/s00604-016-1994-1.

[67] Ramezani M, Danesh NM, Lavaee P, Abnous K, Taghdisi SM (2016) A selective and sensitive fluorescent aptasensor for detection of kanamycin based on catalytic recycling activity of exonuclease III and gold nanoparticles. Sens. Actuators B Chem. 222:1–7. doi: 10.1016/j.snb.2015.08.024.

[68] Kalunke RM, Grasso G, D'Ovidio R, Dragone R, Frazzoli C (2018) Detection of ciprofloxacin residues in cow milk: A novel and rapid optical β-galactosidase-based screening assay. Microchem. J. 136:128–132. doi: 10.1016/j.microc.2016.12.014.

[69] Wang S, Liu J, Yong W, Chen Q, Zhang L, Dong Y, Su H, Tan T (2015) A direct competitive assay-based aptasensor for sensitive determination of tetracycline residue in honey. Talanta 131:562–569. doi: 10.1016/j.talanta.2014.08.028.

[70] Chen M, Gan N, Zhou Y, Li T, Xu Q, Cao Y, Chen Y (2017) A novel aptamer- metal ions- nanoscale MOF based electrochemical biocodes for multiple antibiotics detection and signal amplification. Sens. Actuators B Chem. 242:1201–1209. doi: 10.1016/j.snb.2016.08.185.

[71] Jiang W, Beloglazova NV, Wang Z, Jiang H, Wen K, Saeger S de, Luo P, Wu Y, Shen J (2015) Development of a multiplex flow-through immunoaffinity chromatography test for the on-site screening of 14 sulfonamide and 13 quinolone residues in milk. Biosens. Bioelectron. 66:124–128. doi: 10.1016/j.bios.2014.11.004.

[72] Yan Z, Gan N, Li T, Cao Y, Chen Y (2016) A sensitive electrochemical aptasensor for multiplex antibiotics detection based on high-capacity magnetic hollow porous nanotracers coupling exonuclease-assisted cascade target recycling. Biosens. Bioelectron. 78:51–57. doi: 10.1016/j.bios.2015.11.019.

[73] Chen D, Yang M, Zheng N, Xie N, Liu D, Xie C, Yao D (2016) A novel aptasensor for electrochemical detection of ractopamine, clenbuterol, salbutamol, phenylethanolamine and procaterol. Biosens. Bioelectron. 80:525–531. doi: 10.1016/j.bios.2016.01.025.

[74] Mehta J, Vinayak P, Tuteja SK, Chhabra VA, Bhardwaj N, Paul AK, Kim K-H, Deep A (2016) Graphene modified screen printed immunosensor for highly sensitive detection of parathion. Biosens. Bioelectron. 83:339–346. doi: 10.1016/j.bios.2016.04.058.

[75] Fang H, Zhang X, Zhang SJ, Liu L, Zhao YM, Xu HJ (2015) Ultrasensitive and quantitative detection of paraquat on fruits skins via surface-enhanced Raman spectroscopy. Sens. Actuators B Chem. 213:452–456. doi: 10.1016/j.snb.2015.02.121.

[76] Tan MJ, Hong Z-Y, Chang M-H, Liu C-C, Cheng H-F, Loh XJ, Chen C-H, Liao C-D, Kong KV (2017) Metal carbonyl-gold nanoparticle conjugates for highly sensitive SERS detection of organophosphorus pesticides. Biosens. Bioelectron. 96:167–172. doi: 10.1016/j.bios.2017.05.005.

[77] Li H, Xie T, Ye L, Wang Y, Xie C (2017) Core-shell magnetic molecularly imprinted polymer nanoparticles for the extraction of triazophos residues from vegetables. Microchim. Acta 184:1011–1019. doi: 10.1007/s00604-017-2096-4.

[78] Chang MMF, Ginjom IR, Ng SM (2017) Single-shot 'turn-off' optical probe for rapid detection of paraoxon-ethyl pesticide on vegetable utilizing fluorescence carbon dots. Sens. Actuators B Chem. 242:1050–1056. doi: 10.1016/j.snb.2016.09.147.

[79] Feng S, Hu Y, Ma L, Lu X (2017) Development of molecularly imprinted polymers-surface-enhanced Raman spectroscopy/colorimetric dual sensor for determination of chlorpyrifos in apple juice. Sens. Actuators B Chem. 241:750–757. doi: 10.1016/j.snb.2016.10.131.

[80] Facure MHM, Mercante LA, Mattoso LHC, Correa DS (2017) Detection of trace levels of organophosphate pesticides using an electronic tongue based on graphene hybrid nanocomposites. Talanta 167:59–66. doi: 10.1016/j.talanta.2017.02.005.

[81] Muthumariappan A, Govindasamy M, Chen S-M, Sakthivel K, Mani V (2017) Screen-printed electrode modified with a composite prepared from graphene oxide nanosheets and Mn_3O_4 microcubes for ultrasensitive determination of nitrite. Microchim. Acta 184:3625–3634. doi: 10.1007/s00604-017-2379-9.

[82] Cui M, Huang J, Wang Y, Wu Y, Luo X (2015) Molecularly imprinted electrochemical sensor for propyl gallate based on PtAu bimetallic nanoparticles modified graphene-carbon nanotube composites. Biosens. Bioelectron. 68:563–569. doi: 10.1016/j.bios.2015.01.029.

[83] Guzman JMCC, Tayo LL, Liu C-C, Wang Y-N, Fu L-M (2018) Rapid microfluidic paper-based platform for low concentration formaldehyde detection. Sens. Actuators B Chem. 255:3623–3629. doi: 10.1016/j.snb.2017.09.080.

[84] Yu H, Du L, Guan L, Zhang K, Li Y, Zhu H, Sun M, Wang S (2017) A ratiometric fluorescent probe based on the pi-stacked graphene oxide and cyanine dye for sensitive detection of bisulfite. Sens. Actuators B Chem. 247:823–829. doi: 10.1016/j.snb.2017.03.101.

[85] Yu P, Liu Y, Zhang X, Zhou J, Xiong E, Li X, Chen J (2016) A novel electrochemical aptasensor for bisphenol A assay based on triple-signaling strategy. Biosens. Bioelectron. 79:22–28. doi: 10.1016/j.bios.2015.12.007.

[86] He M-Q, Wang K, Wang J, Yu Y-L, He R-H (2017) A sensitive aptasensor based on molybdenum carbide nanotubes and label-free aptamer for detection of bisphenol A. Anal. Bioanal. Chem. 409:1797–1803. doi: 10.1007/s00216-016-0123-7.

[87] Sajid M, Basheer C, Alsharaa A, Narasimhan K, Buhmeida A, Al Qahtani M, Al-Ahwal MS (2016) Development of micro-solid phase extraction using natural sorbent for determination of phthalate esters in milk samples. Anal. Chim. Acta 924:35–44. doi: 10.1016/j.aca.2016.04.016.

[88] Leonardo S, Rambla-Alegre M, Samdal IA, Miles CO, Kilcoyne J, Diogène J, O'Sullivan CK, Campàs M (2017) Immunorecognition magnetic supports for the development of an electrochemical immunoassay for azaspiracid detection in mussels. Biosens. Bioelectron. 92:200–206. doi: 10.1016/j.bios.2017.02.015.

[89] Boundy MJ, Selwood AI, Harwood DT, McNabb PS, Turner AD (2015) Development of a sensitive and selective liquid chromatography-mass spectrometry method for high throughput analysis of paralytic shellfish toxins using graphitized carbon solid phase extraction. J. Chromatogr. A 1387:1–12. doi: 10.1016/j.chroma.2015.01.086.

[90] He Y, Mo F, Chen D, Xu L, Wu Y, Fu F (2017) Capillary electrophoresis inductively coupled plasma mass spectrometry combined with metal tag for ultrasensitively determining trace saxitoxin in seafood. Electrophoresis 38:469–476. doi: 10.1002/elps.201600411.

[91] Yu L, Shi Z, Fang C, Zhang Y, Liu Y, Li C (2015) Disposable lateral flow-through strip for smartphone-camera to quantitatively detect alkaline phosphatase activity in milk. Biosens. Bioelectron. 69:307–315. doi: 10.1016/j.bios.2015.02.035.

[92] Zhang Y, Zhou H, Zhang Z-H, Wu X-L, Chen W-G, Zhu Y, Fang C-F, Zhao Y-G (2017) Three-dimensional ionic liquid functionalized magnetic graphene oxide nanocomposite for the magnetic dispersive solid phase extraction of 16 polycyclic aromatic hydrocarbons in vegetable oils. J. Chromatogr. A 1489:29–38. doi: 10.1016/j.chroma.2017.02.010.

[93] Gao F, Hu Y, Chen D, Li-Chan ECY, Grant E, Lu X (2015) Determination of Sudan I in paprika powder by molecularly imprinted polymers-thin layer chromatography-surface enhanced Raman spectroscopic biosensor. Talanta 143:344–352. doi: 10.1016/j.talanta.2015.05.003.

[94] Yu L, Shi M, Yue X, Qu L (2015) A novel and sensitive hexadecyltrimethyl ammonium bromide functionalized graphene supported platinum nanoparticles composite modified glassy carbon electrode for determination of sunset yellow in soft drinks. Sens. Actuators B Chem. 209:1–8. doi: 10.1016/j.snb.2014.10.098.

[95] Lim J, Kim G, Mo C, Kim MS, Chao K, Qin J, Fu X, Baek I, Cho B-K (2016) Detection of melamine in milk powders using near-infrared hyperspectral imaging combined with regression coefficient of partial least square regression model. Talanta 151:183–191. doi: 10.1016/j.talanta.2016.01.035.

[96] Zhong Y, Chen Y, Yao L, Zhao D, Zheng L, Liu G, Ye Y, Chen W (2016) Gold nanoparticles based lateral flow immunoassay with largely amplified sensitivity for rapid melamine screening. Microchim. Acta 183:1989–1994. doi: 10.1007/s00604-016-1812-9.

[97] Chen Z, Chengjun S, Zewei L, Kunping L, Xijian Y, Haimin Z, Yongxin L, Yixiang D (2018) Fiber optic biosensor for detection of genetically modified food based on catalytic hairpin assembly reaction and nanocomposites assisted signal amplification. Sens. Actuators B Chem. 254:956–965. doi: 10.1016/j.snb.2017.07.174.

[98] Jayasena SD (1999) Aptamers: An Emerging Class of Molecules That Rival Antibodies in Diagnostics. Clinical Chemistry 45:1628–1650.

[99] Bunka DHJ, Stockley PG (2006) Aptamers come of age - at last. Nature reviews. Microbiology 4:588–596. doi: 10.1038/nrmicro1458.

[100] Hamula C, Guthrie J, Zhang H, Li X, Le X (2006) Selection and analytical applications of aptamers. Trends Anal. Chem. 25:681–691. doi: 10.1016/j.trac.2006.05.007.

[101] Oh SS, Ahmad KM, Cho M, Kim S, Xiao Y, Soh HT (2011) Improving aptamer selection efficiency through volume dilution, magnetic concentration, and continuous washing in microfluidic channels. Anal. Chem. 83:6883–6889. doi: 10.1021/ac201269f.

[102] Sellergren B (ed) (2001) Molecularly imprinted polymers: Man-made mimics of antibodies and their applications in analytical chemistry, 1st edn. Techniques and instrumentation in analytical chemistry v. 23. Elsevier, Amsterdam, New York.

[103] Salam F, Tothill IE (2009) Detection of *Salmonella typhimurium* using an electrochemical immunosensor. Biosens. Bioelectron. 24:2630–2636. doi: 10.1016/j.bios.2009.01.025.

[104] Luo C, Tang H, Cheng W, Yan L, Zhang D, Ju H, Ding S (2013) A sensitive electrochemical DNA biosensor for specific detection of *Enterobacteriaceae* bacteria by Exonuclease III-assisted signal amplification. Biosens. Bioelectron. 48:132–137. doi: 10.1016/j.bios.2013.03.084.

[105] Lermo A, Campoy S, Barbé J, Hernández S, Alegret S, Pividori MI (2007) In situ DNA amplification with magnetic primers for the electrochemical detection of food pathogens. Biosens. Bioelectron. 22:2010–2017. doi: 10.1016/j.bios.2006.08.048.

[106] Farabullini F, Lucarelli F, Palchetti I, Marrazza G, Mascini M (2007) Disposable electrochemical genosensor for the simultaneous analysis of different bacterial food contaminants. Biosens. Bioelectron. 22:1544–1549. doi: 10.1016/j.bios.2006.06.001.

[107] Bruno JG, Phillips T, Carrillo MP, Crowell R (2009) Plastic-adherent DNA aptamer-magnetic bead and quantum dot sandwich assay for Campylobacter detection. J. Fluoresc. 19:427–435. doi: 10.1007/s10895-008-0429-8.

[108] Wu S, Duan N, Shi Z, Fang C, Wang Z (2014) Simultaneous aptasensor for multiplex pathogenic bacteria detection based on multicolor upconversion nanoparticles labels. Anal. Chem. 86:3100–3107. doi: 10.1021/ac404205c.

[109] Li F, Zhao Q, Wang C, Lu X, Li X-F, Le XC (2010) Detection of *Escherichia coli* O157:H7 using gold nanoparticle labeling and inductively coupled plasma mass spectrometry. Anal. Chem. 82:3399–3403. doi: 10.1021/ac100325f.

[110] Piliarik M, Párová L, Homola J (2009) High-throughput SPR sensor for food safety. Biosens. Bioelectron. 24:1399–1404. doi: 10.1016/j.bios.2008.08.012.

[111] Tawil N, Sacher E, Mandeville R, Meunier M (2012) Surface plasmon resonance detection of *E. coli* and methicillin-resistant *S. aureus* using bacteriophages. Biosens. Bioelectron. 37:24–29. doi: 10.1016/j.bios.2012.04.048.

[112] Kuang H, Chen W, Xu D, Xu L, Zhu Y, Liu L, Chu H, Peng C, Xu C, Zhu S (2010) Fabricated aptamer-based electrochemical "signal-off" sensor of ochratoxin A. Biosens. Bioelectron. 26:710–716. doi: 10.1016/j.bios.2010.06.058.

[113] Guo X, Wen F, Zheng N, Luo Q, Wang H, Wang H, Li S, Wang J (2014) Development of an ultrasensitive aptasensor for the detection of aflatoxin B1. Biosens. Bioelectron. 56:340–344. doi: 10.1016/j.bios.2014.01.045.

[114] Wang J, Leung D (2007) Analyses of macrolide antibiotic residues in eggs, raw milk, and honey using both ultra-performance liquid chromatography/quadrupole time-of-flight mass spectrometry and high-performance liquid chromatography/tandem mass spectrometry. Rapid Commun. Mass Spectrom. 21:3213–3222. doi: 10.1002/rcm.3207.

[115] Lara FJ, García-Campaña AM, Alés-Barrero F, Bosque-Sendra JM, García-Ayuso LE (2006) Multiresidue method for the determination of quinolone antibiotics in bovine raw milk by capillary electrophoresis-tandem mass spectrometry. Anal. Chem. 78:7665–7673. doi: 10.1021/ac061006v.

[116] Font G, Juan-García A, Picó Y (2007) Pressurized liquid extraction combined with capillary electrophoresis-mass spectrometry as an improved methodology for the determination of sulfonamide residues in meat. J. Chromatogr. A 1159:233–241. doi: 10.1016/j.chroma.2007.03.062.

[117] Fagerquist CK, Lightfield AR, Lehotay SJ (2005) Confirmatory and quantitative analysis of beta-lactam antibiotics in bovine kidney tissue by dispersive solid-phase extraction and liquid chromatography-tandem mass spectrometry. Anal. Chem. 77:1473–1482. doi: 10.1021/ac040138q.

[118] Fernández F, Hegnerová K, Piliarik M, Sanchez-Baeza F, Homola J, Marco M-P (2010) A label-free and portable multichannel surface plasmon resonance immunosensor for on site analysis of antibiotics in milk samples. Biosens. Bioelectron. 26:1231–1238. doi: 10.1016/j.bios.2010.06.012.

[119] Zhang Q, Lian M, Liu L, Cui H (2005) High-performance liquid chromatographic assay of parabens in wash-off cosmetic products and foods using chemiluminescence detection. Anal. Chim. Acta 537:31–39. doi: 10.1016/j.aca.2005.01.027.

[120] Mei Z, Chu H, Chen W, Xue F, Liu J, Xu H, Zhang R, Zheng L (2013) Ultrasensitive one-step rapid visual detection of bisphenol A in water samples by label-free aptasensor. Biosens. Bioelectron. 39:26–30. doi: 10.1016/j.bios.2012.06.027.

[121] Zhang K, Mei Q, Guan G, Liu B, Wang S, Zhang Z (2010) Ligand replacement-induced fluorescence switch of quantum dots for ultrasensitive detection of organophosphorothioate pesticides. Anal. Chem. 82:9579–9586. doi: 10.1021/ac102531z.

[122] Scherpenisse P, Bergwerff AA (2005) Determination of residues of malachite green in finfish by liquid chromatography tandem mass spectrometry. Anal. Chim. Acta 529:173–177. doi: 10.1016/j.aca.2004.08.009.

[123] Kuang H, Chen W, Yan W, Xu L, Zhu Y, Liu L, Chu H, Peng C, Wang L, Kotov NA, Xu C (2011) Crown ether assembly of gold nanoparticles: Melamine sensor. Biosens. Bioelectron. 26:2032–2037. doi: 10.1016/j.bios.2010.08.081.

[124] Balabin RM, Smirnov SV (2011) Melamine detection by mid- and near-infrared (MIR/NIR) spectroscopy: A quick and sensitive method for dairy products analysis including liquid milk, infant formula, and milk powder. Talanta 85:562–568. doi: 10.1016/j.talanta.2011.04.026.

[125] Ramalhosa MJ, Paíga P, Morais S, Delerue-Matos C, Oliveira MBPP (2009) Analysis of polycyclic aromatic hydrocarbons in fish: Evaluation of a quick, easy, cheap, effective, rugged, and safe extraction method. J. Sep. Sci. 32:3529–3538. doi: 10.1002/jssc.200900351.

[126] Bianchi F, Careri M, Mangia A, Musci M (2006) Development and validation of a solid phase micro-extraction-gas chromatography-mass spectrometry method for the determination of furan in baby-food. J. Chromatogr. A 1102:268–272. doi: 10.1016/j.chroma.2005.10.056.

[127] Kamath R (2018) Food Traceability on Blockchain: Walmart's Pork and Mango Pilots with IBM. The JBBA 1:1–12. doi: 10.31585/jbba-1-1-(10)2018.

[128] Mayer M, Baeumner AJ (2018) ABC Spotlight on Analytics 4.0. Anal. Bioanal. Chem.:5095–5097. doi: 10.1007/s00216-018-1191-7

2 Motivation and Structure of the Thesis

The focus of this thesis lies on the development of different production strategies for magnetized fluorescent liposomes as multifunctional labels for analytic sensing purposes, and on studying their performance when applied in (bio-)analytical assays.

One fast growing application field for analytical chemistry is food safety analysis, as food is an essential element of daily life, whose production and trade is increasing global, and as such, it is mandatory that everyone can trust the high quality and low risk of the food, which they consume every day. Important parameters for the development of point of need analysis for food safety are the field portability of the analysis system as well as short assay times, ease of use and reliable results, to enable the highest possible secureness for the end consumer. Risks that come from food involve biohazards like microorganisms or mycotoxins, residues of security sustainers in the production such as veterinary drugs and pesticides, and even technically legal additives, e.g., preservatives and colorants [1]. **Chapter 1** compares the advantages and disadvantages of new trends in this fast developing field and especially emphasizes the biological and synthetic macro- and nanomaterials that are developed and applied for this purpose. It was found that a common approach to yield low detection limits and high sensitivity is to utilize the principle of signal amplification by certain nanomaterials. A lot of different analysis systems relying on this strategy have been reported over the years, beginning with electrochemical sensors employing gold nanoparticles as electrode material [2, 3], graphene oxide or silver nanoplates deposited on SERS substrates for microbe detection [4, 5], and silica microbeads that are used as nanocarriers for fluorescence and electrochemical signal generation [6, 7]. Similar to silica microbeads, liposomes are also applied as dye carriers to achieve highly sensitive feedback of binding events [8, 9].

Liposomes are artificial vesicles surrounded by a phospholipid bilayer and are classified according to their size and lamellarity. Multilamellar vesicles are huge and consist of several phospholipid bilayers with onion-like stacking, while unilamellar vesicles show only one bilayer and can be discriminated into small and large ones [10]. The features of liposomes depend on the phospholipids of which the membrane consists. The chain length and degree of saturation influence the vesicles characteristics, as they are significant for the phase transition temperature of the lipids [11]. The polar head groups of the amphiphilic lipids point towards either the hydrophilic exterior or the inner volume of the liposomes and can either be uncharged, anionic or cationic [12]. Charged head groups are mostly favored as the resulting repulsion reduces the aggregation of the liposomes [13]. The unpolar tails on the other hand are oriented towards each other, forming a hydrophobic space in the bilayer core [10, 14], in which lipophilic molecules can

intercalate. In contrast to that, the inner compartment of liposomes is lipophobic, which enables the inclusion of hydrophilic substances, e.g., drugs, dyes, enzymes or nanoparticles [14].

These liposomes can then be used for drug transport or signal amplification. For that purpose, the encapsulant is set free by lysis, i.e., the destruction of the lipid bilayer, e.g., by addition of amphiphilic molecules. In the case of signal molecules, this enables enormous signal amplification, as not only single dye molecules are bound to the receptors and responsible for the signal, but one liposome linked to a bioreceptor can set free a large number of dye molecules at once [15]. A drawback of liposomes is their large size, which limits their diffusion in comparison with small dye molecules [16, 17], necessitating long assay times and reducing the efficiency of binding. The development of multifunctional liposomes with target binding as well as signal generating and externally manipulable properties are able to overcome this limitation and significantly improve assay times and efficiency. **Chapters 3 and 4** investigate different strategies to equip fluorescent liposomes with magnetic features to enable their directed attraction towards the sensing surface. In former studies, liposomes with incorporated magnetic nanoparticles (MNPs) in the lipid bilayer were developed [18]. In **Chapter 3**, this incorporation into the hydrophobic bilayer core as well as an alternative strategy of encapsulation in the hydrophilic inner compartment of liposomes are further examined. Therefore, small 8 nm MNPs with hydrophobic surface coating were synthesized, the size of which is a compromise between being small enough for intercalation into the narrow bilayer space [19] and having a large enough size to yield sufficient magnetic properties for attraction [20]. In contrast, commercially available particles with 30 nm in diameter and positively charged amino surface modification were chosen for incorporation of MNPs into the hydrophilic interior, as larger particles show stronger magnetization [20] and a negative surface potential might be repelled by the negatively charged liposomes. Different liposome synthesis methods and parameters are compared to optimize the system with respect to lipid composition, extrusion method and overall synthesis strategy, and the as-prepared liposomes were characterized with respect to their hydrodynamic diameter, zeta-potential, phospholipid concentration and the encapsulation efficiency, i.e., how large the fraction of magnetized liposomes is in comparison to the fraction of their non-magnetic counter parts. The various resulting systems are applied in a DNA sandwich hybridization assay in the presence and absence of an external magnetic field to evaluate their performance improvement regarding limits of detection and quantification, sensitivity, maximum signal to noise ratio and linear range and thus compare their ability of enhancing diffusion-based assays.

In **Chapter 3** the magnetic particles were directly encapsulated in the liposomes during synthesis, incorporating them either into the lipid bilayer or the hydrophobic core. A third possible

association strategy involves the linkage of magnetic particles to the surface of liposomes after synthesis. **Chapter 4** studies this approach and shows that the linking of both components in bulk solution leads to severe crosslinking. To circumvent this complication, a microfluidic chip was developed to enable directed coupling from one side only. The concept provides that first magnetic particles are captured at the bottom of the channel, then liposomes are flushed over to bind only from the top side and finally crosslinking after magnetic release is prevented by deactivation of the active carboxy groups on the surface of the liposomes. The channel was laser cut into double adhesive tape and closed by PMMA slides, and the design was optimized to achieve high binding capacities. The coupling of two different magnetic particles - magnetic beads with a diameter of 1 µm and magnetic nanoparticles with 30 nm in diameter - as well as determination of the coupling efficiency is described, and by application of liposomes with an additional biotin functional group the performance of the coupling product was investigated in a biotin-streptavidin-binding assay.

Apart from the controlled attraction in diffusion-based bioassays, a possible application area for magnetized liposomes is the immunomagnetic separation of analytes. Magnetic particles are commonly used for this strategy of preconcentrating diluted biomolecules from complex sample matrices, which is conducted by modification of the particles with initially antibodies, but meanwhile also with other bioreceptors, to capture the analyte and separate it from the sample solution [7, 21–23]. A drawback of this method is that for many strategies the bond between particle and analyte has to be broken prior to analysis as the particles can disturb further analysis and detection [21, 24]. The immunomagnetic separation technique is also employed for the detection of the HIV capsid protein p24 with single-particle-fluorescence-imaging of a sandwich assay between magnetic microparticles, p24 and a fluorescent label. Due to the large size of the particles (5 µm) and thus an about 25 times slower diffusion than liposomes (compare calculations in Chapter 4), an improvement of the detection limit of the described assay by the use of magnetized liposomes is imaginable. Their manipulable features were investigated for the preconcentration of p24, as they can be detached from the analyte easily by, e.g., the addition of mild detergent solutions or by complement lysis [25], setting the analyte free without changing its conformation or binding sites. **Chapter 5** describes preliminary studies regarding the feasibility of this approach. When first results showed that the binding of liposome-bound analyte to microparticles might be hindered due to steric reasons as well as because p24 is a quite lipophilic molecule that possibly interacts with liposomes, studies were conducted towards proof of principle of the strategy with the less lipophilic protein neutrophil gelatinase-associated lipocalin (NGAL).

The mentioned findings and results of this thesis are concluded in **Chapter 6**. The developed magnetic liposome systems are compared regarding their advantages and disadvantages and various ways for their optimization are described as well as completely new strategies for the association of magnetic particles with liposomes. In addition, this chapter shows the perspectives for future applications of magnetic liposomes in (bio-)analysis and the transfer of the microfluidic magnetic-coupling strategy to other nanomaterials.

2.1 References

[1] Dzantiev BB, Byzova NA, Urusov AE, Zherdev AV (2014) Immunochromatographic methods in food analysis. Trends Anal. Chem. 55:81–93. doi: 10.1016/j.trac.2013.11.007.

[2] Huang K-J, Shuai H-L, Chen Y-X (2016) Layered molybdenum selenide stacking flower-like nanostructure coupled with guanine-rich DNA sequence for ultrasensitive ochratoxin A aptasensor application. Sens Actuator B 225:391–397. doi: 10.1016/j.snb.2015.11.070.

[3] Yin J, Guo W, Qin X, Zhao J, Pei M, Ding F (2017) A sensitive electrochemical aptasensor for highly specific detection of streptomycin based on the porous carbon nanorods and multifunctional graphene nanocomposites for signal amplification. Sens Actuator B 241:151–159. doi: 10.1016/j.snb.2016.10.062.

[4] Duan N, Shen M, Wu S, Zhao C, Ma X, Wang Z (2017) Graphene oxide wrapped Fe_3O_4@Au nanostructures as substrates for aptamer-based detection of *Vibrio parahaemolyticus* by surface-enhanced Raman spectroscopy. Microchim Acta 184:2653–2660. doi: 10.1007/s00604-017-2298-9.

[5] Wang W, Hynninen V, Qiu L, Zhang A, Lemma T, Zhang N, Ge H, Toppari JJ, Hytönen VP, Wang J (2017) Synergistic enhancement via plasmonic nanoplate-bacteria-nanorod supercrystals for highly efficient SERS sensing of food-borne bacteria. Sens Actuator B 239:515–525. doi: 10.1016/j.snb.2016.08.040.

[6] Wang C, Qian J, Wang K, Wang K, Liu Q, Dong X, Wang C, Huang X (2015) Magnetic-fluorescent-targeting multifunctional aptasensor for highly sensitive and one-step rapid detection of ochratoxin A. Biosens. Bioelectron. 68:783–790. doi: 10.1016/j.bios.2015.02.008.

[7] Yan Z, Gan N, Wang D, Cao Y, Chen M, Li T, Chen Y (2015) A "signal-on" aptasensor for simultaneous detection of chloramphenicol and polychlorinated biphenyls using multi-metal ions encoded nanospherical brushes as tracers. Biosens. Bioelectron. 74:718–724. doi: 10.1016/j.bios.2015.07.024.

[8] Jiang W, Beloglazova NV, Wang Z, Jiang H, Wen K, Saeger S de, Luo P, Wu Y, Shen J (2015) Development of a multiplex flow-through immunoaffinity chromatography test for the on-site screening of 14 sulfonamide and 13 quinolone residues in milk. Biosens. Bioelectron. 66:124–128. doi: 10.1016/j.bios.2014.11.004.

[9] Miao Y-B, Ren H-X, Gan N, Cao Y, Li T, Chen Y (2016) Fluorescent aptasensor for chloramphenicol detection using DIL-encapsulated liposome as nanotracer. Biosens. Bioelectron. 81:454–459. doi: 10.1016/j.bios.2016.03.034.

[10] Jesorka A, Orwar O (2008) Liposomes: Technologies and analytical applications. Annu Rev Anal Chem 1:801–832. doi: 10.1146/annurev.anchem.1.031207.112747.

[11] Zook JM, Vreeland WN (2010) Effects of temperature, acyl chain length, and flow-rate ratio on liposome formation and size in a microfluidic hydrodynamic focusing device. Soft Matter 6:1352. doi: 10.1039/B923299K.

[12] Karmali PP, Chaudhuri A (2007) Cationic liposomes as non-viral carriers of gene medicines: Resolved issues, open questions, and future promises. Med Res Rev 27:696–722. doi: 10.1002/med.20090.

[13] Grit M, Crommelin DJA (1993) Chemical stability of liposomes: Implications for their physical stability. Chem Phys Lipids 64:3–18. doi: 10.1016/0009-3084(93)90053-6.

[14] Liu Q, Boyd BJ (2013) Liposomes in biosensors. The Analyst 138:391–409. doi: 10.1039/c2an36140j.

[15] Wang J (2005) Nanomaterial-based amplified transduction of biomolecular interactions. Small 1:1036–1043. doi: 10.1002/smll.200500214.

[16] Gendron P-O, Avaltroni F, Wilkinson KJ (2008) Diffusion coefficients of several rhodamine derivatives as determined by pulsed field gradient-nuclear magnetic resonance and fluorescence correlation spectroscopy. J Fluoresc 18:1093–1101. doi: 10.1007/s10895-008-0357-7.

[17] Stokes AM, Wilson JW, Warren WS (2012) Characterization of restricted diffusion in uni- and multi-lamellar vesicles using short distance iMQCs. J Magn Reson 223:31–40. doi: 10.1016/j.jmr.2012.07.021.

[18] Edwards KA, Baeumner AJ (2014) Enhancement of heterogeneous assays using fluorescent magnetic liposomes. Anal Chem 86:6610–6616. doi: 10.1021/ac501219u.

[19] Amstad E, Kohlbrecher J, Muller E, Schweizer T, Textor M, Reimhult E (2011) Triggered release from liposomes through magnetic actuation of iron oxide nanoparticle containing membranes. Nano Lett 11:1664–1670. doi: 10.1021/nl2001499.

[20] Lim J, Lanni C, Evarts ER, Lanni F, Tilton RD, Majetich SA (2011) Magnetophoresis of nanoparticles. ACS nano 5:217–226. doi: 10.1021/nn102383s.

[21] Li H, Xie T, Ye L, Wang Y, Xie C (2017) Core-shell magnetic molecularly imprinted polymer nanoparticles for the extraction of triazophos residues from vegetables. Microchim Acta 184:1011–1019. doi: 10.1007/s00604-017-2096-4.

[22] Sun Y, Quyen TL, Hung TQ, Chin WH, Wolff A, Bang DD (2015) A lab-on-a-chip system with integrated sample preparation and loop-mediated isothermal amplification for rapid and quantitative detection of *Salmonella spp.* in food samples. Lab Chip 15:1898–1904. doi: 10.1039/c4lc01459f.

[23] Madonna AJ, Basile F, Furlong E, Voorhees KJ (2001) Detection of bacteria from biological mixtures using immunomagnetic separation combined with matrix-assisted laser desorption/ionization time-of-flight mass spectrometry. Rapid Commun Mass Spectrom 15:1068–1074. doi: 10.1002/rcm.344.

[24] Fisher M, Atiya-Nasagi Y, Simon I, Gordin M, Mechaly A, Yitzhaki S (2009) A combined immunomagnetic separation and lateral flow method for a sensitive on-site detection of *Bacillus anthracis* spores - assessment in water and dairy products. Lett Appl Microbiol 48:413–418. doi: 10.1111/j.1472-765X.2008.02542.x.

[25] Edwards KA, Baeumner AJ (2006) Liposomes in analyses. Talanta 68:1421–1431. doi: 10.1016/j.talanta.2005.08.044.

3 Evaluation of Different Encapsulation Strategies for Magnetosomes

3.1 Abstract

The application of magnetic liposomes (magnetosomes) as new labels in analysis can overcome diffusion dependent bioassays through fast and easy magnetic attraction. In a previous study, magnetosomes were produced by the incorporation of magnetic nanoparticles (MNPs) into the bilayer of liposomes resulting in a significantly improved DNA hybridization assay under magnetic conditions. Our aim was to increase the understanding of how different encapsulation strategies and synthesis parameters influence the generation of these magnetosomes, and to determine the percentage of magnetization to smartly design for higher performance in functional bioassays. Here, the incorporation of MNPs into the hydrophobic bilayer core (b-liposomes) was compared with their entrapment in the hydrophilic inner cavity (i-liposomes), and encapsulation efficiencies for both systems were evaluated. Small hydrophobic MNPs (8 – 10 nm) as well as hydrophilic MNPs (30 nm) were used. Liposomes were characterized by DLS, zeta-potential measurements and ICP-OES, and optimized with respect to lipid composition, extrusion method and synthesis strategy.

B-liposomes presented as Janus-like particles with a fraction of 15% magnetization. It is assumed that the bilayer integration renders liposomes thermodynamically less stable and hence supports the formation of non-magnetic liposomes. Still, with this degree of magnetization, a 3-fold lowered limit of detection in a DNA sandwich hybridization assay was achieved in comparison to non-magnetic conditions. Surprisingly, no further improvement could be obtained by magnetically concentrating b-liposomes and using only those in analysis. This suggests that non-magnetic liposomes are dragged to the surface through the movement of magnetosomes as well to participate in the bioassay. In the case of i-liposomes, the situation is surprisingly reverse. Since no highly concentrated MNP solutions could be used for encapsulation, a theoretical yield of 2% was targeted. Instead, 5% of magnetosomes were achieved even through the hydrodynamic diameter of MNPs would theoretically not promote their encapsulation. Furthermore, unlike with b-liposomes, by eliminating the high amount of non-magnetic liposomes an 8-fold LOD increase could be achieved compared to non-magnetic conditions. We assume that 5% magnetosomes within a liposome population see less benefit by an external magnetic field due to the repulsion observed by the many liposomes in solution counteracting a directed magnetic field movement. In the end, both strategies provide viable options for the improvement of bioassays and thus offer

high degrees of freedom in assay design as surface tags are unhindered and additional marker molecules can be entrapped into the liposome cavity.

This chapter is intended to be submitted for publication.

Author contributions:

The experimental work was carried out by the author. Vanessa Tomanek and Sandy Himmelstoß provided 3D graphics. Carola Hofmann, Thomas Hirsch, Axel Duerkop and Antje J. Baeumner contributed with strategic discussions. Antje J. Baeumner was the leader of this project.

3.2 Introduction

Cryptosporidium parvum is an intestinal parasite, which causes diarrhea amongst a wide range of human communities. At the moment, there only exists one proven anti-parasitic drug for cryptosporidiosis, but even this treatment is not effective for all groups of patients and especially infants and immunocompromised persons are still threatened by this pathogen [1–3]. This makes clear that a high necessity exists to detect this threat early, especially as it can even occur in treated drinking water [1].

A common technique for the recognition of pathogens is to detect their genome by DNA hybridization. Amongst these, sandwich assays hold the advantage of twofold recognition by one capture and one reporter probe, which yields higher selectivity. DNA sandwich hybridization assays have been reported for the detection of many pathogens, e.g., *Salmonella* [4], *Hepatitis B* [5], *B. anthracis* [6] and also *C. parvum* [7]. But this assay format heavily relies on diffusion and accidental meeting of the reaction partners in solution or, even worse, on the surface of a sensor platform or microtiter plate. By overcoming these diffusion-based processes, faster and more efficient binding of the reaction partners would be possible, resulting in the possibility to apply these assays even more efficiently in sensors to achieve higher field portability and point of care devices, e.g., to detect low numbers of *C. parvum* in contaminated drinking water and food or in infected patients. One possible strategy for the overcoming of diffusion barriers is the directed attraction in an external electromagnetic field as established in many bioanalytical approaches taking advantage of immunomagnetic separation strategies [8–10]. Thus, bioanalytical labels should be modified to have a dual functionality: signal generation as well as magnetic attraction.

Liposomes - artificial vesicles filled with signal molecules - are applied often as bioanalytical labels due to their high biocompatibility and the attribute of signal amplification due to the release of a high number of dye molecules by one bound liposome [11]. By incorporation of magnetic material into a liposome, a so-called magnetosome, a liposome with magnetic properties, is formed. These cannot only be transported to their point of destination by diffusion, but also directed by a magnetic field, and a greater amount of magnetosomes should be able to bind in shorter time than in a conventional diffusion-based assay, as shown in Figure 1. By removal of the magnetic field and convection, the unspecifically bound magnetosomes should be detached and the signal-to-noise ratio may be considerable improved [12]. As magnetic material for incorporation, magnetic nanoparticles (MNPs) can be used, e.g., iron oxide nanoparticles.

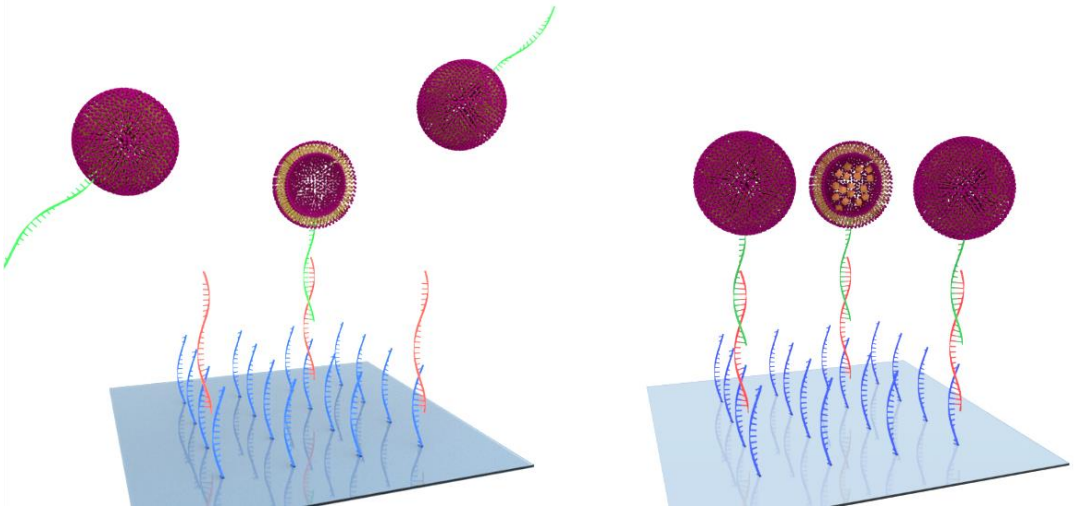

Figure 1: Comparison of a DNA hybridization assay with liposomes used for signal enhancement without (left) and with (right) MNPs incorporated into the liposomes under the influence of an external magnetic field. By magnetic attraction, more liposomes can bind to the target DNA. (provided by Dr. Sandy Himmelstoß)

For the synthesis of magnetosomes the reverse phase evaporation [7] as well as the thin film rehydration method [13] were employed. Both display the efficient encapsulation of molecules and yield long-term stable liposomes and therefore were promising for the successful encapsulation of MNPs. With both methods, it is possible to either encapsulate MNPs in the hydrophilic inner volume together with signal molecules, or separate from them in the hydrophobic lipid bilayer core.

For the encapsulation into the hydrophilic inner volume, shown in Figure 2, surface modification of MNPs is necessary as after synthesis they are coordinated by hydrophobic oleic acid. These modified nanoparticles can then be added together with the signal molecules as aqueous encapsulation solution.

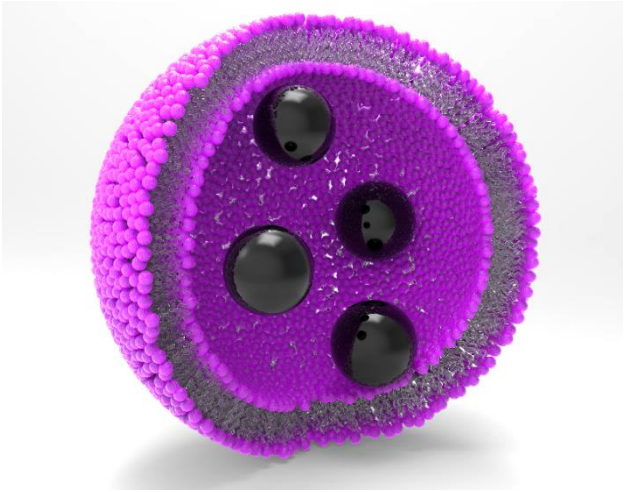

Figure 2: Scheme of a liposome with nanoparticles (10 nm in diameter) encapsulated into the hydrophilic lumen inside the liposome. Note: the diameter of liposomes is not to scale. (provided by Vanessa Tomanek)

Alternatively, the as-synthesized hydrophobic MNPs can be incorporated into the lipid bilayer by simply adding them to the lipids dissolved in organic solvents. The magnetization power of MNPs scales with their size [14], at the same time, they must fit into the ~4 nm lipid bilayer of the liposomes. While some studies and theoretical models show, that the maximum particle diameter for insertion into the bilayer is about 5 nm [15], the successful insertion of particles with up to 15 nm diameter has been reported [12]. Figure 3 left shows an ideal scheme of this incorporation, where the particles are statistically distributed across the membrane. As the membrane has only about four nm in thickness and the particles have a diameter of around 10 nm, the membrane has to wrap around the particles, being distorted to a heavy degree. For this reason, the particles will most likely tend to agglomerate at one point and form kind of Janus shaped vesicles [16], as shown in Figure 3 right. As reporter molecules are distributed across the membrane of the vesicles, this asymmetry is not suspected to influence the binding efficiency.

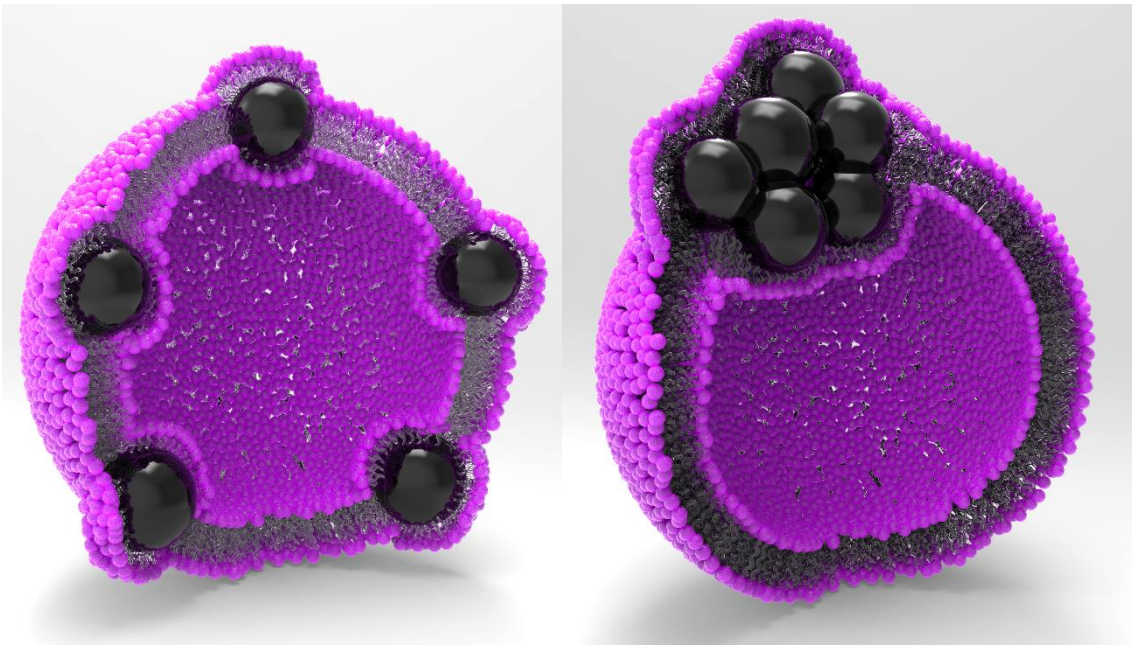

Figure 3: Scheme of liposomes with nanoparticles (10 nm in diameter) incorporated into the lipid bilayer core (4 nm in thickness). Left: This ideal scheme shows a statistical distribution of particles and the vast distortion of the membrane by the particles. Right: The more likely to be found liposome form will equal this Janus shaped liposome with agglomerated MNPs on one side and the hydrophilic department on the other. Note: the diameter of liposomes is not to scale. (provided by Vanessa Tomanek)

To use magnetosomes as analytical tool their surface must be modified enabling coupling to bioreceptors. Appropriately modified lipids can be inserted directly during synthesis, or they can be inserted after synthesis by intercalation of the hydrophobic chains into the outer lipid bilayer [17, 18], or covalent coupling reactions can be performed with purified liposomes. Due to the simplicity and high reliability of the approach, insertion of cholesterol-tagged DNA reporter was chosen. For quality control of the resulting magnetosomes, their performance in bioassays in

presence or absence of an external electromagnetic field was compared. Sulforhodamine B was used as signal generating molecule, a fluorescent dye that in high concentrations is self-quenching, ensuring that while encapsulated in liposomes the dye is not detectable. By lysis of the liposomes the dye is set free and diluted, which disables self-quenching of the fluorescence. Therefore, by a very small amount of bound liposomes a clearly measurable signal can be generated [11]. With this assay, the ability of magnetosomes to improve a DNA sandwich hybridization assay for *Cryptosporidium parvum*, and the optimum conditions for their synthesis were investigated.

3.3 Materials and Methods

3.3.1 Materials

Iron (III) chloride hexahydrate (≥ 99%) and sodium oleate (≥ 82%) were bought from Sigma Aldrich (www.sigmaaldrich.com). Oleic acid and 1-octadecene (both 90%, technical grade) were obtained from Alfa Aesar (www.alfa.com).

1,2-dipalmitoyl-sn-glycero-3-phosphocholine (DPPC), 1,2-dipalmitoyl-sn-glycero-3-phospho-(1'-rac-glycerol) (sodium salt) (DPPG), 1,2-dipalmitoyl-sn-glycero-3-phosphoethanolamine-N-(biotinyl) (sodium salt) (biotin-DPPE), 1,2-dipalmitoyl-sn-glycero-3-phosphoethanolamine-N-(glutaryl) (sodium salt) (N-glutaryl-DPPE) were purchased from Avanti Polar Lipids, Inc. (www.avantilipids.com), cholesterol and sulforhodamine B were obtained from Sigma Aldrich (www.sigmaaldrich.com) and n-octyl-β-D-glucopyranoside (OG) was bought from Roth (www.carlroth.com).

A DNA derived from the *C. parvum* heat shock protein 70 (hsp70) mRNA was used as model analyte for DNA hybridization assays. Three different sequences were employed, specified as capture probe (CP), target sequence (tDNA) and reporter probe (RP) [CP: 5′-biotinyl-AGA TTC GAA GAA CTC TGC GC-3′; tDNA: 5′-AAGGACCAGCATCCTTGAGTA CTTTCT C AA CTG GAG CTA AAG TTG CAC GGA AGT AAT CA GCG CAG AGT TCT TCG AAT CT AG CTC TAC TGA TGG CAA CTG A-3′; RP: 5′-GTG CAA CT T TAG CTC CAG TT-cholesteryl-3′]. This DNA was obtained from Metabion (www.metabion.com).

Chloroform, cyclohexane and methanol were purchased from Fisher Scientific (www.fishersci.com).

Hydroxyethyl)piperazine-1-ethanesulfonic acid (HEPES) and sodium azide were bought from Sigma Aldrich (www.sigmaaldrich.com). BSA (albumin fraction V from bovine serum), di-potassium hydrogen phosphate trihydrate, di-sodium hydrogen phosphate dihydrate, formamide, potassium chloride, potassium dihydrogen phosphate and tri-sodium citrate dihydrate were bought from Merck (www.merckmillipore.com). Ficoll 400 and sodium chloride were obtained from Roth (www.carlroth.com) and sucrose was purchased from VWR (de.vwr.com).

All other chemicals were of analytical grade and obtained from either VWR (de.vwr.com), Merck (www.merckmillipore.com), Roth (www.carlroth.com) or Sigma Aldrich (www.sigmaaldrich.com). Double distilled water was used for the preparation of all aqueous solutions.

HEPES buffer consisted of 10 mM HEPES, 200 mM NaCl and 0.01% (w/v) NaN_3 and pH was adjusted to 7.5. For HSS buffer (HEPES-saline-sucrose) a varying amount of sucrose was added to adjust right osmolality for liposome outer buffer. Phosphate buffered saline (PBS) contained 137 mM NaCl, 2.7 mM KCl, 10 mM Na_2HPO_4 and 1.8 mM KH_2PO_4 at pH 7.4. For production of washing buffer, 0.05% (v/v) Tween 20 and 0.01% (w/w) bovine serum albumin were added to PBS. Potassium phosphate buffer consisted of 50 mM K_2HPO_4, 50 mM KH_2PO_4 and 1 mM EDTA and pH was adjusted to 7.5. Hybridization buffer was prepared from 1.35 M NaCl, 0.135 M sodium citrate, 0.01% (w/v) NaN_3, 30% (v/v) formamide and 0.2% (w/v) Ficoll 400 with pH 7.0.

For extrusion of liposomes, an extruder equipped with syringes, filter supports and membranes from Avanti Polar Lipids, Inc. (www.avantilipids.com) was employed. Sephadex G50 for column chromatography was purchased from Sigma Aldrich (www.sigmaaldrich.com).

Black MaxiSorp 96 well microtiter plates from Nunc for stability testing and magnetic washing experiments were purchased from Sigma Aldrich (www.sigmaaldrich.com). For DNA hybridization assays, white streptavidin coated microtiter plates (KaiSA 96) with a biotin binding capacity of >14 pmol/well from Kaivogen Oy (kaivogen.com) were used.

3.3.2 Synthesis and Characterization of Magnetic Nanoparticles

MNPs were synthesized by thermal decomposition, adapting a method developed by Park et al. [19], where a precursor is decomposed at high temperatures.

For the precursor synthesis, typically 2.703 g $FeCl_3 \cdot 6H_2O$ (1 equiv., 10 mmol) and 9.133 g sodium oleate (3 equiv., 30 mmol) are dissolved in a solvent mixture of 20 mL ethanol, 15 mL water and 35 mL hexane and heated to reflux for 4 h. After cooling to room temperature, the organic phase was washed with 10 mL water three times and the solvent was removed at the rotary evaporator at reduced pressure.

For particle synthesis, typically 0.9 g precursor (1 equiv., 1 mmol) and 120 mg oleic acid (0.4 equiv., 0.4 mmol) were dissolved in 10 mL octadecene in a three necked round bottom flask. The flask is heated to 120 °C, flushed with nitrogen for 15 min and then set under vacuum for another 15 min. Again nitrogen is applied and the solution is heated to reflux (>320 °C) for 1 h. After cooling to room temperature rapidly, the nanoparticles are washed with cyclohexane and ethanol via centrifugation (3 times, 5 min, 4,000 g) and aggregates are removed by centrifugation for 3 min at 1,000 g. Afterwards the nanoparticles are stored at 4 °C as dispersion in cyclohexane.

The method of choice for determination of diameter and uniformity of the particles was transmission electron microscopy (TEM). Therefore, a 120 kV Philips CM12 (ww.fei.com) microscope was employed and the obtained images were evaluated with ImageJ software (http://rsbweb.nih.gov/ij/). Liposome samples were stained with phosphotungstic acid for TEM. The hydro- and solvodynamic diameters were determined by Dynamic Light Scattering (DLS) at 20 °C with a Malvern Zetasizer Nano-ZS (www.malvern.com) in disposable poly(methyl methacrylate) (PMMA) cuvettes (semi-micro). ζ-potential measurements were carried out at the same instrument in disposable capillary cells. Hydro-/solvodynamic diameters were determined 13 times for each sample and averaged. The zeta potential was measured 25 to 37 times and averaged.

3.3.3 Magnetic Characterization of Particles

To compare the magnetization of different magnetic particles with another, the particles were filled in a semi-micro PMMA cuvette (~1 mL volume, path length 10 mm) and placed next to a magnet. The time until most of the particles were migrated towards the magnet was determined. Ten iterations were performed for commercial 30 nm MNPs and 1 µm MBs, both at a concentration of about 1 mg·mL^{-1}. For self-synthesized 8 nm MNPs with oleic acid as surface ligand, the magnetic attraction could only be measured after addition of an antidispersant, as these particles form stable ferrofluids in organic solvents and are not attractable without moving the whole liquid. The particles were diluted to a concentration of around 20 mg·mL^{-1} with cyclohexane and further to 10 mg·mL^{-1} by addition of the antidispersant ethanol before magnetic attraction.

3.3.4 Liposome Synthesis and Characterization

Liposomes were synthesized either by reverse phase evaporation according to an established procedure from Edwards et al. or by thin film rehydration according to a modified procedure by Bangham et al. [13]. Typically, 10 mg cholesterol (26 µmol, 46% of lipid composition), 15 mg DPPC (20 µmol, 36%) and 7.5 mg DPPG (10 µmol, 18%) are dissolved in 0.5 mL methanol and 3 mL chloroform. The solution is sonicated for 1 min.

For reverse phase evaporation, 2 mL encapsulant (10 mM SRB in 20 mM HEPES, pH 7.5) are added and the mixture is sonicated for further 4 min. Organic solvents are evaporated at the rotary evaporator at 60 °C under reduced pressure. The mixture is vortexed thoroughly and 2 mL encapsulant are added. The flask is transferred back to the rotary evaporator to get rid of any remaining organic solvent.

For thin film rehydration, first organic solvents are evaporated at the rotary evaporator at 60 °C under reduced pressure. Then 4 mL encapsulant are added for rehydration of the lipid film by rotating at atmospheric pressure at 60 °C at the rotary evaporator for 1 h. After 30 min the liposome solution was vortexed thoroughly.

In both cases, the liposomes are extruded each 21 times at 60 °C through two polycarbonate membranes with 1.0 and 0.4 µm pores. The solution is purified by size exclusion column chromatography (1.5 x 20 cm, Sephadex G50). Liposome containing fractions are collected as medium and high concentrated solutions and transferred to dialysis (pore size 12 – 14 kD, spectrumlab.com) against HEPES buffer.

To achieve modified liposomes, different additions are possible: Reporter probe modified liposomes are achieved by addition of 25 µL of a 300 µM solution of DNA tagged with cholesterol (15 nmol) with the lipid ingredients. For incorporation of hydrophobic-coated MNPs into the lipid bilayer, 2.5 mg MNPs dispersed in cyclohexane are transferred into 1 mL chloroform by precipitation with ethanol and centrifugation. This dispersion replaces 1 of 3 mL chloroform as lipid solvent. For encapsulation of MNPs with hydrophilic surface coating, the aqueous MNP solution is added to the encapsulation solution.

Concentrations are determined by ICP-OES measurements on a Spectroflame-EOP inductively coupled plasma optical emission spectrometer (ICP-OES) from Spectro (www.spectro.com), hydrodynamic diameters by DLS at 20 °C with a Malvern Zetasizer Nano-ZS (www.malvern.com) in disposable PMMA cuvettes (semi-micro). ζ-potential measurements were carried out at the same instrument in disposable capillary cells. Hydrodynamic diameters were determined 12 to 15 times for each sample and averaged, zeta potential 25 to 37 times.

3.3.5 DNA Hybridization Assay

Streptavidin coated microtiter plates were used for the following assay. All steps are performed in parallel on two identical MTPs.

Each well is washed with washing buffer (2 x 200 µL/well) and PBS (1 x 200 µL/well) and biotinylated capture probe (*C. parvum*, 0.1 µM in potassium phosphate buffer, 100 µL/well) is added. MTPs are incubated for 30 min at 23 °C on an Eppendorf ThermoMixer C (online-shop.eppendorf.de). Unbound capture probe is removed and the wells are washed with washing buffer (2 x 200 µL/well) and hybridization buffer (1 x 200 µL/well).

Synthetic target DNA (*C. parvum*, different concentratoins in hybridization buffer, 100 µL/well) is added and MTPs are incubated for 30 min at 23 °C on Eppendorf ThermoMixer C. Unbound target DNA is removed and the wells are washed with HEPES buffer (2 x 200 µL/well).

Liposome-reporter DNA (50 µM total lipid in HEPES buffer, 100 µL/well) is added and incubated for 60 min at room temperature, where only one MTP is placed on a permanent magnet. During this time, both MTPs are transferred two times to the ThermoMixer C and shaken for 10 s. Unbound liposomes are removed and the wells are washed with HEPES buffer (2 x 200 µL/well)

Fluorescence is measured in 100 µL HEPES buffer once either with a BioTek SYNERGY neo2 (www.biotek.com) or a FLUOstar® OPTIMA microtiter plate reader from BMG LABTECH (www.bmglabtech.com). Then the supernatant is removed and octyl glycoside (30 mM, 100 µL/well) is added to induce lysis of the liposome bilayer. After 5 min incubation, fluorescence is measured again.

3.4 Results and Discussion

3.4.1 Characterization of Magnetic Nanoparticles and Liposomes

Iron oxide magnetic nanoparticles were synthesized using previously established protocols [19] and characterized with DLS and TEM. With DLS, a solvodynamic diameter of 18.2 nm in cyclohexane was determined, while by TEM the diameter of the bare particles was determined as (8.1±1.1) nm. This difference is caused by the oleic acid groups on the surface and the solvent corona formed around it. As shown in Figure 4, the particles are of uniform cubic shape and monodisperse.

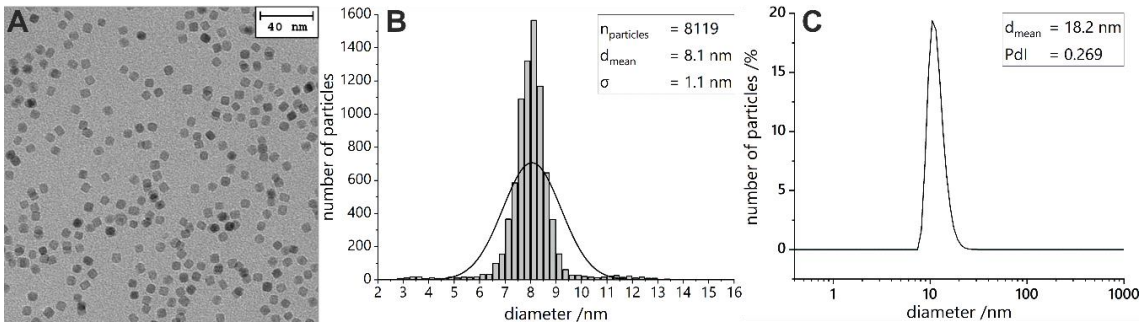

Figure 4: TEM image (A), particle size distribution as obtained from TEM images (B) and DLS (C) of MNPs. The particles possess an average diameter d_{mean} of 8.1 nm with a standard deviation σ of 1.1 nm and a solvodynamic diameter d_{mean} of 18.2 nm with a polydispersity index (PdI) of 0.269.

The magnetic properties of these particles were compared to commercially available iron oxide nanoparticles with 30 nm diameter and magnetic beads with 1 µm in diameter (see SI for more information). Surprisingly, the self-synthesized 8 nm MNPs showed better magnetic properties than large 1 µm beads, but expectedly were less magnetic than the 30 nm particles.

Liposomes were characterized according to their hydrodynamic diameter determined by DLS measurements, which is around 170 nm for original liposomes extruded through 1.0 and 0.4 µm membranes, and 234 nm for optimized liposomes with only one extrusion step at 1 µm pore size. The zeta potential of all liposomes is ~20 mV, which is characteristic for liposomes with this lipid composition and typically leads to high colloidal stability (for more information see SI). TEM images show the expected Janus shaped incorporation of particles in the bilayer (see Figure S1 right).

As the liposome mixture is composed of magnetically modified liposomes as well as liposomes without incorporated particles, this fraction was determined by measuring the fluorescence signal after magnetic separation compared to the signal of the unaltered liposome mixture. Therefore, liposomes were washed twice in absence or presence of a magnetic field, respectively, and the

resulting intensity values were subtracted to eliminate nonspecific binding effects. The value was then compared to unwashed liposomes with the same starting concentration. For optimized liposomes with MNPs incorporated into the lipid bilayer (b-liposomes) it was found that (14.5±0.2)% of the liposomes were magnetic in the original solution, while for encapsulating MNPs in the hydrophilic inner cavity of the liposomes together with marker molecules (i-liposomes) only a fraction of (5.4±0.9)% was determined to be magnetic (Figure 5). An explanation for this phenomenon is on the one hand the lower amount of particles used for i-liposomes due to the higher cost and lower concentration of commercial particle solutions and on the other hand the large hydrodynamic diameter of these particles, which prevents incorporation of high particle quantities per liposome.

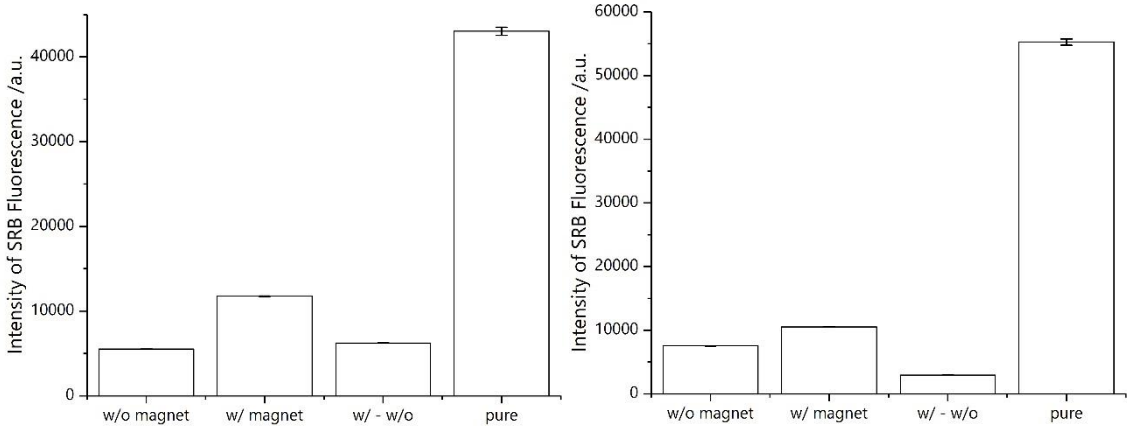

Figure 5: Encapsulation efficiency of optimized b-liposomes (left) and i-liposomes (right) as determined by magnetic separation and fluorescence measurements.

3.4.2 Development of Optimized Bilayer Insertion Liposomes

To validate the magnetic abilities of the synthesized magnetosomes, a DNA hybridization sandwich assay was performed in parallel with and without the presence of an external magnetic field. In a first attempt with b-liposomes (Figure S3 left), limits of detection (LOD) and quantification (LOQ) (zero value plus three and ten times standard deviation, respectively) and the maximum signal-to-noise ratio (max S/N) got surprisingly poorer when applying a magnetic field (1.1 to 1.2 fold higher without than with magnet, see Table 1). We assume that this was due to increased non-specific binding of the b-liposomes occurring. Therefore, optimization of these liposomes was necessary.

Three synthesis parameters were investigated regarding possible optimization of the system: the cholesterol fraction of the total lipid composition, the pore size of employed extrusion membranes and the overall synthesis method.

Cholesterol is added to the lipid composition to stabilize the membrane, as it reduces on the one hand the repulsion of charged headgroups by increasing the headgroup spacing, and on the other hand, the motion of hydrocarbon chains by increased Van der Waals interactions [20]. But this effect also stiffens the membrane, which likely hinders the intercalation of nanoparticles between the two rigid bilayer sheets as the membrane has to arrange in a more distorted structure. Therefore, reduction of the cholesterol content was investigated to yield higher membrane fluidity and thus higher MNP encapsulation. Unfortunately, as shown in Figure 6A, a reduction of the cholesterol content did not improve the assay. With 7.5% cholesterol the assay in presence of a magnetic field still yields better results, but in total the results are worse than with 46% cholesterol, while without any cholesterol an inversion of *with* versus *without magnet* takes place. A possible explanation for this phenomenon is that, without a stabilizing cholesterol present, lipid coated nanoparticles form, which cover the surface of the microtiter plate and hinder binding of dye-filled liposomes to the target DNA. This would also explain why some data points show lower fluorescence than the blank solutions. In presence of target DNA, the coated particles can bind and shield the plate surface against unspecific binding of dye-filled liposomes, which lowers the background signal, while without target DNA in the blank samples, some of the particles can be removed by shaking and washing and liposomes can adsorb.

Secondly, thin film rehydration was investigated and compared to reverse phase evaporation, assuming that the pre-formation of lipid films will favor MNP integration into the lipid bilayer. Unfortunately, no improvement of the assay could be achieved by changing the synthesis method (Figure 6B).

Finally, the pore size of the applied extrusion membranes was investigated. Extrusion is performed to yield uniform unilamellar vesicles with a narrow size distribution. These are more stable than a liposome dispersion with a broad size distribution, as those can fuse or grow by Ostwald ripening and get unstable due to an unfavored surface curvature [21]. Also, uniform liposomes are preferred in analytical assays to improve the reproducibility of binding events. However, a visibly high loss of magnetic particles was observed during the extrusion process, when liposomes are ripped apart to form in a uniform and unilamellar way again at the other side of the membrane. Therefore, it was investigated if the use of only one extrusion through a membrane with 1.0 µm pores instead of two consecutive extrusions through membranes with 1.0 and 0.4 µm pores would yield better results, finding a compromise between homogenizing the liposome size and severe particle loss. In fact, it was found that through reducing the number of extrusion steps higher signals and a steeper slope of the signal curve could be achieved (Figure 6C). The liposome

diameter went from 170 to 230 nm, which remains in the stable unilamellar size range for these bioanalytical liposomes [22].

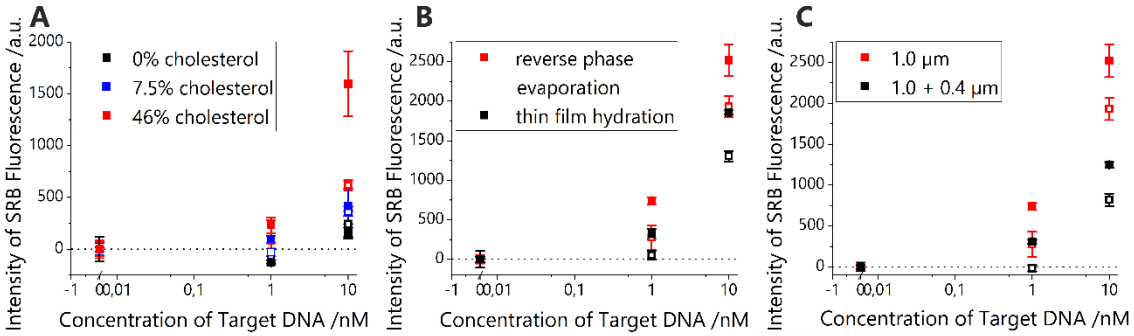

Figure 6: DNA hybridization assays performed for different b-liposomes systems once in absence and once in presence of an external magnetic field. Cholesterol content (A), synthesis method (B) and extrusion steps (C) were varied.

3.4.3 Comparison of Magnetic Liposome Systems

For an optimized b-liposome system, synthesis by reverse phase evaporation, a cholesterol content of 45% and only one extrusion step with a pore size of 1.0 µm were chosen. Performance investigation by DNA hybridization revealed very low LOD and LOQ, and a high improvement with the use of an external magnetic field could be achieved (~3-fold reduction of LOD/LOQ and increase of max S/N, respectively, see Table 1). Interestingly, after magnetic separation and concentration adjustment to 14.5%, improvement factors were in the same range as prior magnetic separation, while the LOD and LOQ rose significantly (Figure 7).

In case of i-liposomes, an assay showed no difference with or without applied external magnetic field (Figure S3 right), yet for the separated magnetic fraction significant improvement for LOD, LOQ, sensitivity as well as max S/N could be achieved, although LOD and LOQ again rose after removal of non-magnetic liposomes.

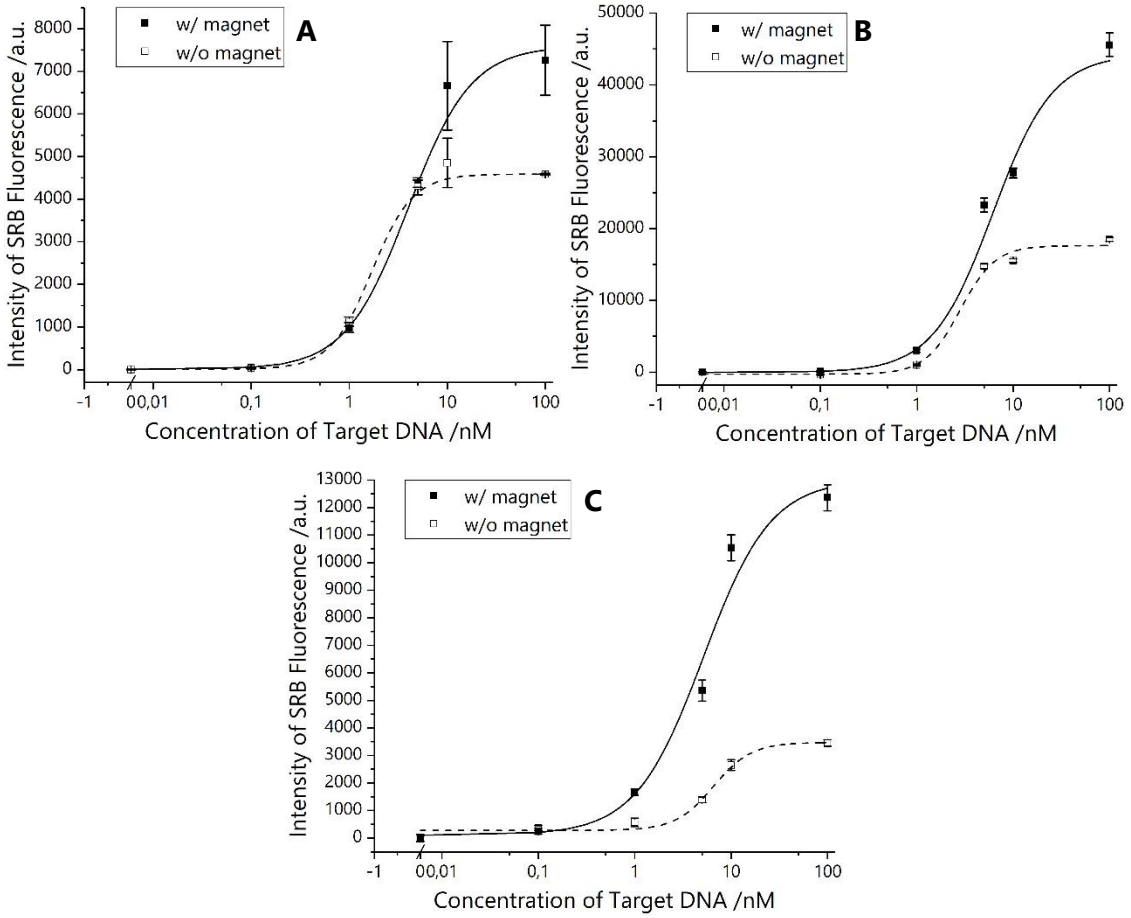

Figure 7: DNA sandwich hybridization assay with optimized b-liposomes before (**A**) and after (**B**) magnetic separation and concentration adjustment to 14.5%, as well as with i-liposomes after magnetic separation and concentration adjustment to 5% (**C**).

When comparing the different magnetosome systems (Table 1, Figure 8), it can be observed that in total the lowest LOD was obtained with optimized b-liposomes at 42 pM, being 3.4 times lower than in the absence of a magnetic field, while i-liposomes showed generally higher LODs, probably due to the lower fraction of liposomes with magnetic features in the mixture (only around 5%). Separating out non-magnetic liposomes in all cases increased the difference between the results for absence and presence of a magnetic field, yielding much better values with magnet, but the overall LODs worsened. We assume that, without magnetic separation, the non-magnetic liposomes present in the solution are dragged towards the magnetic field by their magnetic counter parts and thus higher binding rates can be observed. In contrast, when the same is done after magnetic clean up, this additional contribution ceases. Here, i-liposomes showed higher improvement than b-liposomes, possibly due to more room for progress as only a twentieth of the liposomes are magnetic instead of a seventh for b-liposomes. For all systems, linear ranges lie between 1 and 12 nM *C. parvum* target DNA, and for optimized systems, they improve in the presence of an external magnetic field.

Table 1: Statistics for magnetosome systems. Improvement for LOD and LOQ (the lower the better) is defined as *without magnet* divided by *with*, for sensitivity and maximum signal to noise ratio (the higher the better) as *with* divided by *without*.

		LOD /pM	LOQ /pM	sensitivity /slope*	max S/N**	linear range /nM
original b-liposomes	w/ magnet	449	1300	228	48	2 – 8
	w/o magnet	386	1070	142	55	2 – 7
	improvement	0.9	0.8	1.6	0.9	
optimized b-liposomes	w/ magnet	42	102	5675	1404	2 - 8
	w/o magnet	141	253	5251	527	1 – 3
	improvement	3.4	2.5	1.1	2.7	
optimized b-liposomes after magnetic separation	w/ magnet	162	388	34171	491	3 – 11
	w/o magnet	525	885	23300	176	2 – 5
	improvement	3.2	2.3	1.5	2.8	
original i-liposomes	w/ magnet	137	257	5966	813	2 – 4
	w/o magnet	97	205	5043	615	2 – 5
	improvement	0.7	0.8	1.2	1.3	
i-liposomes after magnetic separation	w/ magnet	314	880	8696	95	2 – 12
	w/o magnet	2459	4899	3843	31	4 – 11
	improvement	7.8	5.6	2.3	3.0	

* a.u.·$\log_{10}$nM^{-1} ** maximum signal to noise ratio

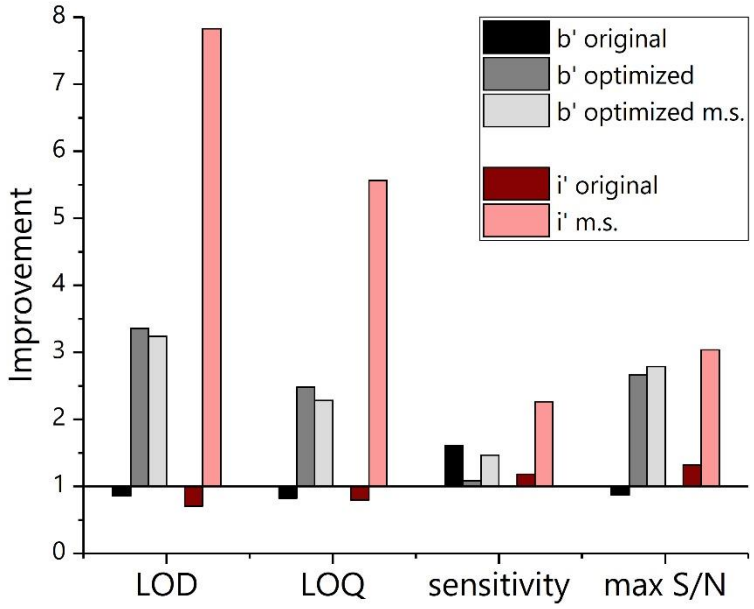

Figure 8: Comparison of improvement factors of different magnetosome systems and their optimizations. (=1: no difference between with and without magnet, >1: improvement with magnet, <1: worsening with magnet) Grey: b-liposomes (b'), original, optimized and optimized after magnetic separation (m.s.) with concentration adjustment to 14.5%. Red: i-liposomes (i'), original and after magnetic separation with concentration adjustment to 5%. LOD and LOQ are improved when the value is lower with magnet than without magnet, sensitivity and signal to noise ratio are improved if the value is rising by application of a magnetic field.

3.5 Conclusion

In previous studies the proof of principle of b-liposome generation and the achievement of an overall improvement factor of 15-fold in a DNA assay have been shown [12]. These liposomes were larger (hydrodynamic diameter of 357 nm) but not further investigated with respect to the percentage of magnetization. Here, we carefully studied two possible strategies to magnetize liposomes while keeping their signal amplification capability intact. Optimization strategies were investigated and liposomes were characterized in detail by DLS, TEM, ICP-OES and fluorescence measurements.

Overall, it was found that the inclusion of magnetic particles in the lipid bilayer was more successful than their encapsulation within the inner cavity. We assume that this is due to the hydrodynamic diameter of the nanoparticles and their concentration within an encapsulant solution. Theoretical calculations could fit a maximum of ~107 MNPs (spherical, 30 nm diameter) inside a liposome (spherical, 166 nm inner diameter), if fully packed. However, this is a purely theoretical number as such concentrated MNP solutions can hardly be prepared and as the hydrodynamic diameter of particles and their electrostatic repulsion is not included in this calculation, which would suggest in fact that only one MNP would fit into one liposome. In addition, achieving a theoretical amount of one particle per liposome would require about US$3500 per liposome batch. With the concentration chosen, 2% of liposomes are supposed to be magnetized, while our results found 5% magnetic liposomes. This suggests that the inner cavity encapsulation strategy is very efficient as it is close to the theoretical value and not many lipids or MNPs get lost during synthesis and purification.

In contrast, the bilayer incorporation synthesis was significantly less efficient. While a more or less 100% magnetization of liposomes was to be expected based on the MNP concentration chosen (5.6 particles per liposome), only a 14.5% efficiency was detectable. We assume that this is caused by the fact that the bilayer-entrapment is sterically and thermodynamically more challenging. Nevertheless, the costs for the production of the required amount of magnetic nanoparticles for insertion into the bilayer is under US$10 per liposome batch and can even be lowered when producing higher amounts per batch of particles. By surface modification with stable hydrophilic ligands, these particles might also be used for inner cavity encapsulation and thus could make this more efficient strategy accessible for higher particle amounts and further optimization.

This approach will be investigated in future studies, as well as MNPs with different size and composition, such as those made of cobalt, to achieve higher magnetization. Another interesting study will be conducted regarding the optimal proportion of magnetic to non-magnetic liposome,

as fascinatingly it was determined that non-magnetic liposomes are dragged towards the sensing surface by their magnetic counter parts and hence further overcome diffusion limitations. In addition it will be determined if strategies of immunomagnetic separation and magnetically enhanced detection can be combined in just one assay.

3.6 References

[1] DuPont HL, Chappell CL, Sterling CR, Okhuysen PC, Rose JB, Jakubowski W (1995) The Infectivity of *Cryptosporidium parvum* in Healthy Volunteers. N Engl J Med 332:855–859. doi: 10.1056/NEJM199503303321304.

[2] Abrahamsen MS, Templeton TJ, Enomoto S, Abrahante JE, Zhu G, Lancto CA, Deng M, Liu C, Widmer G, Tzipori S, Buck GA, Xu P, Bankier AT, Dear PH, Konfortov BA, Spriggs HF, Iyer L, Anantharaman V, Aravind L, Kapur V (2004) Complete genome sequence of the apicomplexan, *Cryptosporidium parvum*. Science 304:441–445. doi: 10.1126/science.1094786.

[3] Sparks H, Nair G, Castellanos-Gonzalez A, White AC (2015) Treatment of *Cryptosporidium*: What We Know, Gaps, and the Way Forward. Curr Trop Med Rep 2:181–187. doi: 10.1007/s40475-015-0056-9.

[4] Polsky-Cynkin R, Parsons GH, Allerdt L, Landes G, Davis G, Rashtchian A (1985) Use of DNA immobilized on plastic and agarose supports to detect DNA by sandwich hybridization. Clin Chem 31:1438–1443.

[5] Keller GH, Huang DP, Shih JW, Manak MM (1990) Detection of hepatitis B virus DNA in serum by polymerase chain reaction amplification and microtiter sandwich hybridization. J Clin Microbiol 28:1411–1416.

[6] Zhang N, Appella DH (2007) Colorimetric detection of anthrax DNA with a Peptide nucleic acid sandwich-hybridization assay. J Am Chem Soc 129:8424–8425. doi: 10.1021/ja072744j.

[7] Edwards KA, Curtis KL, Sailor JL, Baeumner AJ (2008) Universal liposomes: preparation and usage for the detection of mRNA. Anal Bioanal Chem 391:1689–1702. doi: 10.1007/s00216-008-1992-1.

[8] Madonna AJ, Basile F, Furlong E, Voorhees KJ (2001) Detection of bacteria from biological mixtures using immunomagnetic separation combined with matrix-assisted laser desorption/ionization time-of-flight mass spectrometry. Rapid Commun Mass Spectrom 15:1068–1074. doi: 10.1002/rcm.344.

[9] Fisher M, Atiya-Nasagi Y, Simon I, Gordin M, Mechaly A, Yitzhaki S (2009) A combined immunomagnetic separation and lateral flow method for a sensitive on-site detection of *Bacillus anthracis* spores - assessment in water and dairy products. Lett Appl Microbiol 48:413–418. doi: 10.1111/j.1472-765X.2008.02542.x.

[10] Wang H, Li Y, Wang A, Slavik M (2011) Rapid, sensitive, and simultaneous detection of three foodborne pathogens using magnetic nanobead-based immunoseparation and quantum dot-based multiplex immunoassay. J Food Prot 74:2039–2047. doi: 10.4315/0362-028X.JFP-11-144.

[11] Edwards KA, Baeumner AJ (2006) Liposomes in analyses. Talanta 68:1421–1431. doi: 10.1016/j.talanta.2005.08.044.

[12] Edwards KA, Baeumner AJ (2014) Enhancement of heterogeneous assays using fluorescent magnetic liposomes. Anal Chem 86:6610–6616. doi: 10.1021/ac501219u.

[13] Bangham AD, de Gier J, Greville GD (1967) Osmotic Properties and Water Permeability of Phospholipid Liquid Chrystals. Chem Phys Lipids 1:225–246. doi: 10.1016/0009-3084(67)90030-8.

[14] Lim J, Lanni C, Evarts ER, Lanni F, Tilton RD, Majetich SA (2011) Magnetophoresis of nanoparticles. ACS nano 5:217–226. doi: 10.1021/nn102383s.

[15] Amstad E, Kohlbrecher J, Muller E, Schweizer T, Textor M, Reimhult E (2011) Triggered release from liposomes through magnetic actuation of iron oxide nanoparticle containing membranes. Nano Lett 11:1664–1670. doi: 10.1021/nl2001499.

[16] Bonnaud C, Monnier CA, Demurtas D, Jud C, Vanhecke D, Montet X, Hovius R, Lattuada M, Rothen-Rutishauser B, Petri-Fink A (2014) Insertion of nanoparticle clusters into vesicle bilayers. ACS nano 8:3451–3460. doi: 10.1021/nn406349z.

[17] Steinhäuser C, Heigl U, Tchikov V, Schwarz J, Gutsmann T, Seeger K, Brandenburg J, Fritsch J, Schroeder J, Wiesmuller K-H, Rosenkrands I, Walther P, Pott J, Krause E, Ehlers S, Schneider-Brachert W, Schutze S, Reiling N (2013) Lipid-labeling facilitates a novel magnetic isolation procedure to characterize pathogen-containing phagosomes. Traffic 14:321–336. doi: 10.1111/tra.12031.

[18] Hofmann C, Roth G, Hirsch T, Duerkop A, Baeumner AJ (2019) Tethering functionality to lipid interfaces by a fast, simple and controllable post synthesis method. Colloids Surf B Biointerfaces 181:325–332. doi: 10.1016/j.colsurfb.2019.05.049.

[19] Park J, An K, Hwang Y, Park J-G, Noh H-J, Kim J-Y, Park J-H, Hwang N-M, Hyeon T (2004) Ultra-large-scale syntheses of monodisperse nanocrystals. Nat Mater 3:891–895. doi: 10.1038/nmat1251.

[20] Ohvo-Rekilä H, Ramstedt B, Leppimäki P, Slotte JP (2002) Cholesterol interactions with phospholipids in membranes. Prog Lipid Res 41:66–97. doi: 10.1016/S0163-7827(01)00020-0.

[21] Casals E, Galán AM, Escolar G, Gallardo M, Estelrich J (2003) Physical stability of liposomes bearing hemostatic activity. Chem Phys Lipids 125:139–146. doi: 10.1016/S0009-3084(03)00086-0.

[22] Jesorka A, Orwar O (2008) Liposomes: Technologies and analytical applications. Annu Rev Anal Chem 1:801–832. doi: 10.1146/annurev.anchem.1.031207.112747.

3.7 Supporting Information

3.7.1 Characterization of Magnetic Nanoparticles and Liposomes

The magnetic properties of the self-synthesized particles were compared to commercially available iron oxide nanoparticles with 30 nm diameter (30 nm MNPs) and magnetic beads with 1 µm in diameter (1 µm MBs). Therefore, the time was measured that is necessary to separate the particles from solution and attract them to a magnet. The self-synthesized particles with oleic acid as hydrophobic surface ligand (MNPs OA) have to be precipitated by addition of an antidispersant to be able to separate them magnetically from the ferrofluid, due to the formation of highly stable dispersions in cyclohexane (no sedimentation over several months). In comparison to that, the commercially available particles dispersed in aqueous solution are not nearly as stable (sedimentation within few days). Very similar attraction times of 40 to 71 seconds in the magnetic field were measured for all particles.

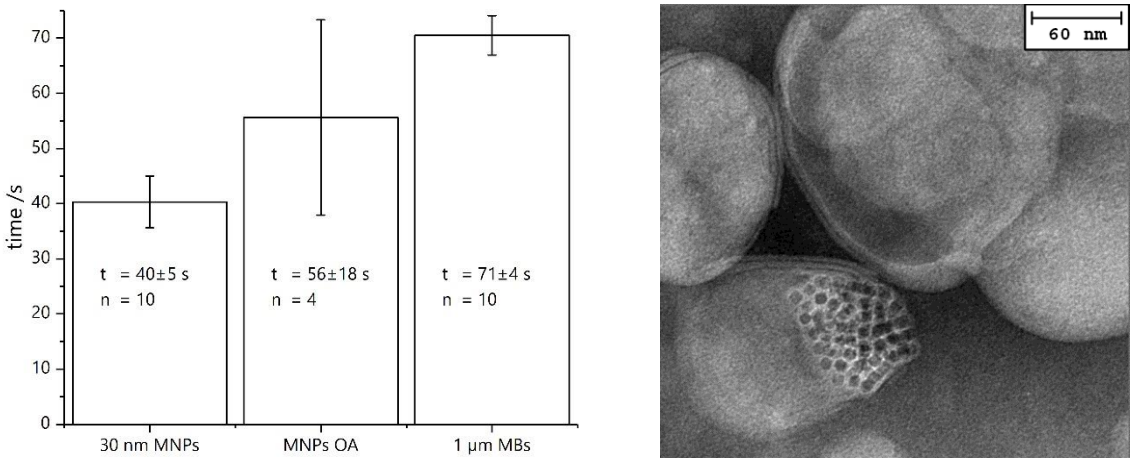

Figure S1: **left**: Magnetic attraction times of different nanoparticles. **right**: TEM image of original b-liposomes with incorporated MNPs with hydrophobic surface coating. To reduce the distortion of the membrane, particles accumulate at one side instead of spreading across the whole bilayer, forming Janus shaped vesicles.

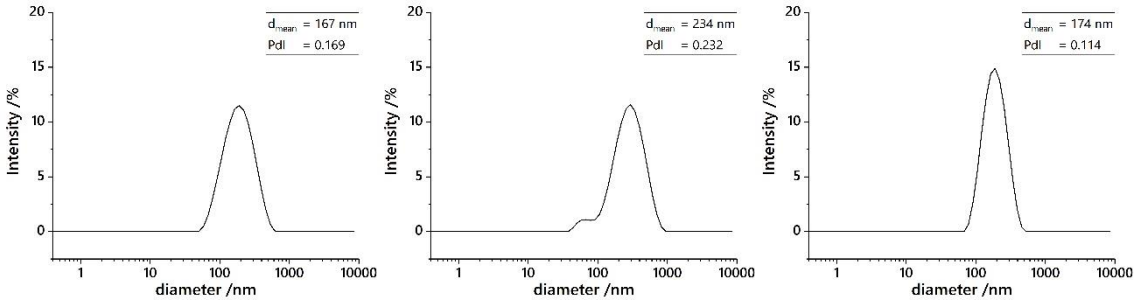

Figure S2: DLS measurement of original b-liposomes (**left**), optimized b-liposomes (**middle**) and i-liposomes (**right**).

Table S1: Hydrodynamic diameter, PdI and zeta potential of compared liposome systems

	hydrodynamic diameter /nm (PdI)	zeta potential /mV
b-liposomes original	167 (0.169)	(-20.6±1.6)
b-liposomes optimized	234 (0.232)	(-20.5±1.0)
i-liposomes original	174 (0.114)	(-21.3±1.4)

3.7.2 DNA Hybridization Assay Pre-Studies

To validate the magnetic abilities of the synthesized magnetosomes, a DNA hybridization sandwich assay was performed in parallel with and without the presence of an external magnetic field (Figure S3 left). In a first assay with original b-liposomes, LOD, LOQ and the maximum signal to noise ratio (max S/N) were 1.2 times better without than with magnet, respectively, although the sensitivity increased to 1.6 times at about the same linear range. Therefore, optimization of this assay was necessary.

Another liposome system encapsulated hydrophilic magnetic particles inside the inner cavity of the liposomes, aside with the signal molecules. A first assay showed no significant change when conducting the assay with or without the presence of an external magnetic field (Figure S3 right).

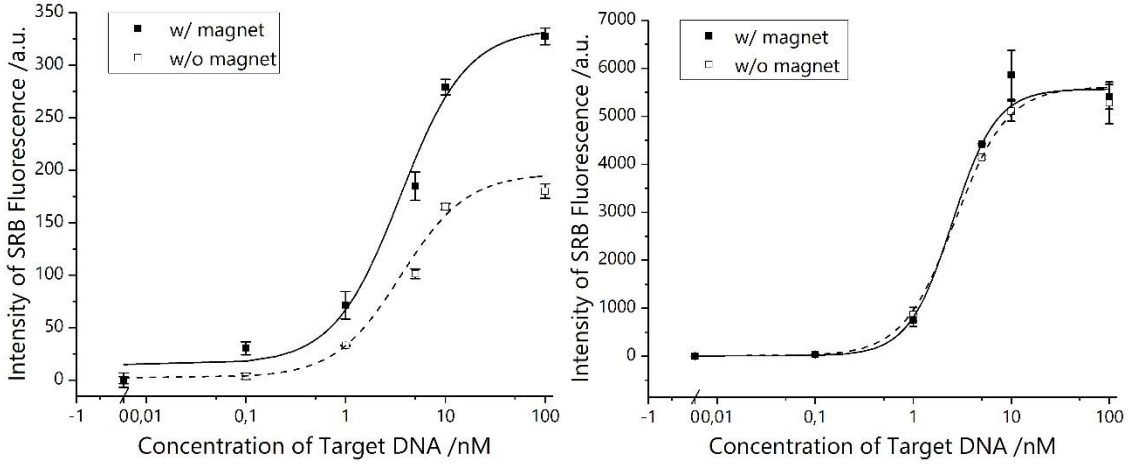

Figure S3: DNA hybridization sandwich assay with original b-liposomes (left) and original i-liposomes (right), performed with and without the presence of an external magnetic field.

4 A Microfluidic Magnetic-Coupling Device for the Production of Multifunctional Conjugates

4.1 Abstract

Bearing multiple functionalities dramatically increases capabilities of nanomaterials to enhance analytical assays by assisting in improving sensitivity, selectivity, sample preparation, or signal read-out strategies. Often these multiple functionalities can only be added post synthesis, especially in the case of surface functionalization or magnetization. Here, we developed a new microfluidic method to generate magnetic nanovesicles, which is impossible to be accomplished in bulk without risking the creation of large conglomerates. Carboxy group bearing, biotinylated, fluorescent liposomes were activated in bulk and covalently bound to amino group presenting magnetic particles immobilized through a magnetic field within microfluidic channels. Microfluidic design and coupling assay optimization resulted in 62% coupling efficiency when using 1 µm magnetic beads. However, this drops to just 13% when 30 nm magnetic nanoparticles (MNPs) are used. It is assumed that either crowding of the MNPs on the magnet and hence less available amino groups result in lower coupling efficiency, or that labeling with more MNPs per liposome is needed to render them sufficiently magnetic. Finally, both populations of tri-functional liposomes were applied to a biological binding assay demonstrating their superior performance in comparison to non-magnetic bi-functional liposomes.

This chapter is intended to be submitted for publication.

Author contributions:

The experimental work was carried out by the author. Franziska Beck assisted in the magnetic setup optimization. Vanessa Tomanek provided 3D graphics. Christian Griesche, Michael Mayer and Antje J. Baeumner contributed with discussions to microfluidic design and setup and strategic ideas. Antje J. Baeumner was the leader of this project.

4.2 Introduction

Liposomes are applied as common labels in analytical assays due to their potential to incorporate dyes that can be set free after binding and thus amplify the signal enormously [1]. This mechanism is especially useful when assays are conducted in microfluidic channels, where very low amounts of solution are applied and thus low binding rates are achieved. By the use of signal-amplifying liposomes instead of single dye molecules, the signal of every binding event can increase enormously and very sensitive microfluidic analysis systems can be designed [2, 3]. Furthermore, microfluidics are not only used to conduct (bio-)analytical assays, but also as synthesis platform, e.g., to produce liposomes with a particular size and size distribution. By varying parameters like flow dynamics or the lipid composition and concentrations, the resulting liposome characteristics can be tailored [4], and also the design of the microfluidic channel can determine aspects like the incorporation efficiency of bioreceptors in the lipid bilayer [5]. By the implementation of analytical tools like asymmetric flow field-flow fractionation combined with quasi-elastic light scattering and multiangle laser-light scattering, the dynamics of vesicle formation and influence of controlled mixing, e.g., by adjusting the ratio of volumetric flow rates of different solvent solutions, can be investigated [6]. Even the implementation of propane jet-freezing inside the microchannel to directly observe the newly formed liposomes *in situ* by cryo electron microscopy was conducted [7].

Although it is possible to tailor the production of liposomes towards their application by the use of microfluidics, a drawback of liposomes remains their large size of about 200 nm in diameter that is preferable to incorporate sufficient amounts of dye molecules for signal amplification, because it results in their slow diffusion to the point of interest compared to single dye molecules (diffusion coefficients can be assumed 150 times lower for liposomes than for Rhodamine dye molecules, for more information see SI). To overcome this problem, bifunctional liposomes with both magnetic and fluorescent properties can be employed to be able to attract them in a controlled manner due to a magnetic field and utilize their fluorescent abilities for signal generation. In previous works, magnetic nanoparticles have been incorporated into the lipid bilayer for analytical assay applications [8], but this method has the drawback that only small nanoparticles with low magnetization can be incorporated due to the distortion of the membrane by larger particles that would be attracted faster [9]. Encapsulation in the inner cavity of liposomes would also be possible, but has the drawback that less dye might be incorporated, as both dye and particles would be located in the same minute volume. A completely different strategy is the coupling of magnetic particles to the outside of liposomes after synthesis. This has the advantage

that particles of different size can be bound and as the same batch of liposomes can be tested in different coupling strategies, comparability of the results and reproducibility are higher.

The innovative properties of microfluidics to precisely control the convergence and mixing of components, have already been employed for the formation of multifunctional particles, e.g., by combination of quantum dots and magnetic particles to single Janus cores inside acrylate droplets [10], or by fusing liposomes of different composition by the use of microelectrodes [11]. In this work, we study the directed coupling of fluorescent liposomes to two different kinds of magnetic particle inside a microfluidic device for the formation of bifunctional labels to be applied in bioanalytical assays (Figure 1).

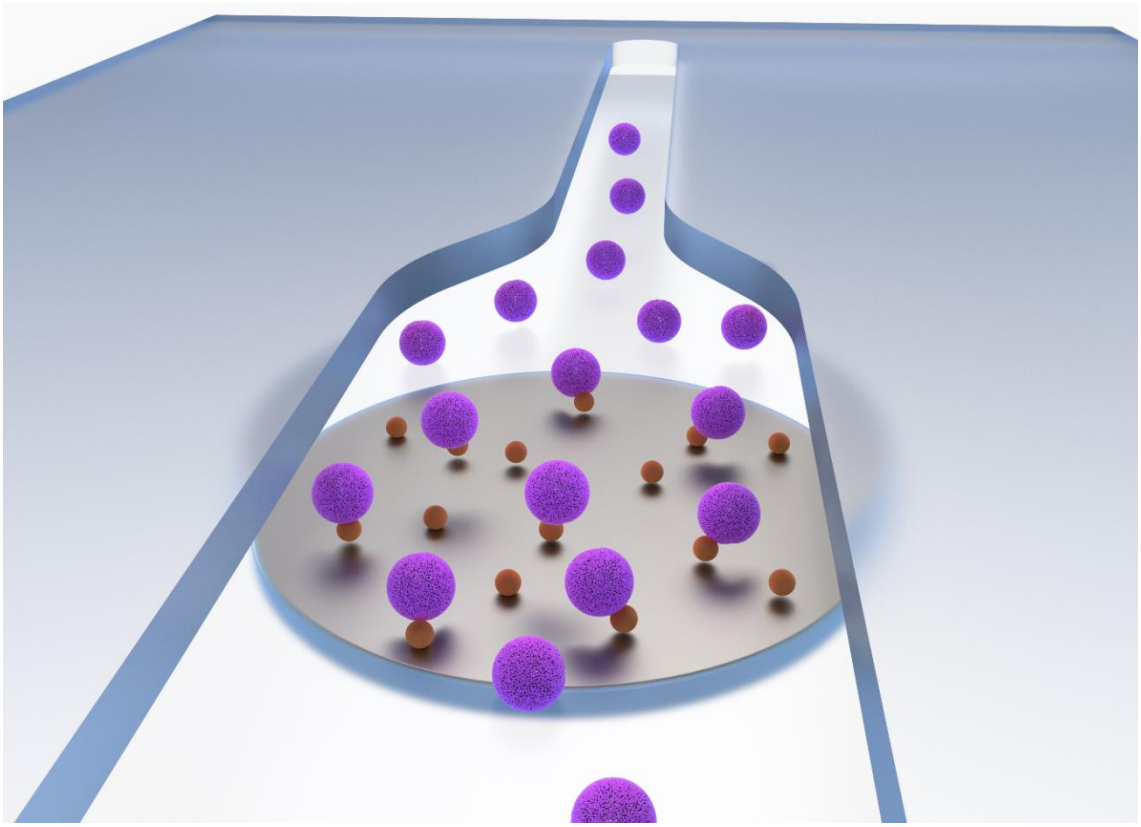

Figure 1: Scheme of the directed coupling of liposomes with magnetic nanoparticles inside a microfluidic channel. The particles are captured on a magnet while liposomes bind to the particles on their way through the channel. (provided by Vanessa Tomanek)

4.3 Materials and Methods

4.3.1 Chemicals and Instruments

Phospholipids, including 1,2-dipalmitoyl-sn-glycero-3-phospho-(1'-rac-glycerol) (sodium salt) (DPPG), 1,2-dipalmitoyl-sn-glycero-3-phosphocholine (DPPC), 1,2-dipalmitoyl-sn-glycero-3-phosphoethanolamine-N-(glutaryl) (sodium salt) (N-glutaryl-DPPE) and 1,2-dipalmitoyl-sn-glycero-3-phosphoethanolamine-N-(biotinyl) (sodium salt) (biotin-DPPE), were obtained from Avanti Polar Lipids, Inc. (www.avantilipids.com), n-octyl-β-D-glucopyranoside (OG) was bought from Roth (www.carlroth.com) and cholesterol and sulforhodamine B were purchased from Sigma Aldrich (www.sigmaaldrich.com).

Iron oxide (II,III) magnetic nanoparticle solution (30 nm diameter, amine functionalized, 1 $mg \cdot mL^{-1}$ in H_2O) and magnetic bead solution (approx. 1 µm in diameter, amine functionalized, 50 $mg \cdot mL^{-1}$ in H_2O) were both obtained from Sigma Aldrich (www.sigmaaldrich.com).

N-Hydroxysulfosuccinimide sodium salt (sNHS) was purchased from Sigma Aldrich (www.sigmaaldrich.com). 1-Ethyl-3-(3-dimethylaminopropyl)carbodiimide hydrochloride (EDC), chloroform, cyclohexane and methanol were purchased from Fisher Scientific (www.fishersci.com).

BSA (albumin fraction V from bovine serum), di-potassium hydrogen phosphate trihydrate, di-sodium hydrogen phosphate dihydrate, formamide, potassium chloride, potassium dihydrogen phosphate and tri-sodium citrate dihydrate were bought from Merck (www.merckmillipore.com). Sodium azide and hydroxyethyl)piperazine-1-ethanesulfonic acid (HEPES) were obtained from Sigma Aldrich (www.sigmaaldrich.com). Ficoll 400 and sodium chloride were purchased from Roth (www.carlroth.com) and sucrose was purchased from VWR (de.vwr.com).

All other chemicals were of analytical grade and purchased from either Roth (www.carlroth.com), Merck (www.merckmillipore.com), VWR (de.vwr.com) or Sigma Aldrich (www.sigmaaldrich.com).

HEPES buffer was prepared from 10 mM HEPES, 200 mM NaCl and 0.01% (w/v) NaN_3 with a pH of 7.5. For production of washing buffer, 0.05% (v/v) Tween 20 and 0.01% (w/w) bovine serum albumin were added to Phosphate buffered saline (PBS), which consisted of 137 mM NaCl, 2.7 mM KCl, 10 mM Na_2HPO_4 and 1.8 mM KH_2PO_4 and was adjusted to pH 7.4.

An extruder equipped with syringes, filter supports and membranes for extrusion of liposomes was obtained from Avanti Polar Lipids, Inc. (www.avantilipids.com). For column chromatography, sephadex G50 was obtained from Sigma Aldrich (www.sigmaaldrich.com).

For fluorescence measurements and determination of coupling efficiency, black or transparent MaxiSorp 96 well microtiter plates (MTPs) from Nunc purchased from Sigma Aldrich (ww.sigmaaldrich.com) or black 96 well half-area MTPs from VWR (de.vwr.com) were used. White streptavidin coated MTPs (KaiSA 96) with a biotin binding capacity of >14 pmol/well were obtained from Kaivogen Oy (kaivogen.com) for biotin-streptavidin assay. Fluorescence and absorbance measurements were performed with a BioTek SYNERGY neo2 (www.biotek.com).

4.3.2 Liposome Synthesis

For liposome synthesis, reverse phase evaporation according to an established procedure from Edwards et al. [12] was employed.

Therefore, 15 mg DPPC (20 µmol, 36%), 10 mg cholesterol (26 µmol, 46% of lipid composition) and 7.5 mg DPPG (10 µmol, 18%) are dissolved in 3 mL chloroform and 0.5 mL methanol. After sonication for 1 min, 2 mL of 10 mM SRB in 2 mM HEPES solution (pH 7.5) are added and the mixture is sonicated for another 4 min to form a microemulsion. Then, organic solvents are vaporized at a rotary evaporator at 60 °C under reduced pressure. After vortexing the mixture thoroughly, 2 mL SRB solution are added. The flask is positioned back at the rotary evaporator to eliminate any remaining organic solvent. The liposomes are extruded each 21 times at 60 °C through two polycarbonate membranes with 1.0 and 0.4 µm pores. Purification by size exclusion column chromatography (1.5 x 20 cm, Sephadex G50) is performed. Medium and high concentrated liposome containing fractions are collected and transferred to dialysis (molecular weight cut-off 12 – 14 kDa, spectrumlab.com) against HEPES buffer.

To achieve DNA reporter probe modified liposomes, 25 µL of a 300 µM solution of DNA tagged with cholesterol (15 nmol) are added with the lipid ingredients. For carboxy or biotin modification, N-glutaryl-DPPE and biotin-DPPE are added to the lipid mixture, respectively. Biotin-DPPE is always added as 2% of total lipids (1.5 µmol), but as liposomes with DPPE contents of more than 8% tend to form harder, N-glutaryl-DPPE is added as 6 (3.5 µmol) and 8% (5 µmol), respectively, depending on the presence or absence of biotin-DPPE.

The concentration of liposome solutions is determined with a Spectroflame-EOP inductively coupled plasma optical emission spectrometer (ICP-OES) from Spectro (www.spectro.com) or an ELAN 9000 (ICP-MS) from Perkin Elmer (www.perkinelmer.com), whereas hydrodynamic diameters and ζ-potentials were measured by dynamic light scattering (DLS) at 20 °C with a Malvern Zetasizer Nano-ZS (www.malvern.com) in disposable PMMA cuvettes (semi-micro) and disposable

PMMA capillary cells, respectively. Hydrodynamic diameters were determined 12 to 15 times for each sample and averaged, zeta potential 25 to 37 times.

4.3.3 Microfluidic Setup and Coupling Procedure

The microfluidic chip is produced with a laser scriber VLS2.30 from Universal Laser Systems (www.ulsinc.com). The channel is cut into double-sided adhesive tape (type 415 from 3M (www.3M.com), 100 µm in thickness), then a PMMA slide (1.6 mm in thickness) is glued on top and inlet holes are cut with the laser scriber. Afterwards a second PMMA slide is clued to the bottom to seal the channel. The PMMA slides were treated directly before mounting with UV/ozone treatment for 5 min with a Model 42 UV-ozone-cleaner from Jelight Company Inc. (www.jelight.com) to increase the hydrophilicity of the channel. The overall dimensions of the microfluidic chip are 3.3 x 60 x 30 mm, with a channel height of 100 µm and width from 1.5 to 3.85 mm (Figures 2A and 2B). Then the chip is inserted into a chip holder with underlying magnet holder plate, as represented in Figures 2C and 2D, and tubing is attached to connect the inlet and outlet holes with syringes mounted in Legato 180 syringe pumps from kd Scientific (www.kdscientific.com).

Before coupling can take place, carboxy modified liposomes have to be activated by EDC-sNHS coupling with a modified procedure by Bogdanov et al. [13]. Activated liposomes solution are prepared freshly each day and always used for three or four consecutive couplings. A typical activation solution contains 60 µM carboxy groups on the surface of liposomes and each 15 mM EDC and sNHS. Activation is performed for 20 min at 23 °C in a ThermoMixer C (online-shop.eppendorf.de).

Magnetic beads (1 µm in diameter, MB) are diluted with liposome outer buffer to 0.11 $mg \cdot mL^{-1}$, equaling 44 $nmol \cdot mL^{-1}$ amino groups, while magnetic nanoparticles (30 nm in diameter, MNP) are diluted to 0.17 $mg \cdot mL^{-1}$ (no number given for concentration of amine groups by producer). Ethanolamine is diluted to 25% (4.2 mM) with liposome outer buffer.

Four syringes are loaded with liposome solution, ethanolamine, buffer and MB/MNP solution, respectively. Liposomes are connected to the top inlet in Figure 2A, MBs/MNPs to the bottom inlet and ethanolamine and buffer are added through the middle inlet, syringes connected by a T-piece. Channels are filled by hand to ensure that no bubble remains. Flow speeds and volumes are given in Table 1. Liposomes are added in two steps: first faster to ensure total coverage of the magnetic particle spot with liposomes, than with very slow flow speed to ensure enough time for

sufficient coupling. After this procedure, the magnet plate is removed and the coupling product is flushed out by hand.

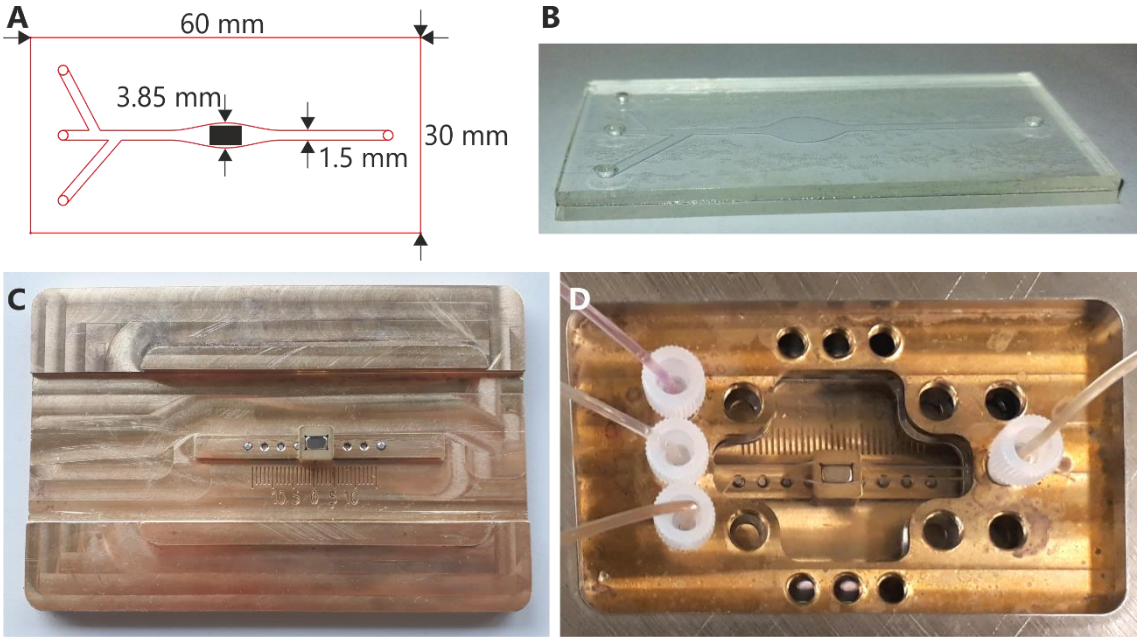

Figure 2: A: Shape and dimensions of the microfluidic chip. The black box represents the underlying magnet with a size of 5 x 3 mm. B: Image of the microfluidic chip made of two PMMA slides glued together by a double-sided adhesive tape in which the channel is laser cut. Inlet and outlet holes are also cut by a laser scriber into the top PMMA slide. C: Magnet holder plate. D: Microfluidic chip holder with magnet holder plate underneath and attached tubing.

Table 1: Microfluidic protocol with flow speed and volumes.

solution	flow speed /µL·min^{-1}	linear velocity /mm·s^{-1}			infused volume /µL	infused amount
		1.50 mm	3.95 mm	6.87 mm		
MB/MNPs	10	1.1	0.42	0.24	150	6.6 nmol amine groups / ~25 µg particles
liposomes	10	1.1	0.42	0.24	10	0.6 nmol carboxy groups
	1	0.11	0.042	0.024	70	4.2 nmol carboxy groups
ethanolamine	10	1.1	0.42	0.24	150	630 nmol amine groups
buffer	15	1.7	0.63	0.36	100	

Three different linear velocities are given as the channel has different widths over its length (see Figure 2 and Figure 4).

4.3.4 Concentration Determination

Concentration determination was performed with three different methods:

For florescence measurements, black 96 well half-area MTPs were used. For each calibration data point (2.5 to 50 µM total lipid) three wells are measured and for the sample 2 wells due to high

material consumption. The solutions are first measured in 25 µL solution in liposome outer buffer for background signal, than 2.7 µL 300 mM OG solution are added for liposome lysis and the fluorescence intensity is measured again.

For ICP-MS and ICP-OES measurements, a Spectroflame-EOP inductively coupled plasma optical emission spectrometer (ICP-OES) from Spectro (www.spectro.com) or an ELAN 9000 (ICP-MS) from Perkin Elmer (www.perkinelmer.com) were employed. Samples are diluted in 0.5 M HNO_3 to an end volume of 3 mL and the average of three measurements is used. A calibration curve from 1 µM to 50 µM phosphor was used.

Bartlett Assay was performed according to a protocol by Edwards et al. [12]. Briefly, 20 µL liposome and calibrations samples (prepared from K_2HPO_4 from 1.25 to 20 mM), respectively, or 400 µL microfluidic product are heated to 180 °C to complete dryness. Then, 15 mL 1.67 M H_2SO_4 are added and heated to 180 °C for 2 h. 100 µL 30% H_2O_2 is added and heated to 180 °C for 1.5 h. After each step, the solutions are cooled to room temperature and mixed thoroughly. 4.6 mL 0.22% ammonium molybdate and 0.2 mL Fiske-Subbarow reagent are added, heated in boiling water for 7 min and then quickly cooled in an ice bath. The absorbance of the solutions is measured in transparent MaxiSorp 96 well MTPs at 830 nm.

4.3.5 Determination of Coupling Efficiency

Consecutive washing steps in black half area microtiter plates were performed to determine fluorescence intensity of unlysed and lysed microfluidic product before and after magnetic separation.

Prior to measurement all wells are blocked with washing buffer (2 x 50 µL/well) and washed with HEPES buffer (2 x 50 µL/well). Then the microfluidic product (each 30 µL per well) is added. Analysis is performed with consecutive washing steps with fluorescence measurement after each step. First, the unaltered sample as collected from the microfluidic chip diluted in HEPES buffer (*pure* in Figure 5) as well as an equally diluted sample in OG solution for lysis (*pure lysed*) are measured. After measurement, the microtiter plate is positioned on a magnetic plate and the supernatant of the pure sample solution in HEPES buffer is taken off. The remaining beads are resuspended in HEPES buffer and measured again (*mag. sep.*). This step is repeated, but with addition of OG solution instead of HEPES buffer (*mag. sep. lysed*).

4.3.6 Biotin-Streptavidin-Binding Assay

Streptavidin coated MTPs were used for the following assay. All steps are performed in parallel on two identical MTPs, with the difference that while liposomes are incubating, one of the plates is positioned on a permanent magnet while the other one is positioned outside the magnetic field.

Before incubating the streptavidin-coated wells with biotin-containing liposome sample, each well is washed with washing buffer (2 x 200 µL/well) and HEPES buffer (2 x 200 µL/well). Then the microfluidic product (varying concentrations, 100 µL/well) is added and incubated for 60 min at room temperature. In between, both MTPs are positioned three times on a ThermoMixer C and shaken for 10 s. Unbound liposomes are removed and the wells are washed with HEPES buffer (2 x 200 µL/well).

Background fluorescence is measured in 100 µL HEPES buffer once. Afterwards, the supernatant is removed and octyl glycoside (30 mM, 100 µL/well) is added to lyse the liposome bilayer. After 5 min incubation, fluorescence is measured again.

4.4 Results and Discussion

4.4.1 Liposome and Magnetic Particle Characterization

Liposomes were synthesized using standard protocols [12] and then characterized regarding their hydrodynamic diameter (135 nm, PdI of 0.116) and zeta potential ((-25.2±1.2) mV) by DLS (see Figure S1), which are typical values for liposomes and yields dispersions with high colloidal stability.

Commercially available magnetic iron oxide nanoparticles (MNPs) were characterized by transmission electron microscopy and DLS, where the size was 30 nm according to TEM. When observing the hydrodynamic diameter of these particles, a significantly larger size and different populations of particles could be observed. Single particles or small aggregates, mainly visible after sonication of the solution, had a hydrodynamic diameter of around 200 nm, which can be caused by the surface modification of the particles and the resulting large solvent-shell. In addition, populations with 1000 and 5000 nm, most likely aggregates of particles, were present in the solution (Table S2, Figure S3). Applying the MNPs to the microfluidic coupling assay conditions (without coupling to liposomes) shows that both single particles and very large agglomerates cannot be found in the eluate anymore. We assume that the single MNPs are either washed out of the device initially or agglomerate mildly (Table S2, Figure S3). The very large MNP agglomerates are successfully eliminated as they either settle down in the channel or tubing or cannot be removed from the magnet anymore. When active liposomes are applied in the microfluidic system and coupling between liposomes and MNPs is performed, a slight increase of MNP diameter could be observed, which indicates that no extensive crosslinking occurs, but successful linkage takes place (Table S2, Figure S3). For commercially available magnetic beads (MBs), also DLS measurements were conducted, finding the expected hydrodynamic diameter of around 1 µm, that did not change significantly upon microfluidic treatment and also showed no crosslinking after the coupling reaction (Table S1, Figure S2).

4.4.2 Bulk Phase Coupling

Initially, the coupling of liposomes and particles in bulk solution was investigated, and the product was recorded via DLS in comparison to free liposomes, free MNPs (after sonication) and an uncoupled mixture of both. The resulting size distribution of the uncoupled mixture presented in Figure 3 shows two distinct peaks at ~100 and ~400 nm that can be assigned to pure liposomes and pure magnetic particles, while in the bulk coupling product the liposome peak at ~100 nm as well as a medium peak at ~1000 nm is visible, indicating some degree of coupling, while a

predominant peak at about 5000 nm indicates severe crosslinking and resulting huge clusters of liposomes and particles. This crosslinking was not surprising and cannot be prevented in bulk coupling strategies, as high concentrations of liposomes are needed in bioanalytical applications.

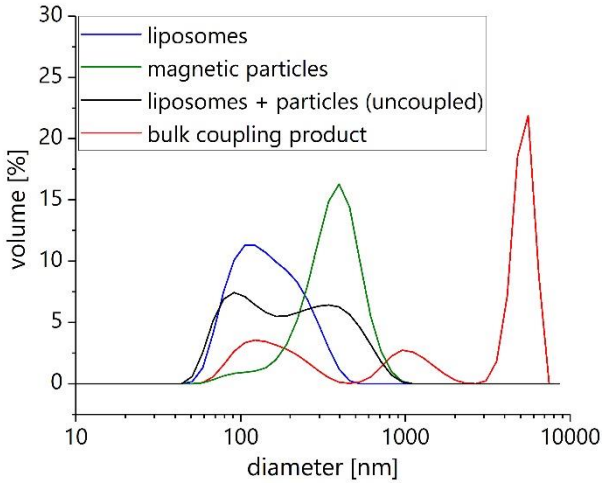

Figure 3: DLS measurement of pure liposomes, pure magnetic particles, a mixture of these two, and the product of a bulk coupling experiment.

Therefore, a strategy that prevents cross-linking was developed through coupling inside a microfluidic channel, enabling binding of the liposomes to the particles only from one side. Two differently dimensioned particles were investigated: MBs with a diameter of 1 µm and MNPs with 30 nm in diameter, both modified with amino groups at the surface. Together with the carboxy-modified liposomes a simple covalent coupling strategy can be realized in which liposomes are activated with a linker (EDC and sNHS), bonded to the MNPs/MBs, and remaining active binding sites are deactivated by flushing ethanolamine before magnetic release.

4.4.3 Channel Optimization

Various microfluidic channel designs were investigated to promote best spreading of magnetic particles on an external magnet, prevent clogging of the channel and create a large surface. In the end, a straight channel with a widened area above the external magnet turned out to be best. Here, depending on the widened channel cross section, magnetic beads collected can be tailored and can be reproducibly carried out (Figure 4A). Here, too narrow channels with respect to the magnet used can cause hotspot capturing which is undesirable for the here intended application. Also, complete coverage of the widened area is not possible with one external magnet due to accumulation at the border of the magnetic field (representation of magnetic field lines in Figure S6). Microfluidic coupling of liposomes to MBs in both chips shown in Figure 4 was done. ICP-OES analysis of the released magnetized liposomes showed that a 1.2-fold better yield could

be achieved in the wider channel design (Figure 4C), which we assume is due to the presented larger surface area and thus higher accessibility by the liposomes.

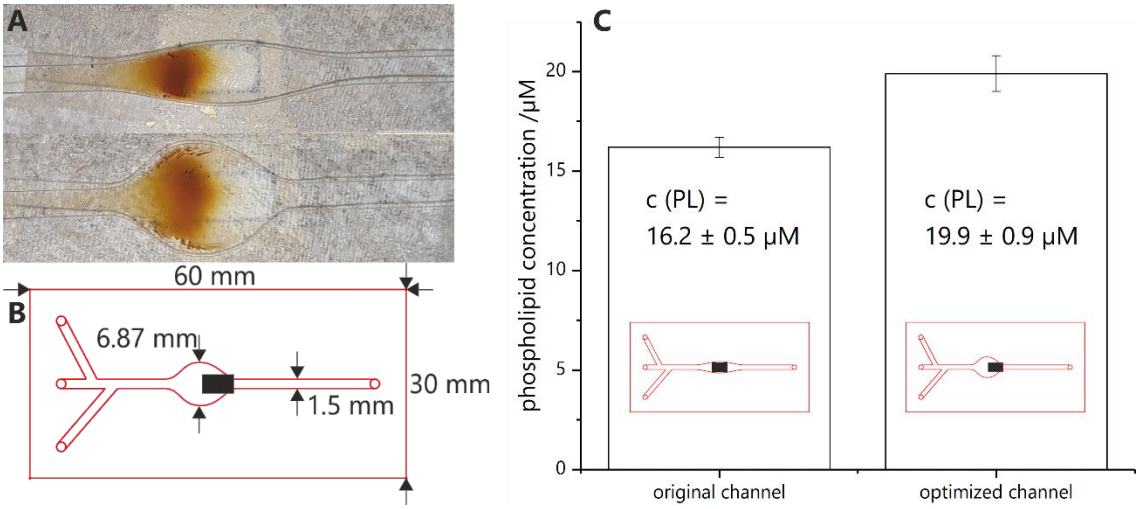

Figure 4: A: Same particle amount caught on original (top) and optimized (bottom) channel. B: Shape and dimensions of the optimized microfluidic chip. The black box represents the underlying magnet with a size of 5 x 3 mm. C: Comparison of phospholipid concentration measured by ICP-OES for original and optimized channel layout.

4.4.4 Coupling Efficiency

Although the channel is flushed substantially after coupling and prior to magnetic release, it must be assumed that a small number of free liposomes remain in the collected product solution. Therefore, the coupling efficiency of the product was determined by measuring the fluorescence of lysed and non-lysed microfluidic product before and after magnetic separation.

For MBs, it was found that (61.6±0.7)% of the liposomes appeared to be conjugated with magnetic particles (Figure 5 left). This is a substantial coupling efficiency considering that other strategies such as bilayer integration or encapsulation of MNPs yield in maximum a 15% magnetization (compare Chapter 3). Some loss of liposomes is observed due to lysis of the liposomes, as indicated by the free SRB dye available in the solution leading to an about 2.5 times higher fluorescence increase in the untreated microfluidic product than in the purified product.

Although the resulting particle diameter of liposome-MNPs is in the same size range as for liposome-MB products, a much lower coupling efficiency of only (12.7±0.4)% was observed (Figure 5 right), probably due to a lower number of amino groups on the surface of MNPs compared to MBs. Other factors are that MNPs are piling up on the magnet and thus less amino groups are available on the surface, resulting in a lower coupling efficiency, or that the coupling of more MNPs to each liposome might be needed to achieve sufficient magnetization Also, an increased fluorescence signal of the magnetically separated liposome-MNP product (2-fold over

non-separated product) indicates some rupture of liposomes as they are bound to more than one MNP and destroyed during their movement in the magnetic field.

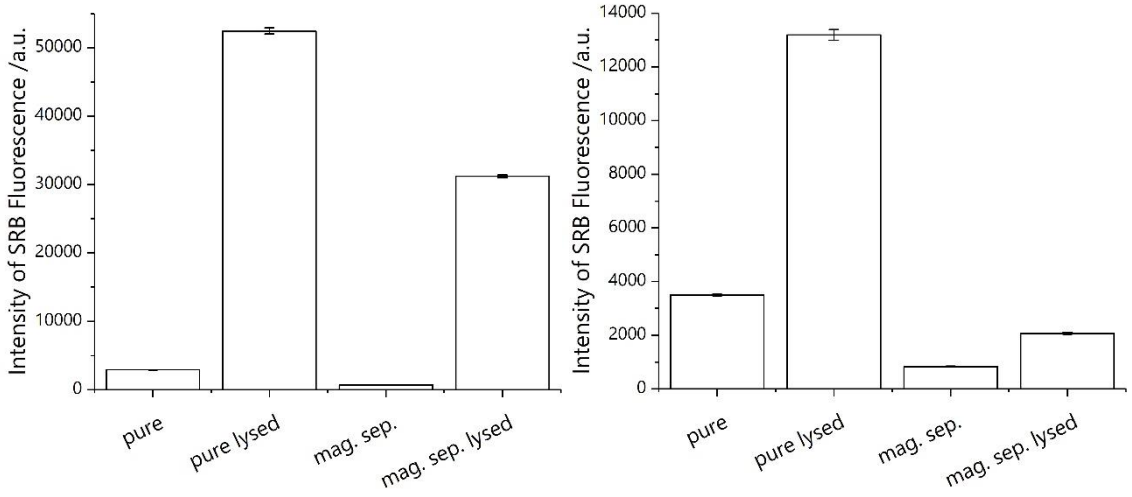

Figure 5: Coupling efficiency determined by fluorescence measurement of unlysed vs. lysed product with and without magnetic separation for coupling of liposomes to MBs (left) and MNPs (right).

4.4.5 Biotin-Streptavidin-Binding Assays

The analytical performance of the microfluidic product was evaluated by conducting biotin-streptavidin-binding assays using biotinylated liposomes. Specifically, these liposomes were synthesized bearing both a carboxy group and a biotin moiety on their outer surface. This moiety can obviously be exchanged for other bioreceptors for varying recognition purposes in the future.

Lipid concentration of the product was determined with fluorescence measurements, by ICP-MS/-OES and with the Bartlett assay. The total lipid concentration of the microfluidic product is determined to be between 34 and 48 µM (Table S3, Figure S7). For the following assays, a concentration of the undiluted microfluidic product of 40 µM was assumed.

When analyzing liposomes bound to MBs and MNPs in a bioassay, it was found that in all cases the magnetic coupling leads to superior bioassay performance in comparison to non-magnetic conditions (Figure 6). Furthermore, when concentrating liposomes coupled to MBs and MNPs via magnetic separation prior to conducting the bioassay, they performed even better, although their concentration was significantly lowered (from 40 µM to a maximum of 25 and 5 µM total lipid, respectively).

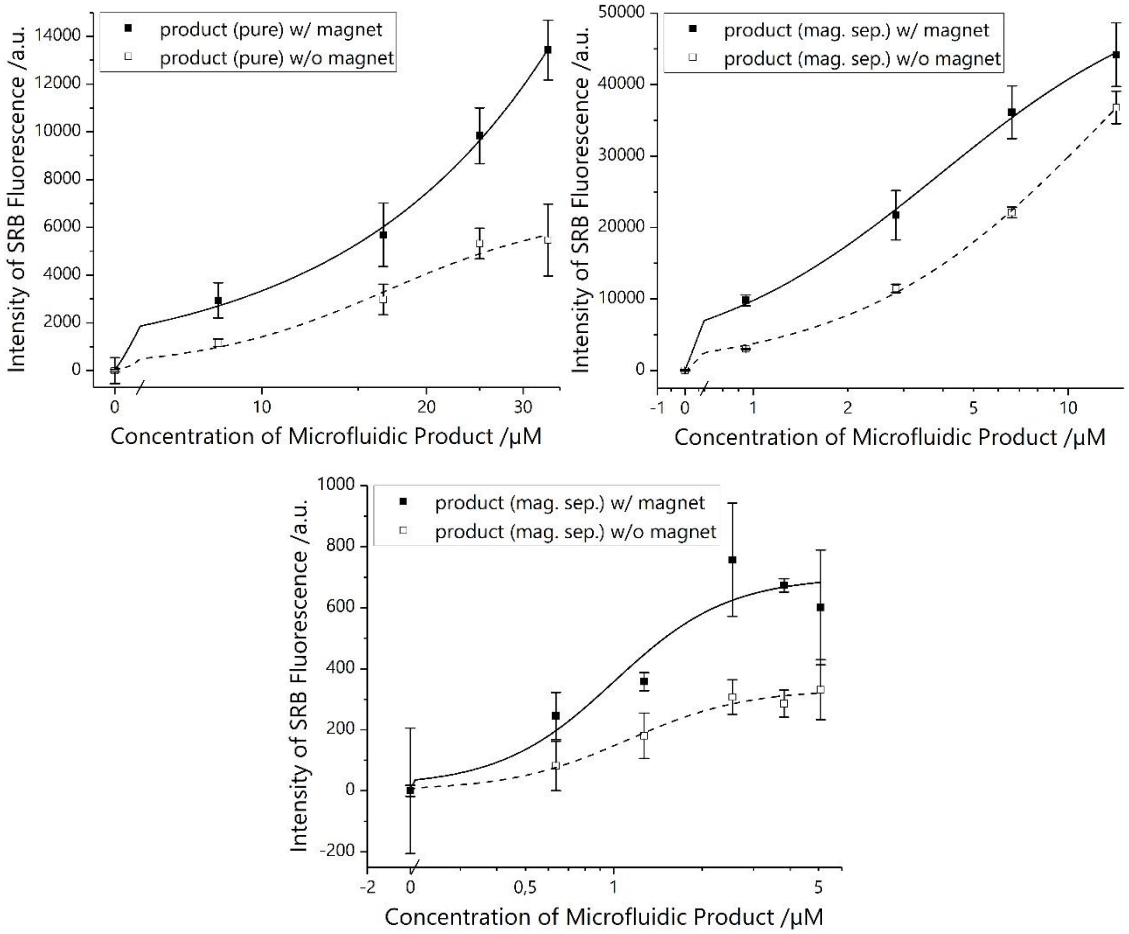

Figure 6: Biotin-streptavidin-binding assay with microfluidic coupling product between magnetic particles and liposomes bearing biotin on the surface, performed in parallel in the absence and presence of an external magnetic field. Left: Pure product with 1 µm MBs without any purification. Right: Product with 1 µm MBs after magnetic separation (mag.sep.), concentration given in percent of pure MB product (undiluted product after magnetic separation equaling 61.6% of pure MB product). Bottom: Product with 30 nm MNPs after magnetic separation (mag.sep.), concentration given in percent of pure MNP product (undiluted product after magnetic separation equaling 12.7% of pure MNP product).

4.5 Conclusion

The successful formation of liposome-magnetic particle conjugates directed by the controlled convergence in a microfluidic channel was accomplished. The resulting multi-functional compounds can be used as versatile label in various assays to amplify signals as well as improve binding affinities and assay times. For the linkage of magnetic microparticles (1 µm) with liposomes bearing biotin groups on the surface, a coupling efficiency of 62% could be observed, while with magnetic nanoparticles (30 nm), only 13% of the liposomes in the collected product were coupled to magnetic particles. A possible explanation for the five times higher coupling efficiency of MBs is that MNPs might bear a lower amount of amino groups on the surface (information is not provided by the supplier). This explanation is supported by the fact that the nanoparticles aggregated rapidly in solution and under the influence of an external magnetic field due to limited stabilization that would have been generated by high amino group concentrations. Overall, the microfluidic coupling strategy was highly successful, especially when compared to magnetization of liposomes using other strategies (see Chapter 3). There encapsulation of MNPs into the inner cavity or integration into the bilayer yields in maximum a magnetization efficiency of 15%. However, in contrast to those methods, MNPs and MBs are not shielded from the sample and may cause unwanted side reactions, which has to be investigated in the future, as well as different deactivation protocols to further reduce loss by crosslinking and mechanical rupture of liposomes during magnetic attraction. Also, assessment of different magnetic particle sizes, e.g., with diameters below and above 30 nm, will provide a better understanding of the binding behaviors of magnetic nanoparticles in the channel.

The developed microfluidic magnetic modification strategy is not limited to liposomes, but can be used also for other nanomaterials such as quantum dots or upconversion nanoparticles or with Raman labels like gold or silver nanomaterials. In addition, this method can easily be upscaled, for instance by parallelization of channels, by expanding the location and size of the magnetic field, etc. Already now, one chip can be reused for at least five coupling procedures. This is currently only limited by apparently low bonding strength as leakage of solution is observed. It is not limited by cleaning of the channels, which indicates that this method is very well suited for mass production of magnetized nanovesicles and nanoparticles.

4.6 References

[1] Edwards KA, Baeumner AJ (2006) Liposomes in analyses. Talanta 68:1421–1431. doi: 10.1016/j.talanta.2005.08.044.

[2] Connelly JT, Kondapalli S, Skoupi M, Parker JSL, Kirby BJ, Baeumner AJ (2012) Micro-total analysis system for virus detection: microfluidic pre-concentration coupled to liposome-based detection. Anal Bioanal Chem 402:315–323. doi: 10.1007/s00216-011-5381-9.

[3] Esch MB, Locascio LE, Tarlov MJ, Durst RA (2001) Detection of viable *Cryptosporidium parvum* using DNA-modified liposomes in a microfluidic chip. Anal Chem 73:2952–2958. doi: 10.1021/ac001508n.

[4] Carugo D, Bottaro E, Owen J, Stride E, Nastruzzi C (2016) Liposome production by microfluidics: potential and limiting factors. Sci Rep 6:25876. doi: 10.1038/srep25876.

[5] Balbino TA, Azzoni AR, La Torre LG de (2013) Microfluidic devices for continuous production of pDNA/cationic liposome complexes for gene delivery and vaccine therapy. Colloids Surf B Biointerfaces 111:203–210. doi: 10.1016/j.colsurfb.2013.04.003.

[6] Jahn A, Vreeland WN, DeVoe DL, Locascio LE, Gaitan M (2007) Microfluidic directed formation of liposomes of controlled size. Langmuir 23:6289–6293. doi: 10.1021/la070051a.

[7] Jahn A, Lucas F, Wepf RA, Dittrich PS (2013) Freezing continuous-flow self-assembly in a microfluidic device: toward imaging of liposome formation. Langmuir 29:1717–1723. doi: 10.1021/la303675g.

[8] Edwards KA, Baeumner AJ (2014) Enhancement of heterogeneous assays using fluorescent magnetic liposomes. Anal Chem 86:6610–6616. doi: 10.1021/ac501219u.

[9] Amstad E, Kohlbrecher J, Muller E, Schweizer T, Textor M, Reimhult E (2011) Triggered release from liposomes through magnetic actuation of iron oxide nanoparticle containing membranes. Nano Lett 11:1664–1670. doi: 10.1021/nl2001499.

[10] Zhao Y, Shum HC, Chen H, Adams LLA, Gu Z, Weitz DA (2011) Microfluidic generation of multifunctional quantum dot barcode particles. J Am Chem Soc 133:8790–8793. doi: 10.1021/ja200729w.

[11] Strömberg A, Karlsson A, Ryttsén F, Davidson M, Chiu DT, Orwar O (2001) Microfluidic device for combinatorial fusion of liposomes and cells. Anal Chem 73:126–130. doi: 10.1021/ac000528m.

[12] Edwards KA, Curtis KL, Sailor JL, Baeumner AJ (2008) Universal liposomes: preparation and usage for the detection of mRNA. Anal Bioanal Chem 391:1689–1702. doi: 10.1007/s00216-008-1992-1.

[13] Bogdanov AA, Klibanov AL, Torchilin VP (1988) Protein immobilization on the surface of liposomes via carbodiimide activation in the presence of N-hydroxysulfosuccinimide. FEBS Lett 231:381–384. doi: 10.1016/0014-5793(88)80854-8.

[14] Stokes AM, Wilson JW, Warren WS (2012) Characterization of restricted diffusion in uni- and multi-lamellar vesicles using short distance iMQCs. J Magn Reson 223:31–40. doi: 10.1016/j.jmr.2012.07.021.

[15] Gendron P-O, Avaltroni F, Wilkinson KJ (2008) Diffusion coefficients of several rhodamine derivatives as determined by pulsed field gradient-nuclear magnetic resonance and fluorescence correlation spectroscopy. J Fluoresc 18:1093–1101. doi: 10.1007/s10895-008-0357-7.

4.7 Supporting Information

4.7.1 Estimation of Diffusion Coefficients for Liposomes versus Dye Molecules

For the estimation of the diffusion coefficient of liposomes, the Stokes-Einstein equation (1) was used and the following approximations were made: liposomes were treated as rigid spheres with a diameter d_L of 200 nm and the viscosity η of pure water ($8.94 \cdot 10^{-4}$ Pa·s) was used [14].

$$D_L = \frac{k_B \cdot T}{3 \cdot \pi \cdot \eta \cdot d_L} \quad (1)$$

where k_B is the Boltzmann constant and T is the temperature (25 °C). A diffusion constant D_L of $2.8 \cdot 10^{-8}$ cm²·s⁻¹ was calculated. Compared to a mean diffusion constant for several Rhodamine dyes of around $4.2 \cdot 10^{-6}$ cm²·s⁻¹ [15], liposomes have an around 150 times smaller diffusion constant.

4.7.2 Liposome Characterization

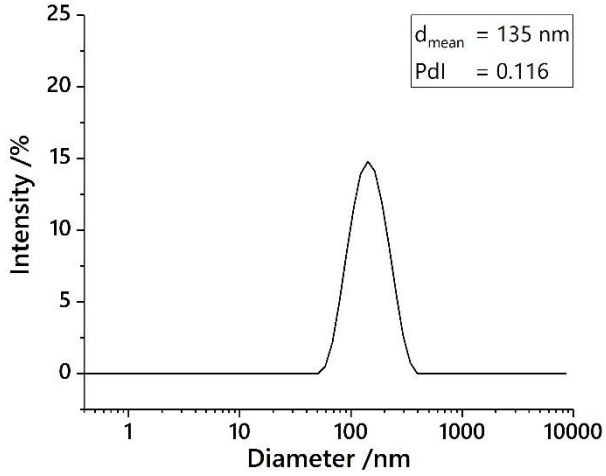

Figure S1: Hydrodynamic diameter of liposomes with 2% biotin-DPPE and 6% N-glutaryl-DPPE as determined by DLS.

4.7.3 Observation of Hydrodynamic Diameter Evolution during Microfluidics

To observe possible aggregation of magnetic particles due to magnetic capture inside the microfluidic channel, particles were captured and washed with buffer. The hydrodynamic diameter of these particles was compared to the diameter of pure particles from the stock solution, as well as with the microfluidic product after coupling with activated liposomes inside the microfluidic channel. MBs (~1 µm in diameter according to producer) show a (1.51±0.26)-fold increase in diameter after microfluidic treatment, which is too low for possible aggregation of particles,

indicating that the particles are stable during magnetic capture and microfluidic treatment. After microfluidic coupling with liposomes, the diameter increases by (1.54±0.24) times and the distribution is much broader than for the other measurements.

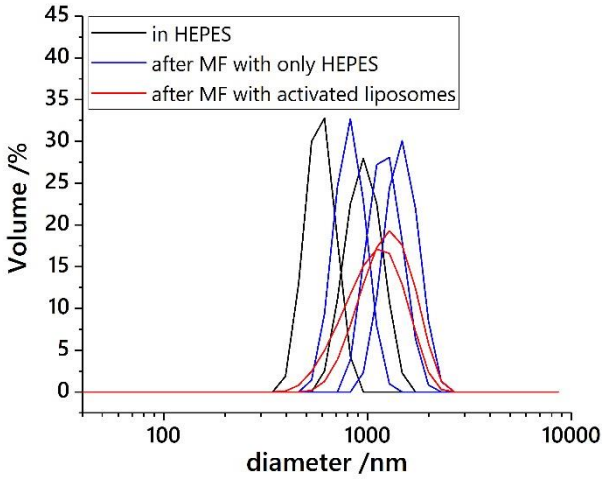

Figure S2: Hydrodynamic diameter of MBs (~1 µm according to producer) dispersed in HEPES buffer, pure (black), after microfluidic treatment with HEPES buffer (no coupling reaction with liposomes) (blue) and after coupling reaction with activated liposomes inside a microfluidic channel (red). (MF = microfluidics)

Table S1: Hydrodynamic diameter of MBs (~1 µm diameter according to producer) dispersed in HEPES buffer, pure, after microfluidic treatment with HEPES buffer (no coupling reaction with liposomes) and after microfluidic coupling with activated liposomes. The diameter ranges between ~950 and ~1100 nm with no clear trend visible.

	MBs in HEPES	**MBs after MF with only HEPES**	**MBs after MF with activated liposomes**
diameter (measurement 1)	(592±96) nm	(830±144) nm	(1121±351) nm
diameter (measurement 2)	(972±190) nm	(1236±233) nm	(1285±359) nm
diameter (measurement 3)		(1485±274) nm	
Z-Average (Average)	(782±106) nm	(1184±129) nm	(1203±251) nm

MF = microfluidics;

MNPs (30 nm in diameter according to producer) in pure stock solution show three different peaks. The peak at ~200 nm is most likely generated either by single particles with a thick water shell due to surface coating and measurement in buffer with high ionic strength, or by small aggregates like dimers or trimers. The other two peaks at ~1000 and ~5000 nm can be assigned to bigger aggregates. This assumption is fortified by the fact that sonication reduces the diameter of particles to a broad peak at ~350 nm, most likely produced by single particles as well as small aggregates, while the peak at ~5000 nm decreases, which indicates that still some huge aggregates are left, but less than in not sonicated solution. After microfluidic treatment with only HEPES buffer, only a peak at ~1000 nm remains. An explanation could be that the particles aggregate under the influence of the magnetic field, leaving no smaller aggregates or single particles in solution, while huge aggregates are caught in the channel or tubing, not finding their

way into the measuring cuvette in the end. After microfluidic coupling with activated liposomes, also only one peak is present, but at a slightly elevated diameter of ~1700 nm, which might contain nanoparticle aggregates in the same size as after microfluidics with only buffer but now coupled to liposomes, as well as larger nanoparticle aggregates.

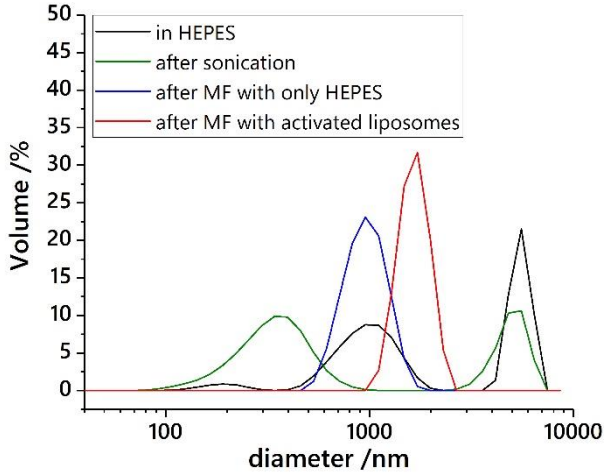

Figure S3: Hydrodynamic diameter of MNPs (30 nm according to producer) dispersed in HEPES buffer, pure (black), after sonication (green), after microfluidic treatment with HEPES buffer (no coupling reaction with liposomes) (blue) and after coupling reaction with activated liposomes inside a microfluidic channel (red). (MF = microfluidics)

Table S2: Hydrodynamic diameter of MNPs (30 nm diameter according to producer) dispersed in HEPES buffer; pure, after microfluidic treatment with HEPES buffer (no coupling reaction with liposomes) and after microfluidic coupling with activated liposomes;

	MNPs in HEPES	MNPs after sonication	MNPs after MF with only HEPES	MNPs after MF with liposomes
diameter (Peak1)	(192±42) nm	(354±139) nm	(974±228) nm	(1668±284) nm
diameter (Peak2)	(1008±307) nm	(4977±862) nm		
diameter (Peak3)	(5498±622) nm			

MF = microfluidics;

4.7.4 Development of Magnetic Setup

Different flow speeds were tested in a straight channel. It was observed that the optimum flow velocity for capturing magnetic beads is 10 µL·min^{-1} (Figure S4), which translates into 3.3 mm·s^{-1} linear velocity. When using a slower flow rate of 5 µL·min^{-1}, less beads were trapped on the magnet, because the particles already settled in the channel before reaching the magnet. With higher velocity, the beads flushed over the magnet, which is not strong enough anymore to accumulate them. These conditions obviously depend on the magnet used (here Ø2 x 1 mm, 130 g adhesive force, obtained from www.supermagnete.de) and the distance between magnet and bottom of the microfluidic channel, which is 100 µm here.

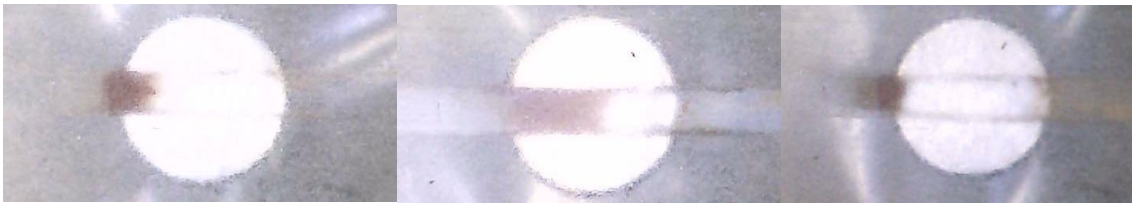

Figure S4: Pictures of three microfluidic channels loaded with the same amount of magnetic beads, but with different flow velocities: 5 µL·min^{-1} (**left**), 10 µL·min^{-1} (**middle**) and 15 µL·min^{-1} (**right**).

A small neodymium magnet (NdFeB, 5 x 5 x 3 mm, ~1 kg adhesive force, obtained from www.supermagnete.de) was employed for further experiments and the optimum orientation regarding the channel was investigated. As can be observed in Figure S5, the magnet captured the highest amount of magnetic beads in vertical arrangement (right image). Therefore, this orientation was used to create a magnet holder, which enables a simple and reproducible arrangement of the experimental setup for further experiments.

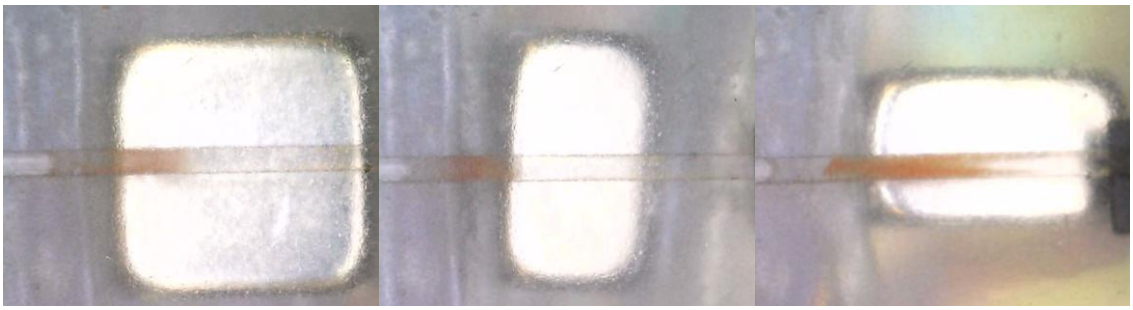

Figure S5: Pictures of three microfluidic channels loaded with the same amount of magnetic beads with same flow velocity, captured on a 5 x 5 x 3 mm magnet in three different orientations.

The magnetic field lines of the magnet were investigated with ferrum powder and are depicted in Figure S6. Their arrangement explains the broad band of particles captured at the front edge of the magnet (compare Figure 4A) as there the particles enter the magnetic field and are stopped.

Figure S6: Images of ferrum powder with underlying magnet, top view as presented in the channel (**left**) and side view perpendicular to the channel (**middle)**. **right**: Scheme of the magnet (grey, top view) with channel (red) and magnetic field lines (black).

4.7.5 Concentration Determination

For concentration determination of the microfluidic product, first the routinely used ICP-MS and –OES detection was employed, but as the microfluidic product is very low concentrated, a huge amount of material (~200 µL for MS, ~500 µL for OES) is necessary to end up in the measureable range. In addition, the measured concentrations (Table S3) are quite inconsistent, especially for magnetically separated samples. Therefore, other methods for determining the vesicle concentration in the microfluidic product were investigated.

Table S3: Measured total lipid concentrations from ICP. Mean concentration without magnetic separation is (41±9) µM, with magnetic separation (23±3) µM.

ICP-MS pure	ICP-OES pure	ICP-MS magnetic separation	ICP-OES magnetic separation
48 µM	40 µM	35 µM	6 µM
71 µM	35 µM	45 µM	
52 µM	28 µM		
21 µM			
(48±18) µM	(34±5) µM	(40±6) µM	6 µM

Fluorescence measurements in half-area MTPs were conducted, where each well is filled with 25 µL solution, which reduces the consumed material by 8 to 20 times. A concentration of (36±1) µM was determined, which deviates from the ICP-determined mean value by 13%. Another drawback of this method is that for the calibration curve pure liposomes are used, while the sample contains magnetic particles, which absorb and scatter light. This effect cannot be controlled totally, as the concentration of particles in the solution is as unknown as the lipid concentration.

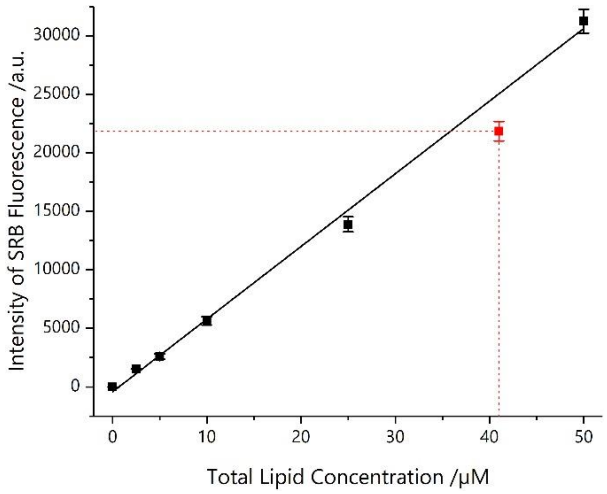

Figure S7: black: Calibration curve of pure liposomes (lipid concentration determined by ICP-OES) and red: total lipid concentration of microfluidic product as determined by ICP-MS/-OES. Fluorescence-determined concentration is (36±1) µM (13% deviation from mean ICP-MS/-OES value).

A third methods examined, the Bartlett assay, unfortunately did not produce reproducible results.

Therefore, a mean concentration of (40±6) µM total lipid, calculated from ICP-MS, ICP-OES and fluorescence measurements, is assumed for the microfluidic product used for the biotin-streptavidin-binding assays, as concentration determination of each individual sample affords a too high material consumption. For the proof-of-principle studies shown here, the assessment suffices. However, in the future, with an upscaled microfluidic setup, ICP-OES can be used for accurate concentration determination as larger volumes and amounts of magnetized nanovesicles are produced.

5 Studies for the Preconcentration of P24 by Liposomes

5.1 Abstract

The HIV capsid protein p24 was detected by single-particle-fluorescence-imaging of a sandwich assay between magnetic microparticles, p24 and a fluorescent label. To increase the sensitivity of this method, preconcentration of p24 with liposomes was tested, where the aim is to use magnetic liposomes for easy accumulation. In this work, preliminary studies were conducted. These studies arrived at the conclusion that the signal of the assay could be doubled by preconcentration. Nevertheless, the reaction of MP-p24 with free liposomes, instead of liposome-p24 with free MPs, was favored, most likely due to steric reasons. As p24 should be quite lipophilic, it possibly interacts with the phospholipids, which might hinder the described assay and block binding sites of p24. Thus, experiments were repeated with neutrophil gelatinase-associated lipocalin (NGAL), a more hydrophilic protein, to verify this theory. The analysis with NGAL showed the same behavior as with p24 regarding preconcentration and the reagent addition order. Unfortunately, significantly higher signals were reached for the reaction of MPs directly binding to liposomes, instead of a construct with NGAL as a sandwich.

This chapter has not been published.

Author contributions:

All experiments described in this chapter were performed by the author herself, and were conducted at Abbott Diagnostics in Lake Forest, IL, in cooperation with Patrick MacDonald, who also conducted preliminary functionalization of antibodies and other reagents and drew parts of the schemes. The author wrote this chapter. Liposome synthesis and functionalization were carried out by Carola Hofmann. Sergey Tetin, Thomas Hirsch, Axel Duerkop and Antje J. Baeumner contributed with strategic discussions. Antje J. Baeumner was the leader of this project.

5.2 Introduction

The protein p24 is a part of the human immunodeficiency virus (HIV) and serves as a marker for HIV infection. The 24 kD domain of the Gag polyprotein, which is a main structural part of HIV-1, forms a capsid around the virus RNA [1, 2]. For HIV diagnosis, the detection of minute amounts of p24 is necessary, and therefore a single-particle-fluorescence-measurement method was used, where images of magnetic microparticles (MPs) located by bright field microscopy are matched with the same images taken under fluorescence excitation [3]. An example can be seen in Figure 1. P24 is captured on the particles by a sandwich antibody assay and fluorescence labeling is performed for detection. This method is very sensitive, but for early diagnosis, the LOD has to be lowered further. As the critical point is the random encounter of p24 and MPs in solution, new methods of preconcentration are necessary. Therefore, liposomes should be used as a capturing element that can be accumulated and easily eliminated.

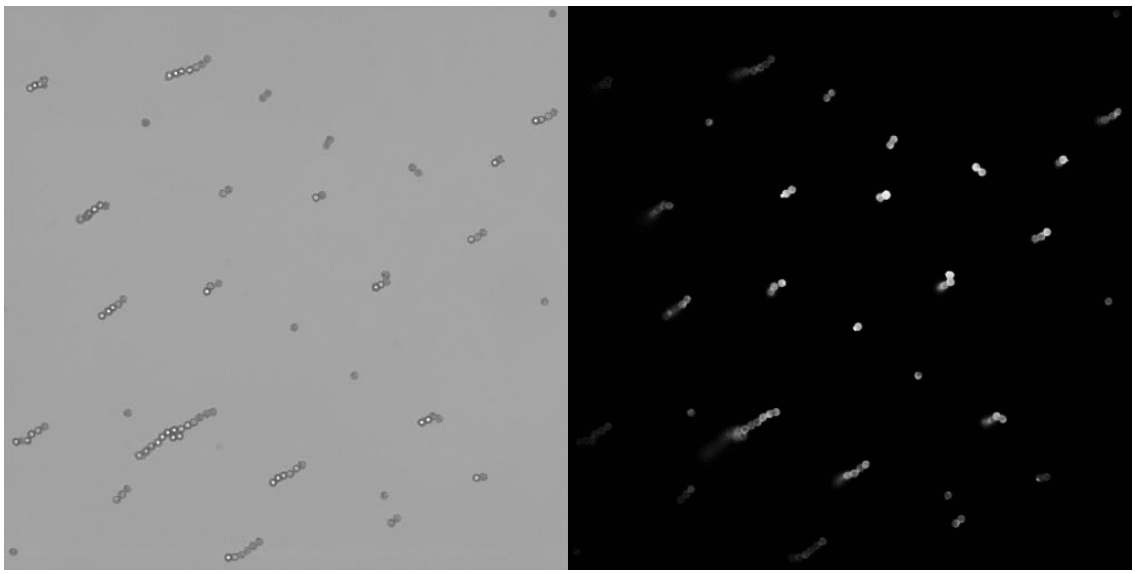

Figure 1: Images of fluorescently labeled MPs taken in bright field (left) and with fluorescence excitation (right).

Liposomes are composed of phospholipids and cholesterol, but additionally functionalized lipids with bioreceptors can be introduced. The bilayer forms a hydrophilic space inside the liposomes and this cavity can be filled with a high variety of aqueous solutions, e.g., dye solutions or buffer. The vesicles have a certain size, in this study they are about 100 to 200 nm in diameter, which is about 30 times smaller than the 5 µm MPs that are used for single-particle-measurements, which lets liposome migrate faster in solution than MPs. Therefore, they should be able to bind p24 more efficient than MPs.

For simple accumulation of the liposome-p24-conjugate, liposomes modified with magnetic elements can be used, which allows magnetic attraction of the conjugate. Then the cohesion of

lipids in the vesicle can be destroyed by detergent addition or mechanical stress like ultrasound or high temperature, to set the p24 free. This is an advantage over the use of smaller magnetic nanoparticles to accumulate p24, as this would hold the necessity to unbind the analyte from the surface of the magnetic particles. Alternatively, liposomes without magnetic features can be accumulated by centrifugation. In the end, both cases yield preconcentrated p24 that is already bound from one side by the bioreceptor on the liposomes. As a fluorescent labeling of p24 is necessary for the described detection method, dye filled liposomes can be used and act directly as fluorescent label without lysis. Alternatively, liposomes can be destroyed to set p24 free. Then a bifunctional bioreceptor should be used to be able to fluorescently label p24.

5.3 Experimental Part

5.3.1 Materials and Methods

1,2-dipalmitoyl-sn-glycero-3-phospho-(1'-rac-glycerol) (sodium salt) (DPPG) and 1,2-dipalmitoyl-sn-glycero-3-phosphocholine (DPPC), as well as extruder kit, polycarbonate membranes and filter supports were obtained from Avanti Polar Lipids, Inc. (www.avantilipids.com), while sulforhodamine B and cholesterol were purchased from Sigma Aldrich (www.sigmaaldrich.com) and n-octyl-β-D-glucopyranoside (OG) was bought from Roth (www.carlroth.com). Dialysis membranes with a molecular weight cut-off of 12 – 14 kDa were purchased from spectrum labs (www.spectrumlabs.com). 4-(2-Hydroxyethyl)piperazine-1-ethanesulfonic acid (HEPES) and sodium azide were obtained from Sigma Aldrich (www.sigmaaldrich.com).

Oligonucleotides with cholesterol and dye-tag were purchased either from Metabion (www.metabion.com) or from Integrated DNA Technologies (www.idtdna.com).

All other chemicals were of analytical grade and obtained from either VWR (de.vwr.com), Merck (www.merckmillipore.com), Roth (www.carlroth.com) or Sigma Aldrich (www.sigmaaldrich.com). Double distilled water was used for the preparation of aqueous solutions.

Each experiment was performed in 100 µL volume in a 96 well plate with glass bottom and for each well four spots were imaged once by bright field and once by fluorescence microscopy.

Different magnetic microparticles, available at Abbott Labs, were used: streptavidin-coated (SA-MPs), anti-p24 antibody-coated (HIV-MPs), anti-NGAL antibody-coated and goat anti-mouse antibody-coated Polymer Labs carboxyl particles (GAM-MPs).

P24 and cy3-p24 were diluted in washing buffer (PBS, 0.05% Tween20, 1% BSA) to the desired concentrations. Neutrophil gelatinase-associated lipocalin (NGAL) was used as ready-to-use kit solutions in phosphate buffer with protein stabilizers provided by Abbott Labs. OG was dissolved in double distilled water. All other solutions for single-particle-fluorescence-analysis were diluted in PBS. Fragment antigen binding (Abbott developed)-sequence 16-biotin (Fab-oligo2-bt) was prelinked by the cooperation partner and purified by HPLC. Also, coupling of oligo1-liposomes with Fab-oligo2-bt and modification of liposomes with monoclonal antibody (mAb, Abbott developed) was conducted by the cooperation partner. Labeling was performed either with streptavidin-phycoerythrin (SA-PE) or with Alexa546 dye labeled anti-p24-antibody (Alexa-Ab).

In the described experiments, an addition of 10 µL Fab-oligo2-liposomes (Fab-lip) correspond to 5 mM lipids in the incubation solution, and microparticle solutions contain 0.1% solids. Incubation was performed at 30 °C during shaking at 750 rpm on a BioShake iQ or at room temperature in a rotating vial holder (in case of samples intended for centrifugation). A magnetic plate washer (BioTek ELx50) was used to wash the magnetic particles, and after the last washing step, solutions were transferred to new wells. An Olympus Ix81 fluorescence microscope at 20x magnification was used for single-particle-fluorescence-analysis (561 nm laser light, 30% power, 100 ms acquisition time, 4 acqs/sample).

5.3.2 Liposome Synthesis

Liposomes were synthesized by Carola Hofmann according to a modified procedure by Edwards et al. [4]. Briefly, 10 mg cholesterol (51.7 µmol), DPPC (40.3 µmol) and DPPG (21 µmol) were dissolved in 0.5 mL methanol and 3 mL choloform. The oligonucleotide (sequence: 5′ AAT CCA CCT TAG AGT ACA AAC GGA ACA CGA GAA AAG 3′), tagged with cholesterol at the 3′-end, was added as solution in a solvent mixture of methanol and water (1:4). The solution was sonicated for 1 min, 2 mL encapsulant (1 mM SRB and 150 mM NaCl in 7.5 mM HEPES, pH 7.5) were added and the mixture was sonicated for a further 4 min. Organic solvents were evaporated at the rotary evaporator at 45 °C under reduced pressure. The mixture was vortexed thoroughly and 2 mL encapsulant was added. The flask was transferred back to the rotary evaporator to get rid of any remaining organic solvent. The resulting liposomes were extruded each 21 times at 50 °C through two polycarbonate membranes with 1.0 and 0.4 µm pores. The solution was purified by column chromatography (1.5 x 20 cm, Sephadex G50). Liposome containing fractions were transferred to dialysis against buffer (10 mM HEPES, 200 mM NaCl, 0.01% NaN_3, pH 7.5).

Phospholipid concentrations were determined by ICP-OES using a Spectroflame-EOP (www.spectro.com). Hydrodynamic diameters measured by dynamic light scattering and zeta potential measurements were conducted with a Malvern Zetasizer Nano-ZS (www.malvern.com) [5].

5.3.3 Comparison of P24 versus Cy3-P24 as well as Fab Fraction 3 versus Fraction 4 Binding Affinity

Table 1: Experimental procedure for the comparison of p24 and cy3-p24 as well as Fab fraction 3 and 4

HIV-MPs	p24	cy3-p24	inc/ wash	Fab-oligo2-bt fraction 4	Fab-oligo2-bt fraction 3	inc/ wash	SA-PE	inc/ wash
2 µL	8 pM 2 pM ✗	✗	30 min	1 nM	✗	30 min	1 nM	15 min
	8 pM ✗	✗		✗	1 nM			
	✗	8 pM ✗		1 nM	✗			

inc = incubate

5.3.4 Effect of Reagent Addition Order and Lipid Interference Study

This experiment was performed twice, once without lysis of liposomes and detection of the fluorescence signal of encapsulated SRB, and once with lysis of liposomes and consecutive labeling with SA-PE.

Table 2: Experimental procedure for analysis regarding reagent addition order without lysis and with detection by SRB encapsulant

MPs/lip	p24	inc/wash	centrifuge	lip/MPs	inc/wash
2 µL HIV-MPs	24 pM	30 min	✗	10 µL Fab-lip	1 h
10 µL Fab-lip 5 µL Fab-lip 1 µL Fab-lip	24 pM	1 h	1x 10 min 10.000 g	2 µL HIV-MPs	30 min
10 µL Fab-lip 5 µL Fab-lip 1 µL Fab-lip	✗				
✗	24 pM	✗	✗	2 µL HIV-MPs	30 min

Table 3: Experimental procedure for analysis regarding reagent addition order with lysis and detection by SA-PE labeling

MPs/lip	p24	inc/ wash	centrifuge	lip/MPs	inc/ wash	lyse	inc/ wash	add	inc/ wash
2 µL HIV-MPs	24 pM	30 min	✗	10 µL Fab-lip	1 h	30 mM OG	30 min	1 nM SA-PE	30 min
10 µL Fab-lip	24 pM	1 h	1x 10 min 10.000 g	2 µL HIV-MPs	30 min				
5 µL Fab-lip									
1 µL Fab-lip									
10 µL Fab-lip	✗	1 h	1x 10 min 10.000 g	2 µL HIV-MPs	30 min				

5.3.5 Binding of P24-Fab151-Sequence 16-Biotin to either Streptavidin-Microparticles or Anti-P24-Microparticles after Lysis

Table 4: Experimental procedure for a bindingstudy of p24-Fab-oligo2-bt to either streptavidin-microparticles or anti-p24-microparticles after lysis

Fab-lip	p24	inc/ wash	centrifuge	lysis	MPs	inc/ wash	dye	inc/ wash
10 µL	72 pM	2 h	1x 10 min 10.000 g	30 mM OG	2 µL SA-MPs	30 min	1 nM Alexa-Ab	30 min
	24 pM							
	✗							
	24 pM		1x 10 min 10.000 g		2 µL HIV-MPs		1 nM SA-PE	
	✗							
	24 pM		✗		2 µL HIV-MPs		1 nM SA-PE	
	✗							

5.3.6 NGAL Experiments

Table 5: Experimental procedure for analysis regarding reagent addition order

anti-NGAL-MPs	NGAL	inc/ wash	NGAL	mAb-lip	inc/ wash	anti-NGAL-MPs	lysis	inc/ wash	dye	inc/ wash
2 µL	10 ng/mL	30 min	✗	10 µL	1 h	✗	30 mM OG	30 min	1 nM SA-PE	15 min
	✗		10 ng/mL			2 µL				

Table 6: Experimental procedure for preconcentration studies

mAb-lip	NGAL	inc/ wash	centrifugation	anti-NGAL-MPs	lysis	inc/ wash	dye	inc/ wash
10 µL	10 ng/mL	1 h	✗	2 µL	30 mM OG	30 min	1 nM SA-PE	15 min
	10 ng/mL		1x 10 min 10.000 g					
	✗		1x 10 min 10.000 g					

Table 7: Experimental procedure for comparison of liposome bound antibody with free antibody

mAb-lip	NGAL	inc/ wash	mAb	NGAL	anti-NGAL-MPs	lysis	inc/ wash	dye	inc/ wash
10 µL	10 ng/mL	1 h	✗	✗	2 µL	30 mM OG	30 min	1 nM SA-PE	15 min
	✗		✗	10 ng/mL					
	✗		5 nM	10 ng/mL					

Table 8: Experimental procedure for comparison of a three-component sandwich assay with a two-component assay

mAb-lip	NGAL	inc/ wash	MPs	inc/ wash
10 µL	10 ng/mL	1 h	2 µL anti-NGAL-MPs	~45 min
10 µL	✗	✗	2 µL GAM-MPs	~1 h

5.4 Results

5.4.1 Experiments with P24

The assay procedure shown in Figure 2 provides that p24 be preconcentrated by being captured by magnetic liposomes, concentrated by magnetic accumulation and set free again by lysis of liposomes. The enriched p24 is then caught by magnetic microparticles and fluorescently labeled. To examine the best assay conditions, first tests were performed with fluorescent liposomes and centrifugation or with fluorescently labeled p24.

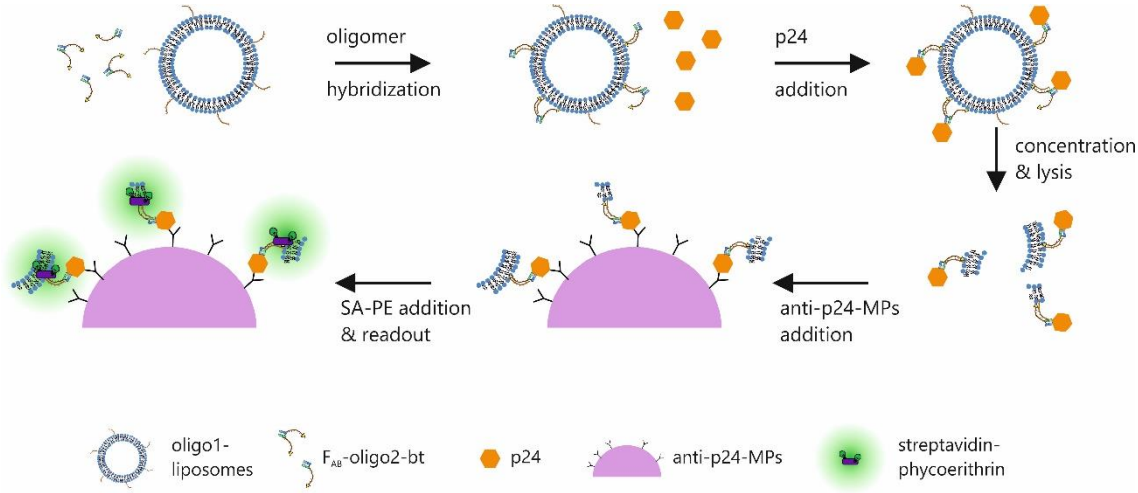

Figure 2: Assay procedure for the detection of p24 as biomarker for HIV.

A first experiment (Figure 3) was performed to compare the binding behavior of free p24 and labeled cy3-p24 as well as the behavior of different fractions of Fab-oligo2-bt conjugate that was purified by HPLC after coupling. Therefore, anti-p24-MPs were mixed with either p24 or cy3 labeled p24 and then labeled by different fractions of Fab-oligo2-bt and SA-PE. This experiment showed restrained binding of cy3-p24 to MPs. Possible reasons might be blocked binding sites, steric or electrostatic hindrance. Therefore, experimental details were reorganized.

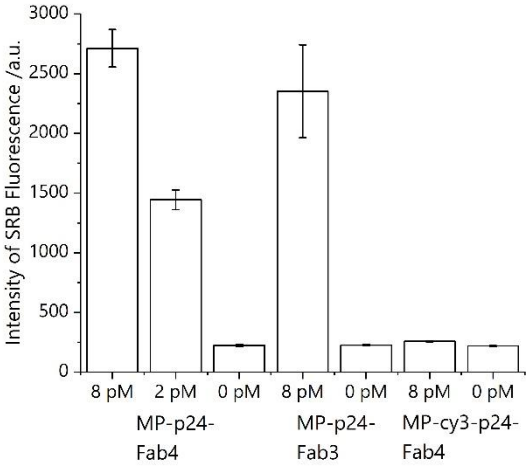

Figure 3: Binding ability of different concentrations of p24 or cy3-p24 to different fractions of the purified Fab. Both fragments bind p24, while cy3-p24 is not bound, most likely due to blocked binding sites.

In addition, an experiment was performed that should give information about the most efficient reagent addition order. The reaction of p24 bound to liposomes with free anti-p24-MPs was compared to the reaction of p24 bound to MPs with free liposomes and a five times higher signal was found for the second case (Figures 4 and 5). A possible explanation could be that p24 is exposed when bound to rigid MPs, while it might be sterically shielded when bound to soft liposomes, although a spacer between p24 and liposomes is inserted. The experiment was performed both with detection of intact liposomes, measuring the signal of encapsulated SRB, as well as with lysed liposomes, binding labeled streptavidin to biotin exposed after lysis. No significant difference could be observed (Figure 5).

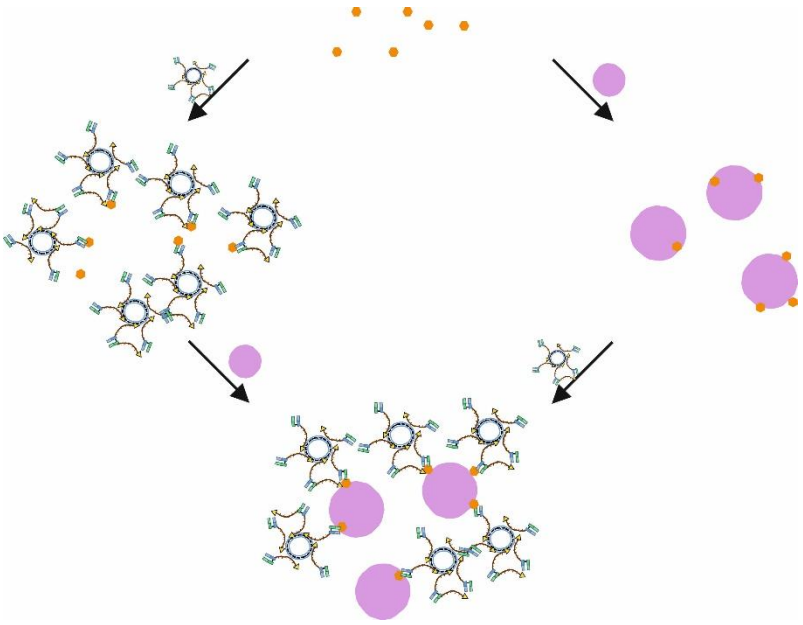

Figure 4: Scheme of an experiment to investigate the effect of reagent addition order. **left**: first binding of p24 (orange hexagon) to liposome-Fab-conjugate, then addition of MPs (pink circles). **right**: first binding of p24 to MPs and then reaction with liposome-Fab-conjugate. In theory, both orders should give the same result.

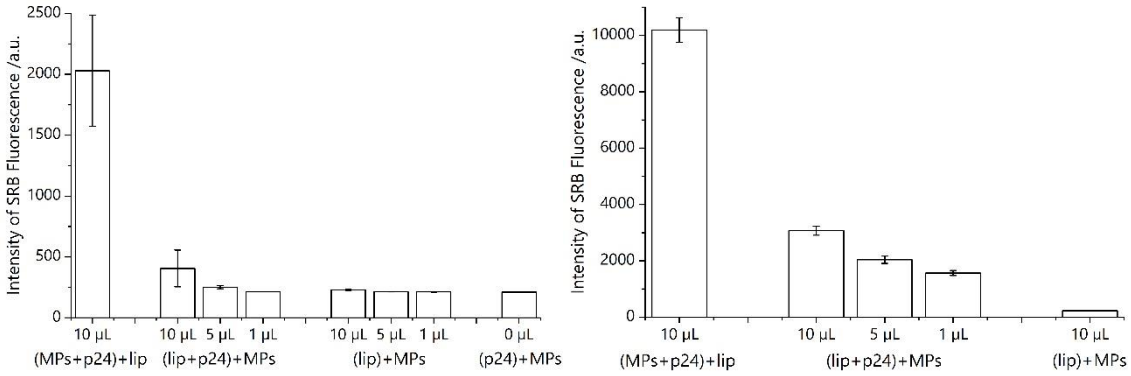

Figure 5: Intensity values measured for the described assay, performed once without (left) and once with (right) lysis of liposomes.

An explanation might be possible hindrance of p24 binding by intact liposomes or free lipids after lysis (also indicated by liposome fragments in Figure 2).

Therefore, MPs with different receptors were used. Binding of p24-Fab-oligo2-**bt** conjugate to **SA**-MPs after lysis of liposomes was investigated, as well as binding of **p24**-Fab-oligo2-bt conjugate to **anti-p24**-MPs (also called HIV-MPs), shown in Figure 6.

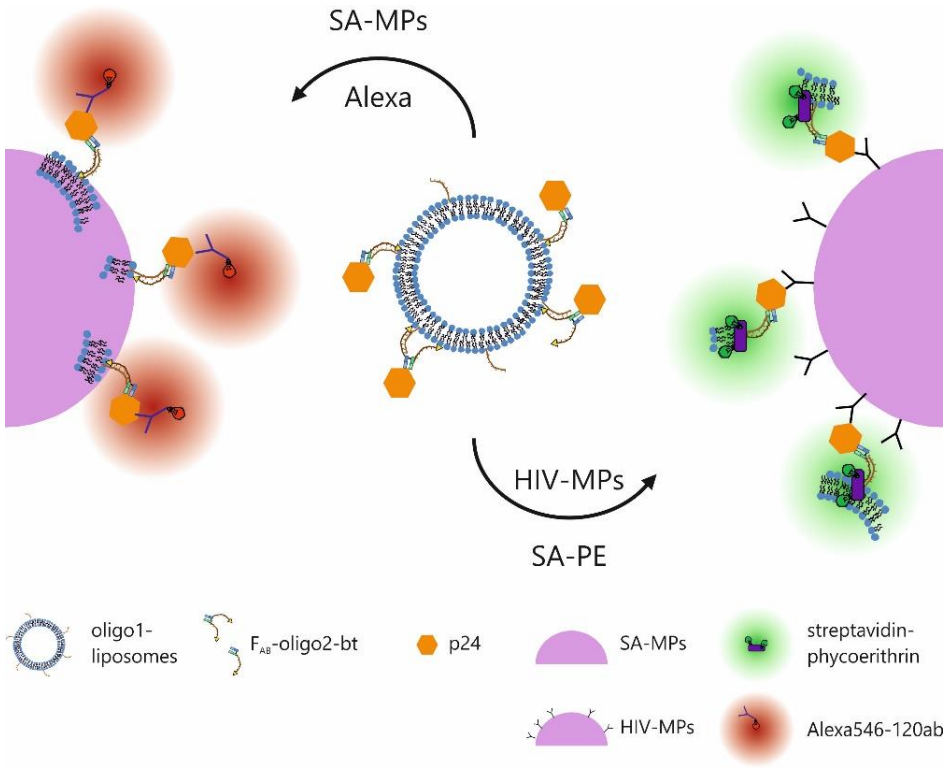

Figure 6: Investigation of binding ability of p24-Fab-oligo2-bt to different receptors on MPs. left: Binding of p24-Fab-oligo2-**bt** conjugate to **SA** particles and signal generation by sandwich of labeled antibody with p24. right: Binding of **p24**-Fab-oligo2-bt conjugate to **anti-p24**-MPs and signal generation by labeled SA binding to bt.

A significant increase of signal for p24 binding to HIV-MPs instead of biotin binding to SA-MPs was found, indicating that biotin might be hindered by liposomal degradation products after lysis, which yields very low binding of **bt**-oligo2-Fab-p24 to **SA**-MPs (Figure 7).

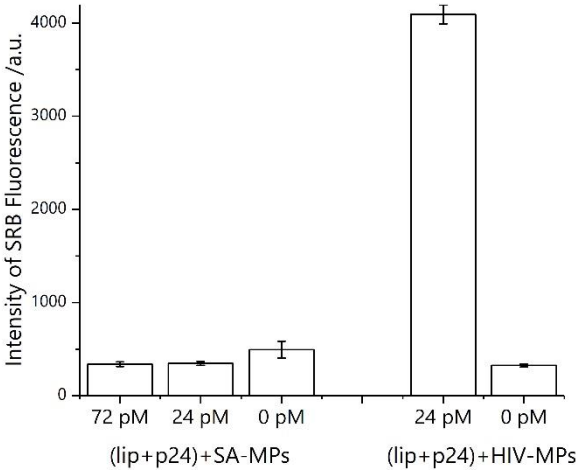

Figure 7: Intensity values for the described experiment. Different concentrations of p24 were mixed with liposomes, lysed and either streptavidin-MPs or anti-p24-MPs (HIV-MPs) were added. A significantly increased signal for binding of p24 to HIV-MPs than for biotin binding to SA-MPs was observed, indicating some blocking of biotin by liposomal degradation products.

As with the use of HIV-MPs in presence of p24 a signal about 10 times higher than the signal for the negative sample could be found, the effect of preconcentration was investigated and it was found that by preconcentration the signal could be doubled (Figure 8).

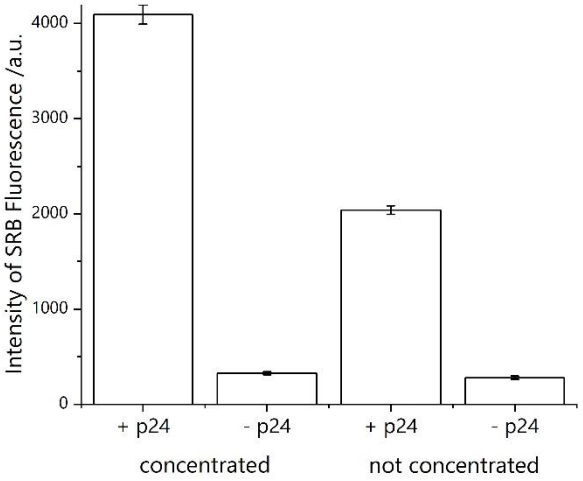

Figure 8: Assay with p24 captured by lipsomes, lysed and bound by HIV-MPs, performed both in absence and presence of p24 as well as with and without preconcentration.

5.4.2 Experiments with NGAL

As p24 is a protein that is encapsulated in the virus envelope, this protein might interact with lipids after lysis. Therefore, different experiments were repeated with NGAL, a less lipophilic

protein. First, it was proven that unfortunately the reagent addition order follows the same rules as with p24 and binding of liposomes to MPs is decreased when involving a target.

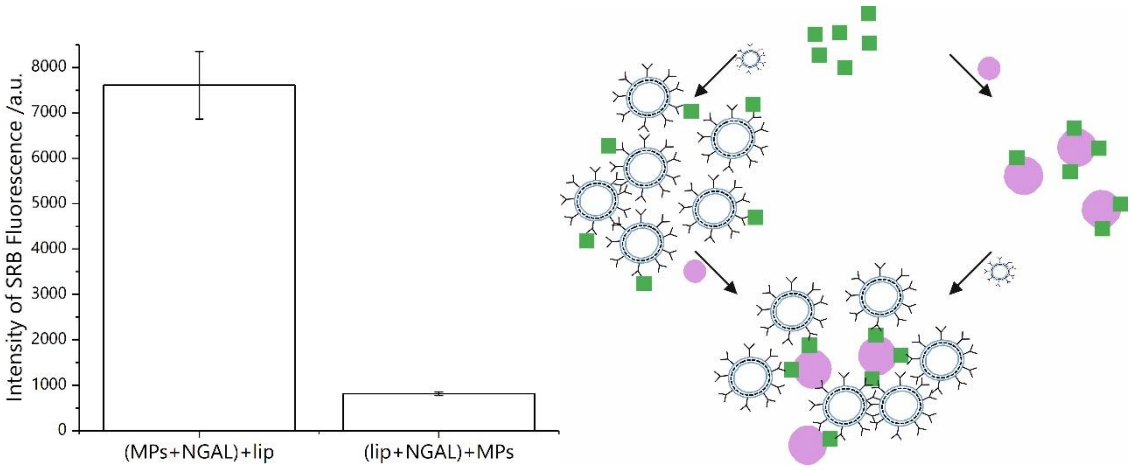

Figure 9: left: Intensity values for reagent addition order test with NGAL. right: Assay scheme, in the left case, first NGAL (green squares) reacts with liposomes and then MPs (pink circles) are added, while in the right case first NGAL reacts with MPs and then liposomes are added.

In a second assay, either a free antibody or an antibody anchored to a liposome were reacted with NGAL. No preconcentration was performed, but liposomes were lysed. Then MPs were added. For signal generation, biotin, coupled to both free and liposome-bound antibodies, was coupled to SA-PE. A significantly (12 times) higher signal could be observed for the free antibody, while the assay with liposome bound antibody showed a signal in the same range as the negative control in absence of any antibody. This indicates hindrance of the binding site by liposome fragments, as in theory, both assays should yield about the same signal.

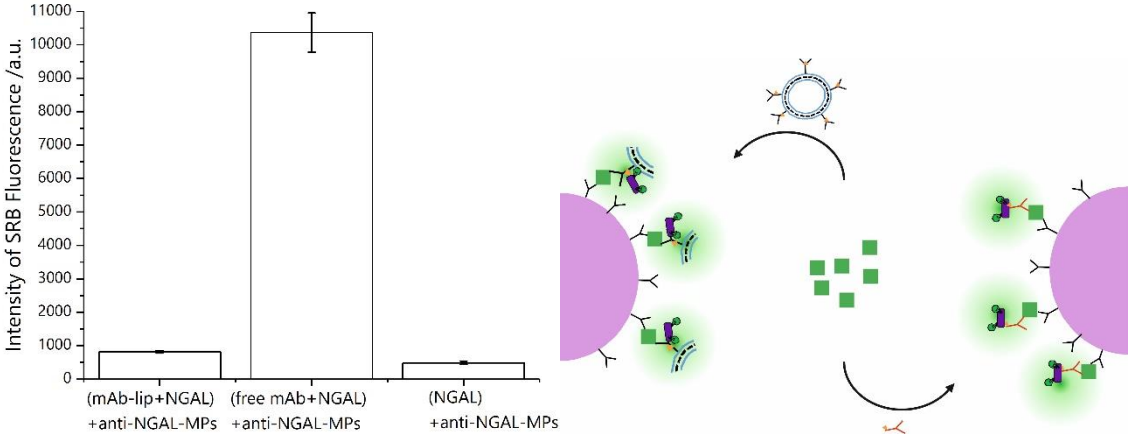

Figure 10: Intensity values for reaction of either free antibody or liposome-bound antibody with NGAL und MPs. Free antibody showed a 12 times higher signal, most likely due to hindrance of the binding site by liposome fragments after lysis. As negative control, the assay was also performed in absence of any antibody. This assay principle is also illustrated in the scheme on the right side, where on the left, antibodies coupled to liposomes are used and on the right, free antibody binds to NGAL.

Preconcentration of the liposome-NGAL conjugate prior to lysis was also investigated for NGAL, and again the signal could be doubled by preconcentration. Unfortunately, the signal was higher for preconcentration in absence of the analyte, than for no preconcentration in presence of the analyte, which indicates severe unspecificity.

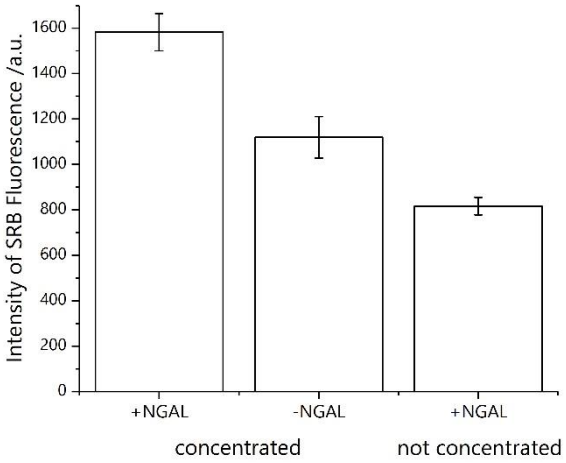

Figure 11: Intensity values for preconcentrated and not preconcentrated assay, in presence and absence of NGAL.

In a last experiment, liposomes were not lysed and the signal of encapsulated SRB was detected. The assay was performed once in presence of NGAL with Anti-NGAL-MPs and once in absence of NGAL with goat anti mouse-MPs (GAM-MPs) binding to the liposome bound antibody. For the latter case, where only two partners had to bind without a sandwich structure, a 10 times higher signal was observed. This is another evidence for blocked binding sites hindering liposome bound analytes to further bind to the particles.

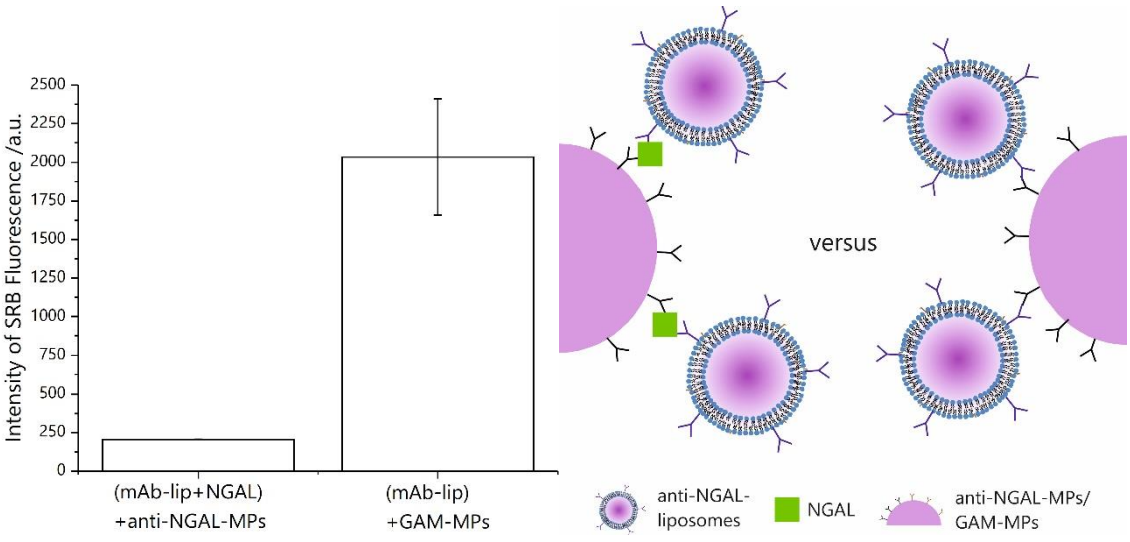

Figure 12: Intensity values for an assay in presence and absence of analyte, relying on the fluorescence of liposome encapsulated SRB. The principle is illustrated in the scheme, where in the left part, liposomes and MPs both bear anti-NGAL-antibodys and therefore build a sandwich with NGAL, while on the right side, MPs bear an antibody that binds to the anti-NGAL-antibody and therefore can bind liposomes without NGAL in between.

5.5 Conclusion

When investigating the reagent addition order, significantly increased binding rates were found for reaction of MP-p24 with free liposomes instead of liposome-p24 with free MPs. Additionally, p24 binding to HIV-MPs instead of biotin binding to SA-MPs was favored when reacting bt-oligo2-Fab-p24 after liposome lysis to the respective MPs. In the end, the signal of the assay could be doubled by preconcentration.

The analysis with NGAL showed the same behavior as with p24 regarding preconcentration and the reagent addition order, where binding of liposomes to MPs was decreased when involving a target. In addition, an assay was performed once with liposomes bound to NGAL and being lysed, compared to a free antibody bound to NGAL, both being labeled at a biotin label, which showed better results without liposomes, again pointing towards a problem with interference of lysis products. Finally, it was investigated if an assay with only two instead of three reaction partners would yield better results and this assumption was verified when significantly higher signals were reached for the reaction of MPs directly binding to liposomes, instead of a construct with NGAL as linker.

Given the overall results, different further analysis is imaginable as these were only preliminary tests, and some tests should be repeated with adaptions. For example, the experiment described in 5.3.4 was carried out to compare the reagent addition order. Therefore, liposome lysis was performed after addition of and incubation with MPs, to yield better comparability with the reaction of MPs with p24 and later addition of liposomes, where lysis can only be carried out after incubation. Nevertheless, the target assay intends to lyse liposomes after preconcentration and before addition of MPs. Therefore, this assay should be repeated in the intended order to yield the desired results. Finally, the results with and without preconcentration should be compared to an assay in absence of liposomes. When achieving positive results, the use of magnetic liposomes instead of preconcentration by centrifugation can be investigated.

5.6 References

[1] Berthet-Colominas C, Monaco S, Novelli A, Sibaï G, Mallet F, Cusack S (1999) Head-to-tail dimers and interdomain flexibility revealed by the crystal structure of HIV-1 capsid protein (p24) complexed with a monoclonal antibody Fab. EMBO J 18:1124–1136. doi: 10.1093/emboj/18.5.1124.

[2] Engelman A, Cherepanov P (2012) The structural biology of HIV-1: mechanistic and therapeutic insights. Nat Rev Microbiol 10:279–290. doi: 10.1038/nrmicro2747.

[3] Ruan Q, Saldana SC, Skinner JP, Tetin SY (2019) Spatially resolved ligand-receptor binding assays: U.S. Patent 10,190,896 B2.

[4] Edwards KA, Curtis KL, Sailor JL, Baeumner AJ (2008) Universal liposomes: preparation and usage for the detection of mRNA. Anal Bioanal Chem391:1689–1702. doi: 10.1007/s00216-008-1992-1.

[5] Hofmann C (2019) Synthesis and Characterization of Liposomes with Controlled Surface Design for Analytical Applications. Unpublished doctoral dissertation, University of Regensburg, Germany.

6 Conclusion and Future Perspectives

The recent progress in food safety analysis is the result of a high demand for rapid reliable techniques for point-of-need detection of numerous contaminants in foodstuff and beverages. Pathogens including bacteria and viruses, natural toxins like mycotoxins or seafood toxins, residues of pesticides, veterinary drugs or packaging components, preservatives or colorants, but also traces of heavy metals, polycyclic aromatic hydrocarbons or polychlorinated biphenyls are among the harmful substances frequently found in food products [1–3]. These analytes display a huge variety of structures, affinities, and chemical behavior and are often embedded in complex matrices, which restrains the application of simple universal detection principles. This thesis found that the complexity of sample preparation and the applied amount and variation of materials is increasing significantly compared to previous literature, while detection principles themselves are focusing on methods with simple readout, like colorimetric or fluorescent detection instead of mass spectrometry. Lots of interesting material composites for this purpose were employed, e.g., in a strategy for sensing of ochratoxin A, a mycotoxin mostly occurring due to incorrect storage of crop plants [4], presented by Wang et al. [5]. For their strategy, they use a material combining quantum dots encapsulated in a silica microsphere conjugated to magnetic particles, which enables magnetic separation as well as fluorescent readout. As quantum dots are highly toxic and of great risk for the environment [6, 7], less harmful alternatives should be investigated for this beneficial combination of magnetic and fluorescent properties. For this purpose, liposomes encapsulating fluorescent dyes are a promising solution, as they not only emit a fluorescent signal but in addition are capable of enormous signal enhancement due to the encapsulation of fluorescent dyes in self-quenching concentrations and release after successful binding to the analyte [8]. By combining liposomes with magnetic particles, a powerful analytical tool is created.

Magnetic liposomes are mainly described for drug delivery, where their magnetic abilities are used for making the membrane permeable and releasing the encapsulant. This is achieved by magnetic actuation of small magnetic nanoparticles (MNPs) in the bilayer by an alternating magnetic field, whereupon the generated heat weakens the bilayer [9, 10]. By this mechanism the encapsulated drug molecules are released at their target location, e.g., in a tumor. Nevertheless, the bilayer incorporated particles are mostly smaller than 6 nm [11, 12]. In this thesis, the successful incorporation of 8 nm MNPs into the bilayer of sulforhodamine B encapsulating liposomes was described and their superior performance in analytical assays under magnetic conditions was shown. By transferring the strategy of encapsulant release by magnetic actuation to the magnetic bilayer incorporation liposomes described in this thesis, signal generation in analytical assays would be possible without further addition of reagents, but instead by using a constant magnetic

field for attracting the magnetic liposomes and then applying an alternating magnetic field for liposome rupture and signal generation. Especially in microfluidic applications, this could yield faster signals by removing a step in the microfluidic protocol where detergent is flushed through the channel to lyse the liposomes and generate the signal, and thus significantly reduce complexity of the system and assay times. In addition, Mayer et al. investigated the effects of different surfactants on the electrochemiluminescence of luminol and one of its derivatives that has also already been encapsulated successfully in liposomes [13], and found that surfactants can both significantly quench and enhance the luminescence. Nevertheless, they found no clear trend or general rules to predict the effect [14]. The use of liposomes with MNPs in the bilayer could overcome this dubiety and prohibit the possibility of severe quenching effects. Of course, a thorough investigation of the lysis efficiency by magnetic actuation would be necessary to be able to estimate the actual advantage of this lysis method.

In this thesis, the synthesis of liposomes with MNPs inserted into the bilayer was investigated and optimized regarding lipid composition, synthesis strategy and purification, and modification. For the encapsulation of magnetic particles into the inner cavity of liposomes, these optimized parameters were adopted and both strategies yielded significantly decreased detection limits under magnetic compared to non-magnetic conditions. Nevertheless, the encapsulation efficiency of inner cavity magnetosomes is only 5% compared to 15% for bilayer magnetosomes, also because fewer particles were used than for bilayer insertion due to high costs of commercially available particle dispersions. Further optimization of this system can be performed to yield higher encapsulation efficiencies, including other strategies to encase particles in the liposome, e.g., by addition of the particles not at the beginning together with the dye encapsulation solution, but after synthesis of the liposomes before extrusion. During this process, the liposomes are pressed through a polycarbonate membrane with pores in the size of the desired liposome diameter. The liposome bilayer is broken and forms again at the other side of the membrane in a more uniform and unilamellar way [15]. Through the addition of MNPs during this step, the particles are enclosed in the newly formed vesicles. The benefit of this method is that MNPs with a surface modification that is not stable in the aqueous-organic solvent mixture at the beginning of the liposome synthesis are added after organic solvents are evaporated and thus the risk of aggregation and precipitation is avoided. Preliminary studies with this method show promising results (Figure 1). However, in its current format, it deemed irreproducible since a lot of particles were lost on the extrusion membrane, where they clogged the pores and led to rupture of the polycarbonate membrane, most likely due to particle aggregates that were larger than the pore

size of the membrane. Thus, particle stability in the liposome mixture applied in extrusion has to be carefully investigated prior to continuing with this interesting strategy.

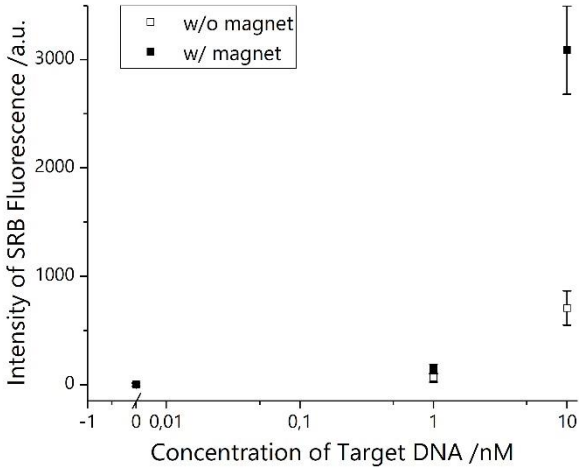

Figure 1: DNA hybridization assay with liposomes encapsulating hydrophilic magnetic nanoparticles in the inner cavity, while particles were added during extrusion.

Another strategy to avoid particle aggregation and precipitation is a more stable surface coating, as described by Amsted et al. [16]. This group uses catechol-derived anchor groups that bind covalently to the particle surface instead of adhering by electrostatic interaction and hydrogen bonds, and thus achieve ultrastable nanoparticle suspensions. Performing this surface coating with self-synthesized nanoparticles as used for bilayer insertion (for synthesis protocol see Chapter 3), much higher concentrated MNP solutions could be applied and thus a higher encapsulation efficiency can be expected. The price of these particles is also much lower than of commercially available MNPs, as the amount of particles to achieve one MNP per liposome is less than US$250 (including chemicals and manpower for the synthesis) compared to US$3500 for commercially available MNPs. In case coating with catechol derivatives is not successful, the formation of a thin silica shell around the nanoparticles is also a possibility [17]. This method bears the advantage of an uncharged but still hydrophilic surface coating, since, while performing these surface modifications, it has to be kept in mind that a negatively charged surface ligand can be rejected by the likewise negative surface of anionic liposomes. Thus, either cationic lipids have to be employed for liposome formation or the coating has to be conducted with positive or uncharged ligands, e.g., the aforementioned silica shells. A crucial aspect to consider here is the thickness of the shell, as there is only limited space inside the inner cavity of liposomes that in addition has to be shared with marker molecules for detection, and the number of particles fitting into the hollow liposome scales with $\frac{1}{d^3}$ to the diameter d of the particles.

The described magnetic liposomes are formed directly during synthesis or by encapsulation of the particles during work-up, but the subsequent modification of liposomes after synthesis is also beneficial, as the same batch of vesicles can be used for different strategies and experiments and no batch-to-batch variation has to be considered. By using silanes bearing amino groups for the formation of silica shells, the resulting particles can also be used for coupling to carboxy-modified liposomes, which should be conducted inside a microfluidic channel to prevent crosslinking. A respective microfluidic chip and a coupling procedure were successfully established in this thesis, obtaining efficiencies of up to 62% of liposomes coupled to magnetic particles in the microfluidic product. A limitation of this strategy is the homogeneous distribution of particles across the bottom of the channel, as the particles accumulate in a hotspot when entering the magnetic field. More investigations in magnet shape, strength and the application of sequentially arranged magnets to capture particles in consecutive spots are necessary for upscaling. The application of electromagnets could also be possible, to be able to switch the magnetic field on and off again and thus achieve higher automation than being dependent on physically removing the magnet from the setup. Modifying the magnetic setup also holds great potential for upscaling, for instance by parallelization of channels, e.g., by stacking chips over each other or applying magnetic fields from both sides to also use the top of the channels as a capturing spot for magnetic particles. At the moment, one chip can already be reused for about 5 coupling procedures, as after several runs solutions start to leak through loosened double-adhesive tape, but by the use of different manufacturing techniques like hot embossing, channels with higher durability can be produced. With a higher throughput und yield, concentration determination will also be more viable, which at the moment displays a drawback due to high material consumption. For this purpose, investigations with different deactivation protocols to further reduce loss by crosslinking and mechanical rupture of liposomes during magnetic attraction are conceivable. The optimized microfluidic magnetic-coupling setup can then be transferred to the linkage of magnetic particles with all kinds of nanomaterials that can be dispersed in solution.

This might be necessary, as some applications offer disadvantageous conditions for liposomes: buffers containing calcium or magnesium can lead to fusion and destabilization of liposomes [18, 19], oxidative conditions like the presence of hydrogen peroxide or transition metal elements and hydrolysis due to ester cleavage under harsh acidic or basic conditions cause increased permeability [20], and temperatures exceeding the phase transition temperature of the lipid bilayer induce leakage of encapsulants [21, 22]. In cases where these conditions cannot be circumvented, the use of liposomes must be thoroughly reconsidered and the use of another material capable of signal enhancement has to be considered. Here, a lot of different carrier

systems have been reported, e.g., composed of mesoporous silica, polymers, proteins, carbon or metal oxides [23]. By equipping these nanoncontainers with carboxy-groups on their surface, the microfluidic magnetic-coupling device developed in this thesis can be used to provide the nanocarriers with magnetic features and use them similar to magnetic liposomes in (bio-)analytical assays. The third functionality of these multifunctional nanomaterials, apart from magnetic and signal-producing features, is the biorecognition element on the surface of the nanocarrier, where a huge variety of receptors is possible. The described microfluidic device was tested with biotin-presenting liposomes, but also nucleic acids, aptamers or antibodies commonly used for analyte capturing. Here, especially for negatively charged DNA molecules, unspecific attachment to the positively charged amino-group presenting magnetic particles, as well as the conjugation of amino groups that are part of the nucleic bases of the DNA strands to the activated carboxy groups on the liposome surface need to be considered. In both cases, the DNA strands would not be available for hybridization with the target DNA and thus analytical sensing would not be possible with this system.

Unlike the microfluidically coupled MNP-liposome conjugates that have so far only been equipped with biotin and applied in biotin-streptavidin-binding assays with great success, bilayer insertion and inner cavity encapsulation magnetosomes were applied in DNA sandwich hybridization assays and their performance was critically compared for different systems and optimizations. In this assay, first, the capture probe was immobilized on the bottom of a microtiter plate, then target DNA was added and incubated and afterwards receptor DNA bearing magnetized liposomes were applied. To enhance the effectivity and assay time, another hybridization order could be investigated: by incubating target DNA and liposomes in bulk solution in parallel to capture probe immobilization, the assay time would be significantly reduced, while the mixing of target DNA and liposomes under agitation can increase the efficiency of binding before the subsequent magnetic attraction of the target DNA – liposome associate to the capture probe modified surface. At the moment, a magnet plate with ring-shaped magnets is used for attraction, which was designed for the application in magnetic bead washing assays, where a particle-free spot in the middle of the well is desired for approach of the pipette tip [24]. As in this assay uniform distribution of the magnetic field across the complete well bottom is preferred, a magnet plate with area magnets could improve the assay by more homogeneous attraction.

Apart from the application as label in (bio-)analytical assays, the use of magnetic liposomes as substrate for immunomagnetic separation purposes was also investigated. Unfortunately, the analytes - the HIV capsid protein p24 and the less lipophilic protein neutrophil

gelatinase-associated lipocalin (NGAL) - were found to interact with liposomes in a way that decreases the likelihood of subsequent binding to magnetic microparticles necessary for the detection. Nevertheless, a signal could still be observed with the use of liposomes, indicating that some degree of binding occurs. This raises hope for the possibility to find the right assay conditions by further optimization. For example, in the investigated assay principle, liposomes were either used without lysis or lysed by detergent addition. By the application of an even more efficient lysis protocol, an interaction with lipid residues might be further reduced. For this purpose, the use of liposomes with MNPs incorporated into the lipid bilayer could be examined for immunomagnetic separation with subsequent magnetic actuation of the MNPs to destroy the lipid bilayer. The efficiency of this method is of course unknown and will only be revealed after thorough experimental investigations.

This thesis investigated the three different locations to associate MNPs with liposomes - in the hydrophilic inner cavity, in the hydrophobic bilayer core and coupled to the outer surface -, compared their efficiency and demonstrated the effectiveness of all routes. For each strategy, specific advantages and disadvantages were found: while the encapsulation of MNPs takes place during synthesis, the coupling to particles in a microfluidic channel offers the possibility to use the same batch of liposomes for different coupling and thus decrease effects of batch-to-batch variations. Nevertheless, this method displays a very low yield and drastic increase in production time compared to direct encapsulation. In addition, in the direct case particles are shielded by lipids while they are prone to unspecific binding when coupled to the outside of liposomes and thus not protected. Also, the surface of liposomes is to some extent covered by particles and thus the availability of lipid-bound bioreceptors for target binding especially at surfaces might be hindered, which favors the application of magnetosomes with direct encapsulation for heterogeneous sensing purposes. On the other hand, the size of MNPs to be encapsulated in the bilayer, and to some extent also in the inner cavity, is limited, while even particles which are larger than the liposome itself can be bound to the outside of liposomes, and thus display high magnetization. This predestines magnetic particle–liposome conjugates for homogeneous applications like, e.g., immunomagnetic separation. Considering these and many more advantages and disadvantages, the knowledge gained provides a useful tool set for the application of magnetic liposomes for different analytic purposes, which additionally offers a lot of potential for further optimization.

As mentioned, the linking of particles to the outside of liposomes has the advantage that the particle size can easily be varied for different applications. Furthermore, this feature is also beneficial when considered the other way around, i.e., not changing the morphology of the

magnetic particles but replacing the liposomes with other nanomaterials. Thus, an undeniable benefit of the microfluidic magnetic-coupling device is the great combinatorial freedom, providing the opportunity that any nanomaterial equipped with carboxy groups that can be activated by EDC/sNHS chemistry, can be introduced into the device, coupled to magnetic particles and thus equipped with magnetic properties. With this method, an enormous variety of multifunctional nanomaterials combining magnetic properties with various other features can be produced. Such multifunctional conjugates can then be applied for sensing, imaging, directed drug transport, etc. in analytical chemistry as well as life science and biomedicine [25].

6.1 References

[1] Dzantiev BB, Byzova NA, Urusov AE, Zherdev AV (2014) Immunochromatographic methods in food analysis. Trends Anal. Chem. 55:81–93. doi: 10.1016/j.trac.2013.11.007.

[2] Joint FAO/WHO Codex Alimentarius Commission (1995 (last amended 2017)) General Standard for Contaminants and Toxins in Food and Feed. Codex Alimentarius CXS 193-1995. World Health Organization; Food and Agriculture Organization of the United Nations.

[3] U.S. Food and Drug Administration Home Page (2018) Foodborne Illness & Contaminants. https://www.fda.gov/food/foodborneillnesscontaminants/default.htm. Accessed 7 August 2018.

[4] Limay-Rios V, Miller JD, Schaafsma AW (2017) Occurrence of *Penicillium verrucosum*, ochratoxin A, ochratoxin B and citrinin in on-farm stored winter wheat from the Canadian Great Lakes Region. PLOS ONE 12. doi: 10.1371/journal.pone.0181239.

[5] Wang C, Qian J, Wang K, Wang K, Liu Q, Dong X, Wang C, Huang X (2015) Magnetic-fluorescent-targeting multifunctional aptasensor for highly sensitive and one-step rapid detection of ochratoxin A. Biosens. Bioelectron. 68:783–790. doi: 10.1016/j.bios.2015.02.008.

[6] Derfus AM, Chan WCW, Bhatia SN (2004) Probing the Cytotoxicity Of Semiconductor Quantum Dots. Nano Lett 4:11–18. doi: 10.1021/nl0347334.

[7] Xu J, He H, Wang Y-Y, Yan R, Zhou L-J, Liu Y-z, Jiang F-L, Maskow T, Liu Y (2018) New aspects of the environmental risks of quantum dots: prophage activation. Environ. Sci.: Nano 5:1556–1566. doi: 10.1039/C8EN00142A.

[8] Edwards KA, Curtis KL, Sailor JL, Baeumner AJ (2008) Universal liposomes: preparation and usage for the detection of mRNA. Anal Bioanal Chem 391:1689–1702. doi: 10.1007/s00216-008-1992-1.

[9] Amstad E, Kohlbrecher J, Muller E, Schweizer T, Textor M, Reimhult E (2011) Triggered release from liposomes through magnetic actuation of iron oxide nanoparticle containing membranes. Nano Lett 11:1664–1670. doi: 10.1021/nl2001499.

[10] Chen Y, Bose A, Bothun GD (2010) Controlled release from bilayer-decorated magnetoliposomes via electromagnetic heating. ACS nano 4:3215–3221. doi: 10.1021/nn100274v.

[11] Bixner O, Reimhult E (2016) Controlled magnetosomes: Embedding of magnetic nanoparticles into membranes of monodisperse lipid vesicles. J Colloid Interface Sci 466:62–71. doi: 10.1016/j.jcis.2015.11.071.

[12] Bonnaud C, Monnier CA, Demurtas D, Jud C, Vanhecke D, Montet X, Hovius R, Lattuada M, Rothen-Rutishauser B, Petri-Fink A (2014) Insertion of nanoparticle clusters into vesicle bilayers. ACS nano 8:3451–3460. doi: 10.1021/nn406349z.

[13] Mayer M, Takegami S, Neumeier M, Rink S, Jacobi von Wangelin A, Schulte S, Vollmer M, Griesbeck AG, Duerkop A, Baeumner AJ (2018) Electrochemiluminescence Bioassays with a Water-Soluble Luminol Derivative Can Outperform Fluorescence Assays. Angew Chem Int Ed 57:408–411. doi: 10.1002/anie.201708630.

[14] Mayer M, Hahn M, Gerstl F, Köwer T, Rink S, Kunz W, Duerkop A, Baeumner AJ (in press) Shedding Light on the Diversity of Surfactant Interactions with Luminol Electrochemiluminescence for Bioanalysis. Anal Chem.

[15] Hope MJ, Nayar R, Mayer LD, Cullis PR (1993) Reduction of liposome size and preparation of unilamellar vesicles by extrusion techniques. In: Gregoriadis G (ed) Liposome Technology, 123–139.

[16] Amstad E, Gillich T, Bilecka I, Textor M, Reimhult E (2009) Ultrastable iron oxide nanoparticle colloidal suspensions using dispersants with catechol-derived anchor groups. Nano Lett 9:4042–4048. doi: 10.1021/nl902212q.

[17] Wu W, He Q, Jiang C (2008) Magnetic iron oxide nanoparticles: synthesis and surface functionalization strategies. Nanoscale Res Lett 3:397–415. doi: 10.1007/s11671-008-9174-9.

[18] Düzgünes N, Wilschut J, Fraley R, Papahadjopoulos D (1981) Studies on the Mechanism of Membrane Fusion: Role of Head-Group Composition in Calcium- and Magnesium-Induced Fusion of Mixed Phospholipid Vesicles. Biochim. Biophys. Acta 642:182–195. doi: 10.1016/0005-2736(81)90148-6.

[19] Ellens H, Bentz J, Szoka FC (1985) H^+- and Ca^{2+}-Induced Fusion and Destabilization of Liposomes. Biochemistry 24:3099–3106. doi: 10.1021/bi00334a005.

[20] Grit M, Crommelin DJA (1993) Chemical stability of liposomes: implications for their physical stability. Chem. Phys. Lipids 64:3–18. doi: 10.1016/0009-3084(93)90053-6.

[21] Blok MC, van Deenen, L. L. M., Gier J de (1976) Effect of the gel to liquid crystalline phase transition on the osmotic behaviour of phosphatidylcholine liposomes. Biochim. Biophys. Acta 433:1–12. doi: 10.1016/0005-2736(76)90172-3.

[22] Blok MC, van der Neut-Kok ECM, van Deenen, L. L. M., Gier J de (1975) The effect of chain length and lipid phase transitions on the selective permeability properties of liposomes. Biochim. Biophys. Acta 406:187–196. doi: 10.1016/0005-2736(75)90003-6.

[23] Hofmann C, Duerkop A, Baeumner AJ (2019) Nanocontainers for Analytical Applications. Angew Chem Int Ed. doi: 10.1002/anie.201811821

[24] Alpaqua Engineering LLC. 96R Ring Magnet Plate. https://www.alpaqua.com/DesktopModules/Bring2mind/DMX/Download.aspx?EntryId=321&PortalId=0&DownloadMethod=attachment. Accessed 22 August 2019.

[25] Sun X-T, Liu M, Xu Z-R (2014) Microfluidic fabrication of multifunctional particles and their analytical applications. Talanta 121:163–177. doi: 10.1016/j.talanta.2013.12.060.

7 Summary

Daily, Consumers all over the world have to rely on the security and high quality of food, which emphasizes the importance and high demand of fast reliable strategies for food safety analysis. These enable us to control the safety of consumable goods during production as well as directly in the supermarket or at home. Recent progress in development of these strategies with focus on the employed biological and synthetic macro- and nanomaterials are examined in this thesis, systematically comparing their advantages and disadvantages. When taking into account less recent literature, it was found that a rethink of useful detection strategies takes place, which is expressed in the fact that purely lab-based strategies are becoming less common, while point-of-need methods are proliferating. This progress involves extensive investigations in sophisticated synthetic materials with much higher research and production effort than biological materials, but will eventually lead to higher field portability and the possibility to enhance food safety directly at the spot where it is needed.

One of the synthetic materials used for food safety analysis are liposomes. These hollow vesicles can encapsulate huge amounts of marker molecules and set them free again after analyte recognition, reaching enormous signal amplification with each binding event. By equipping fluorescent liposomes with magnetic properties, multifunctional labels for the application in analytical assays are obtained, which can overcome diffusion limits due to directed approach under magnetic conditions, and thus can improve assay times as well as sensitivity. Two different strategies for the production of magnetic liposomes were investigated:

The first possibility is the incorporation of magnetic nanoparticles (MNPs) directly during synthesis: Either MNPs with hydrophobic surface coating were inserted into the hydrophobic core of the lipid bilayer (b-liposomes), or MNPs modified with hydrophilic surface ligands were incorporated into the likewise hydrophilic interior of the liposomes (i-liposomes). The resulting liposomes were characterized regarding their hydrodynamic diameter, zeta-potential and phospholipid concentration and optimization of lipid composition, synthesis strategy and work up procedure was conducted. The different systems were then validated by their performance in a DNA hybridization assay and compared between each other, before and after optimization, and with and without purification by further magnetic separation. Encapsulation efficiencies were determined to be 15% for b-liposomes and 5% for i-liposomes. In the DNA assay, it was found that the lowest limit of detection was obtained with optimized b-liposomes at 42 pM target DNA, which was over three times lower than without a magnetic field. Interestingly, when further clean-up procedures were employed and non-magnetic liposomes were sorted out, the overall

LOD increased. A possible explanation is that without magnetic purification, non-magnetic liposomes are dragged towards the magnetic field by their magnetic peers and this positive contribution improves the assay performance. Furthermore, under these conditions, i-liposomes outperformed their bilayer counterparts, which is likely due to a lower fraction of liposomes with magnetic features and thus a higher potential for improvement. Eventually, both strategies represent viable possibilities for the production of magnetic liposomes.

A completely different strategy to obtain multifunctional fluorescent-magnetic liposomes is the external coupling of both components after synthesis, which bears a risk of increased unspecific binding, but also allows the use of larger magnetic particles with higher magnetization and the recombination of different ready-synthesized components. As the linkage in bulk solution yields, as expected, severe crosslinking, a microfluidic device was designed for the directed coupling of both species by magnetically immobilizing a confluent layer of magnetic particles at the bottom of the channel and enabling the binding of liposomes only from the top side while being flushed over the particles. The microfluidic channel was created from PMMA and double adhesive tape by laser cutting and channel design and flow rates were optimized to enhance binding capacities. Carboxy-modified liposomes and two differently sized amino-modified magnetic particles were employed, and the coupling efficiency in the microfluidic product was determined by fluorescence measurements after magnetic separation. The coupling with 1 µm magnetic beads was found to be 5 times more efficient than with smaller 30 nm MNPs and additionally 4 times more efficient than bilayer insertion. Nevertheless, both coupling products showed the ability to significantly improve the assay performance under magnetic conditions, when liposomes with additional biotin functionalization were used in a biotin-streptavidin-binding assay.

A possible application of the resulting magnetosomes is their use for immunomagnetic separation strategies. Thus, preliminary studies were conducted for the preconcentration of the HIV capsid protein p24, before a sandwich assay between magnetic microparticles, p24 and a fluorescent label was conducted followed by single particle fluorescence imaging. Unfortunately, we found that, possibly due to steric reasons, the binding of the concentrated liposome-p24 conjugate to magnetic particles was hindered. Therefore, a less lipophilic protein, neutrophil gelatinase-associated lipocalin (NGAL), was employed for further studies, which was expected to not interact in such a high degree with liposomes as p24 seemed to do. However, the same results as for p24 were yielded, and additionally it was found that the assay performance was much better for the direct binding of liposomes to magnetic particles than with NGAL as a sandwich. Nevertheless, using a preconcentration with liposomes, a two-fold increase of the signal could be achieved compared to an assay without preconcentration. As these were only preliminary studies,

these are still promising results that highlight the great benefit of multifunctional fluorescent magnetic liposomes.

8 Zusammenfassung

Täglich müssen sich weltweit Konsumenten drauf verlassen können, dass ihre Nahrung sicher und von hoher Qualität ist. Dies hebt die Bedeutung der Lebensmittelanalytik und den hohen Bedarf an schnellen zuverlässigen Methoden hervor, welche es uns ermöglichen, die Sicherheit der konsumierten Güter sowohl während der Produktion als auch direkt im Supermarkt oder zu Hause zu kontrollieren. Die neuesten Fortschritte bei der Entwicklung dieser Strategien werden in dieser Arbeit untersucht und ihre Vor- und Nachteile systematisch abwogen, wobei ein besonderer Schwerpunkt auf den verwendeten biologischen und synthetischen Makro- und Nanomaterialien liegt. Im Vergleich mit weniger aktueller Literatur zu diesem Thema fällt auf, dass ein Umdenken bezüglich der nützlichsten Strategien stattfindet, was sich dadurch auszeichnet, dass rein laborbasierte Arbeitsweisen weniger häufig verwendet werden, während anwendernahe Methoden auf dem Vormarsch sind. Diese Entwicklung schließt die Notwendigkeit der intensiven Erforschung von immer ausgefeilteren synthetischen Substanzen mit höherem Forschungs- und Produktionsaufwand - verglichen mit biologischen Materialien - ein, wird aber letztendlich zu gesteigerter Transportfähigkeit führen und zu einer Erhöhung der Lebensmittelsicherheit an dem Punkt, an dem sie am dringendsten benötigt wird.

Eines dieser synthetischen Materialien, die für die Lebensmittelanalytik verwendet werden, ist das Liposom. Diese hohlen Vesikel können große Mengen von Markermolekülen einschließen und nach dem Erkennen des Analyten wieder freisetzen, was eine enorme Signalverstärkung für jede einzelne Bindung bedeutet. Stattet man nun fluoreszierende Liposomen mit magnetischen Eigenschaften aus, so erhält man multifunktionelle Marker für die Anwendung in analytischen Fragestellungen, welche Diffusionslimits durch die gerichtete Annäherung unter magnetischen Bedingungen außer Kraft setzen und damit sowohl die Analysezeit als auch die Sensitivität der Methode signifikant verbessern können. Zwei verschiedene Ansätze für die Herstellung dieser multifunktionellen Lipsomen wurden untersucht:

Die erste Möglichkeit ist die Einlagerung von magnetischen Nanopartikeln (MNPs) direkt während der Liposomsynthese. Hierbei wurden entweder MNPs mit hydrophober Oberflächenmodifikation in den genauso hydrophoben Kern der Lipiddoppelschicht eingelagert (b-Liposomen) oder MNPs, die mit einer hydrophilen Oberfläche ausgestattet wurden, in das ebenfalls hydrophile Innere der

Liposomen eingeschlossen (i-Liposomen). Die entstandenen magnetisierten Liposomen wurden bezüglich ihres hydrodynamischen Durchmessers, ihres Zeta-Potentials und ihrer Phospholipidkonzentration charakterisiert und die Lipidzusammensetzung, die Synthesemethode und die Aufreinigung wurden optimiert. Die verschiedenen Systeme wurden dann anhand ihrer Effizienz in einem DNA-Hybridisierungsassay bewertet und miteinander vergleichen, einerseits sowohl vor als auch nach der Optimierung, andererseits mit und ohne Aufreinigung durch Trennung der magnetischen von den nicht-magnetischen Liposomen. Die Effizienz der Einlagerung von MNPs in die Liposomen wurde bestimmt und diese lag bei 15% für b-Liposomen und bei 5% für i-Liposomen. Im DNA-Assay wurde außerdem herausgefunden, dass das niedrigste zu erreichende Detektionslimit bei 42 pM Ziel-DNA lag, was über dreimal geringer war als ohne Magnetfeld. Interessanterweise stieg das Detektionslimit allgemein an, wenn als weiterer Aufreinigungsschritt eine Abtrennung der nicht-magnetisierten Liposomen vorgenommen wurde. Eine mögliche Erklärung hierfür ist, dass ohne magnetische Aufreinigung die nicht-magnetischen Liposomen von ihren magnetischen Partnern in Richtung des Magnetfeldes gezogen werden und dieser positive Beitrag die Leistung bei der Analyse verbessert. Zudem übertrafen i-Liposomen ihre b-Gegenstücke unter diesen Umständen, was vermutlich daran liegt, dass hier ein geringerer Anteil der Liposomen magnetisiert ist und damit ein größeres Verbesserungspotential besteht. Letztendlich stellen beide Systeme eine erfolgreiche Lösung für die Herstellung von magnetischen Liposomen dar.

Eine komplett andere Strategie um multifunktionelle fluoreszierende magnetische Liposomen zu erhalten verfolgt dagegen der Ansatz, beide Komponenten nach der Synthese extern aneinander zu koppeln. Dies birgt einerseits das Risiko für vermehrte unspezifische Bindungen, erlaubt es andererseits aber auch größere und damit stärker magnetisierte Partikel zu verwenden und verschiedene bereits vorsynthetisierte Komponenten immer wieder neu zu kombinieren. Wie erwartet wurde bei der Verknüpfung in großen Volumina gravierende Quervernetzung zwischen Liposomen und Partikeln beobachtet, weswegen ein mikrofluidisches Instrument entwickelt wurde, welches das kontrollierte Koppeln beider Komponenten ermöglicht. Dies wird realisiert, indem die Partikel magnetisch als durchgängige Schicht am Boden des Kanals immobilisiert werden und so die Bindung der Liposomen, die durch den Kanal fließen, nur von der Oberseite der Partikel erfolgen kann. Der Mikrofluidikkanal wurde aus Plexiglas und doppelseitigem Klebeband gefertigt, aus welchem der Kanal mithilfe eines Lasers ausgeschnitten wurde. Dieser wurde hinsichtlich des Designs des Kanals und der Fließgeschwindigkeit optimiert, um die Bindungskapazität zu erhöhen. Liposomen mit Carboxylgruppen und magnetische Partikel mit Aminogruppen an der Oberfläche wurden für die Bindung gewählt, und die Kopplungseffizienz

des Mikrofluidikprudukts wurde durch Fluoreszenzmessungen nach magnetischer Abtrennung bestimmt. Es stellte sich heraus, dass die Kopplung von Liposomen an 1 µm große magnetische Teilchen etwa fünfmal so effizient ist wie die Kopplung an kleinere 30 nm große MNPs, und zusätzlich viermal effizienter als die Einlagerung von Partikeln in die Lipiddoppelschicht. Trotzdem zeigten *beide* Systeme bei der Verwendung von Liposomen mit zusätzlicher Biotinfunktionalisierung in Biotin-Streptavidin-Bindungsassays die Fähigkeit, das Analyseergebnis unter magnetischen Bedingungen signifikant zu verbessern.

Eine mögliche Anwendung der entstandenen Magnetosomen ist ihr Einsatz für immunomagnetische Abtrennungsstrategien. Deshalb wurden Vorläuferstudien durchgeführt, um das HIV-Kapselprotein p24 aufzukonzentrieren, bevor ein Sandwichassay zwischen magnetischen Mikropartikeln, p24 und einem Fluoreszenzlabel durchgeführt wurde, und vor der Detektion mithilfe von Einzelpartikel-Fluoreszenzimaging. Leider stelle sich heraus, dass - vermutlich aus sterischen Gründen - die Bindung des aufkonzentrierten Liposom-p24-Konjugats an die magnetischen Partikel gehemmt war. Deshalb wurde ein weniger lipophiles Protein, das Neutrophilengelatinase-assoziierte Lipocalin (NGAL), für weitere Studien eingesetzt, welches theoretisch nicht in solch hohem Grade mit den Liposomen interagieren sollte wie scheinbar p24. Jedoch wurden dieselben Ergebnisse wie für p24 erzielt, und zusätzlich herausgefunden, dass die Assayleistung wesentlich besser ist, wenn die Liposomen direkt an die magnetischen Partikel binden können als im Falle, dass NGAL dazwischengeschaltet wird. Nichtsdestotrotz wurde bei der Aufkonzentrierung mit Liposomen tatsächlich ein doppelt so hohes Signal erreicht wie bei einem Assay ohne Aufkonzentrierung. Da dies nur Vorläuferstudien waren, sind das trotz allem vielversprechende Ergebnisse, welche die großen Vorteile von multifunktionellen fluoreszierenden magnetischen Liposomen hervorheben.

EIDESSTATTLICHE ERKLÄRUNG

Ich erkläre hiermit an Eides statt, dass ich die vorliegende Arbeit ohne unzulässige Hilfe Dritter und ohne Benutzung anderer als der angegebenen Hilfsmittel angefertigt habe; die aus anderen Quellen direkt oder indirekt übernommenen Daten und Konzepte sind unter Angabe des Literaturzitats gekennzeichnet.

Weitere Personen waren an der inhaltlich-materiellen Herstellung der vorliegenden Arbeit nicht beteiligt. Insbesondere habe ich hierfür nicht die entgeltliche Hilfe eines Promotionsberaters oder anderer Personen in Anspruch genommen. Niemand hat von mir weder unmittelbar noch mittelbar geldwerte Leistungen für Arbeiten erhalten, die im Zusammenhang mit dem Inhalt der vorgelegten Dissertation stehen.

Die Arbeit wurde bisher weder im In- noch im Ausland in gleicher oder ähnlicher Form einer anderen Prüfungsbehörde vorgelegt.

Ort, Datum Unterschrift